AD-A110 886 OKLAHOMA STATE UNIV STILLWATER DEPT OF PHYSICS F/G 7/4
CHARACTERIZATION OF THE OPTICAL PROPERTIES OF LASER AND PHOSPHO--ETC(U)
JAN 82 R C POWELL DAAG29-80-C-0052

UNCLASSIFIED ARO-16182.11-P NL

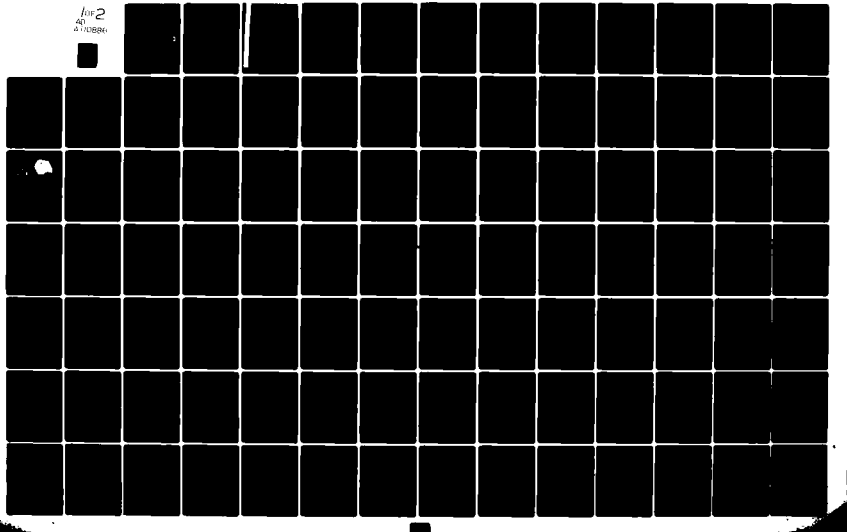

SECURITY CLASSIFICATION OF THIS PAGE (When Data Entered)

REPORT DOCUMENTATION PAGE

READ INSTRUCTIONS BEFORE COMPLETING FORM

1. REPORT NUMBER: FINAL REPORT ARO 16182.11-1
2. GOVT ACCESSION NO.: AD A11 [illegible]
3. RECIPIENT'S CATALOG NUMBER: 6

4. TITLE (and Subtitle): Characterization of the Optical Properties of Laser and Phosphor Crystals
5. TYPE OF REPORT & PERIOD COVERED: Final Report Jan. 1 , 1979 - Jan. 14, 1982
6. PERFORMING ORG. REPORT NUMBER:

7. AUTHOR(s): Richard C. Powell
8. CONTRACT OR GRANT NUMBER(s): DAAG29 79 G 0048; DAAG 29-80-C-0052

9. PERFORMING ORGANIZATION NAME AND ADDRESS: Oklahoma State University, Physics Department, Stillwater, Oklahoma 74078
10. PROGRAM ELEMENT, PROJECT, TASK AREA & WORK UNIT NUMBERS:

11. CONTROLLING OFFICE NAME AND ADDRESS: U.S. Army Research Office, Post Office Box 12211, Research Triangle Park, NC 27709
12. REPORT DATE: January 14, 1982
13. NUMBER OF PAGES: 112

14. MONITORING AGENCY NAME & ADDRESS(if different from Controlling Office)
15. SECURITY CLASS. (of this report)
15a. DECLASSIFICATION/DOWNGRADING SCHEDULE

16. DISTRIBUTION STATEMENT (of this Report)

Approved for public release; distribution unlimited.

17. DISTRIBUTION STATEMENT (of the abstract entered in Block 20, if different from Report)

18. SUPPLEMENTARY NOTES

THE VIEW, OPINIONS, AND/OR FINDINGS CONTAINED IN THIS REPORT ARE THOSE OF THE AUTHOR(S) AND SHOULD NOT BE CONSTRUED AS AN OFFICIAL DEPARTMENT OF THE ARMY POSITION, POLICY, OR DECISION, UNLESS SO DESIGNATED BY OTHER DOCUMENTATION.

19. KEY WORDS (Continue on reverse side if necessary and identify by block number)

LASERS
RARE EARTHS
EXCITON

20. ABSTRACT (Continue on reverse side if necessary and identify by block number)

This report covers the work done in the Department of Physics of Oklahoma State University under contract number DAAG 29-80-C-0052 supported by the U.S. Army Research Office, Research Triangle Park, North Carolina from January 15, 1979 through January 14, 1982. The research involves the utilization of laser optics techniques such as time-resolved site-selection spectroscopy, photo-acoustic spectrosopy, and four-wave mixing spectroscopy to characterize dynamical optical properties such as energy transfer and radiationless relaxation

DD FORM 1 JAN 73 1473 EDITION OF 1 NOV 65 IS OBSOLETE

SECURITY CLASSIFICATION OF THIS PAGE (When Data Entered)

Processes in phosphor and laser materials. The materials investigated included stoichiometric laser materials such as neodymium pentaphosphate and neodymium aluminum borate, and lightly doped laser materials such as neodymium doped yttrium vanadate, garnets and glasses. In addition, several theoretical approaches and computer modeling techniques were developed for analyzing the properties of energy transfer among ions in solids. Some of the important results obtained in this work include the direct measurement of the exciton diffusion coefficient in $Nd_xLa_{1-x}P_5O_{14}$ crystals, the measurement of the quantum efficiency of Nd^{3+} in various hosts, and the development of Monte Carlo modeling techniques for describing energy migration on a random lattice.

OKLAHOMA STATE UNIVERSITY

Department of Physics

CHARACTERIZATION OF THE OPTICAL PROPERTIES OF LASER AND PHOSPHOR CRYSTALS

Richard C. Powell, Ph.D.
Principal Investigator

FINAL REPORT

Contract Number DAAG 29-80-C-0052
(ARO Proposal Number DRXRO-PH-16182-P)
U.S. Army Research Office
Research Triangle Park, North Carolina

January 15, 1979 - January 14, 1982

ABSTRACT

This report covers the work done in the Department of Physics of Oklahoma State University under contract number DAAG 29-80-C-0052 supported by the U.S. Army Research Office, Research Triangle Park, North Carolina from January 15, 1979 through January 14, 1982. The research involves the utilization of laser optics techniques such as time-resolved site-selection spectroscopy, photoacoustic spectroscopy, and four-wave mixing spectroscopy to characterize dynamical optical properties such as energy transfer and radiationless relaxation processes in phosphor and laser materials. The materials investigated included stoichiometric laser materials such as neodymium pentaphosphate and neodymium aluminum borate, and lightly doped laser materials such as neodymium doped yttrium vanadate, garnets and glasses. In addition, several theoretical approaches and computer modeling techniques were developed for analyzing the properties of energy transfer among ions in solids. Some of the important results obtained in this work include the direct measurement of the exciton diffusion coefficient in $Nd_xLa_{1-x}P_5O_{14}$ crystals, the measurement of the quantum efficiency of Nd^{3+} in various hosts, and the development of Monte Carlo modeling techniques for describing energy migration on a random lattice.

CONTENTS

I. INTRODUCTION

The purpose of this research was to enhance our understanding of the dynamical properties of optically pumped solids having potential applications as laser and phosphor materials. The major research goals stated in the original proposal have all essentially been accomplished. The important results obtained during the three years of this contract are briefly outlined in this section and presented in detail in the remainder of the report.

I.1 Summary of Research Accomplishments

The research work performed under this contract can be divided into four thrust areas as listed in Table I. The first of these is Materials Characterization. It is important to compile as much information as possible about the properties of optically active materials to be available when specific design requirements are generated. This is especially important in a field such as electro-optic technology which is advancing rapidly and finding many new applications. The second thrust area is to obtain a better understanding of the fundamental physical processes underlying the optical properties of active materials. Of special interest are processes which lead to the enhancement or quenching of the optical emission. The third thrust area is the development of new theoretical approaches and computer modeling techniques to provide greater accuracy in interpreting experimental data obtained on energy transfer among ions in solids. This has become especially important with the availability of microcomputers which can be easily interfaced to laboratory equipment for data acquisition and analysis. The ability to use a three-pronged attack on a problem involving experimental, theoretical, and modeling work provides a powerful method for investigating the physical properties of solids. The final thrust area is the development of new experimental techniques. These involve using the

Table 1

Research Thrust Areas

CHARACTERIZATION OF MATERIALS	DEVELOPMENT OF THEORETICAL AND MODELING TECHNIQUES
$Nd_xY_{1-x}P_5O_{14}$	Monte Carlo methods for energy migration on a random lattice
$Nd_xLa_{1-x}P_5O_{14}$	Fast diffusion energy transfer with direct interaction
$NdAl_3(BO_3)_4$	Energy transfer on a discrete lattice
$YVO_4:Nd^{3+}$	Theory of degenerate four-wave mixing for diffusion measurements
$Y_xAl_5O_{12}:Nd^{3+}$	
$Y_3(Al_{0.5}Ga_{0.5})_5O_{12}:Nd^{3+}$	
$Nd_3Ga_5O_{12}$	
Nd:Silicate glass	
Nd:Germinate glass	
Nd:Phosphate glass	
Nd:Pentaphosphate glass	
$Eu_xY_{1-x}P_5O_{14}$	
$Al_2O_3:Cr^{3+}$	

UNDERSTANDING OF PHYSICAL PHENOMENA	DEVELOPMENT OF EXPERIMENTAL TECHNIQUES
Exciton dynamics	Time-Resolved Site-Selection Spectroscopy
Ion-ion interaction	Photoacoustic Spectroscopy
Radiationless and vibronic decay processes	High Pressure Spectroscopy
Concentration quenching	Four-wave mixing spectroscopy

special properties of lasers in new spectroscopy methods.

The materials characterization effort focused on Nd^{3+}-doped samples, especially mixed pentaphosphate crystals, mixed garnet crystals, and glasses. Other samples which we initially anticipated studying were not investigated because of the lack of time and the greater interest in those materials which were chosen to study. Three results of major interest came from this work. The first is a better understanding of the low quantum efficiency of YAG:Nd^{3+} laser crystals. Our phtoacoustic work described in Sec. V.1 verified the quantum efficiency of controversy in the literature. This result coupled with the results of the work performed on our previous Army contract (DAAG 29-76-G-0099) showing that efficient energy transfer takes place among Nd^{3+} ions in nonequivalent crystal field sites in this material has led Dr. L.G. DeShaser of Hughes Research Laboratories to perform an investigation of the effects of hydroxal ions in YAG crystals and he has developed a model attributing the low quantum efficiency to energy migration and transfer to "killer sites" which are Nd^{3+} ions near to hydroxyl ions. This points the way to new crystal growth and heat treatment methods which will greatly improve the efficiency of YAG lasers.

The second result of major importance is a better understanding of the concentration quenching mechanisms in stoichiometric laser materials such as NdP_5O_{14}. The various measurements performed for the characterization of this type of material are reported in Sec. III. The final results indicate that below about 10% Nd^{3+} concentration, ion-ion cross-relaxation causes the fluorescence quenching whereas at higher concentrations the quenching occurs by efficient migration to killer sites. These sites are not associated with hydroxal ions and approximately 10% of them may be surface sites. The exact nature of these defect centers has not yet been determined.

The third important result involved with material characterization is described in Sec. IV.3, where the properties of energy transfer among

Nd^{3+} ions in different types of glass hosts are discussed. The efficiency of energy transfer is found to vary with host composition as the spectral overlap and Judd-Ofelt parameters change. Also the phonon-assisted nature of the energy transfer is found to be very sensitive to the type of glass host involved.

One of the major goals in the thrust area of understanding physical phenomena was to elucidate properties of energy migration in heavily doped materials. Studies of mixed neodymium pentaphosphate crystals described in Sec. III.3 show that at room temperature migration occurs by a diffusive mechanism. Spatial migration takes place without spectral transfer and the excitons travel over distances of the order of 0.3 μm. Time did not permit extending these measurements to low temperatures to attempt to observe coherent migration but this work will be careied out in the near future. For other rare-earth pentaphosphates such as Eu^{3+} it was found that spectral energy transfer takes place by a single step process at both high and low temperatures (see Sec. II.2).

The two results of greatest importance in the are of theory and modeling techniques involved the development of methods for using microcomputers such as our LSI-11 system for doing complex simulations of physical situations. The first of these uses a Monte Carlo method for describing energy migration among ions on a random lattice. It is shown in Sec. II.1 that explicitly accounting for the random nature of the distribution of ions in this way can result in values for energy transfer parameters which differ by a factor of two from those obtained from analytical theories which assume a uniform distribution of ions. The second modeling technique involves explicitly accounting for the discrete structure of the lattice in describing single step energy transfer. The work described in Sec. II.2 show that for low concentrations of active ions the results are equivalent to those found from analytical expressions which are obtained after making a continuum

lattice approximation. However, for highly concentrated materials there can be more than an order of magnitude difference in the parameters predicted by the two approaches.

Three major areas were developed involving new experimental techniques. The first of these was the use of photoacoustic spectroscopy to measure quantum efficiencies of laser materials as described in Sec. V.1. Although it was shown that this can be done, the technique is not more accurate or easy to perform than other methods currently in use. In Secs. III.2 and V.2 spectroscopy methods using high pressure diamond cells in conjunction with laser excitation sources are discussed. Pressure measurements add a new parameter to vary in spectroscopic studies along with temperature, concentration and time. The ability to highly focus laser light makes a laser an ideal source to use with small diamond anvil cells. This has greatly enhanced the potential importance of high pressure spectroscopy. Four-wave mixing spectroscopy was developed to establish and prove transient gratings in doped solids as described in Sec. III.3. This has distinct advantages over other coherent transient techniques such as free induction decay since the mestastable state under investigation does not have to be pumped directly. This is a powerful tool for measuring spatial migration of energy without spectral diffusion and our results represent the first direct measurement in the exciton diffusion length of a stoichiometric laser material. In addition to the development of specific experimental methods as discussed above, much time was spent in interfacing our LSI-11 microcomputer system to our laboratory equipment. This has greatly extended the capabilities efficiency with which data can be acquired and analyzed.

I.2 Publications and Personnel

The work performed during the three years of this contract resulted in ten publications and twenty-five unpublished presentations and colloquia. These are listed in Table II.

The personnel making major contributions to this work include the principal investigator, Richard C. Powell, professor of physics, and two graduate research assistants C.M. Lawson and D.K. Sardar who received their doctoral degrees during this time period. Their theses are listed in Table II. One other graduate student, J.K. Tyminski, as well as three undergraduate students, D.P. Neikirk, E.E. Freed, and G.P. Quarles, have been supported by this contract. Two visiting professors in the Physics Department also worked on this project, R.C. Chow and L.D. Merkle. Also it was a pleasure to collaborate with J.G. Gualtieri of the Army Night Vision and Electro-Optics Laboratory, W.K. Zwicker of Philips Research Laboratories, and M.J. Weber of Lawrence Livermore National Laboratory on certain aspects of this project.

Supplemental support for some parts of this research was provided by a grant from the Materials Research Division of the National Science Foundation.

TABLE II

Publications, Theses, and Presentations

I. Publications

1. R.C. Powell, D.P. Neikirk, J.M. Flaherty and J.G. Gualtieri, "Lifetime Measurements, Infrared and Photoacoustic Spectroscopy of NdP_5O_{14}," J. Phys. Chem. Solids 41, 345 (1980).

2. R.C. Powell, D.P. Neikirk, and D. Sardar, "Radiationless Decay Processes of Nd^{3+} Ions in Solids," J. Opt. Soc. American 70, 486 (1980).

3. H.C. Chow and R.C. Powell, "Models for Energy Transfer in Solids," Phys. Rev. 21, 3785 (1980).

4. D.K. Sardar and R.C. Powell, "Energy Transfer Process in $YVO_4:Nd^{3+}$," J. Appl. Phys. 51, 2829 (1980).

5. L.D. Merkle, I.A. Spain, and R.C. Powell, "Effects of Pressure on the Spectra and Lifetimes of $Nd_xLa_{1-x}P_5O_{14}$ and Ruby," J. Phys. C., 14, 2070 (1981).

6. C.M. Lawson, R.C. Powell, W.K. Zwicker, "Measurements of Exciton Diffusion Lengths in $Nd_xLa_{1-x}P_5O_{14}$ by Four-Wave Mixing Techniques," Phys. Rev. Letters, 46, 1020 (1981).

7. D.K. Sardar and R.C. Powell, "Time-Resolved Site-Selection Spectroscopy Studies of $NdAl_3(BO_3)_4$ Crystals," J. Luminescence 22, 340 (1981).

8. R.C. Powell and W.K. Zwicker, "Spectroscopic Properties of Nd-Laser Materials," Proceedings of Int. Conf. on LASERS '80, Edited by C.B. Collins (STS Press, McLean, VA, 1981), p. 350 (held in New Orleans, Dec. 15-19, 1980).

9. L.D. Merkle, R.C. Powell, E.E. Freed and M.J. Weber, "Energy Transfer Among Neodymium Ions in Glass Hosts," J. Luminescence, in press.

10. R.C. Powell and W.K. Zwicker, "Energy Transfer in Stoichiometric Rare-Earth Crystals", Proceedings of Int. Conf. on Lasers '81, Edited by C.B. Collins (STS Press, McLean, VA, 1982), (held in New Orleans, Dec. 14-18, 1981).

II. Doctoral Theses

1. D.K. Sardar, "Laser Spectroscopy Studies of $YVO_4:Nd^{3+}$ and $NdAl_3(BO_3)_4$ Crystals", May, 1979.

2. C.M. Lawson, "Studies of Spectral and Spatial Energy Transfer in Solids", Dec., 1981.

III. Presentations

1. R.C. Powell, "Laser Spectroscopy Studies of Energy Transfer," Physics Colloquium, University of Kansas, March 1979.

2. R.C. Powell, "Energy Transfer in Solids," Physical and Earth Sciences Colloquium, Oklahoma State University, April 1979.

3. R.C. Powell, "Laser Spectroscopy of Solids," Chemistry Department Colloquium, University of Missouri-Kansas City, December 1979.

4. R.C. Powell, D.P. Neikirk, and E.E. Freed, "Host-Sensitized Energy Transfer in Bismuth Germanage and Lithium Niobate Crystals," American Physical Society Meeting, Chicago, IL, March 1979. Bull. Am. Phys. Soc. 24, 376 (1979).

5. R.C. Powell, "Energy Transfer in Nd^{3+}-Doped Garnets and Pentaphosphates," Second Conference on Dynamical Processes in Excited States of Ions and Molecules in Solids," Madison, Wisconsin, June 1979.

6. R.C. Powell, D.P. Neikirk, and D. Sardar, "Radiationless Decay Processes of Nd^{3+} Ions in Solids," Photoacoustic Spectroscopy Meeting, Ames, Iowa, August 1979.

7. H.C. Chow and R.C. Powell, "Recent Investigations of Energy Transfer in Nd-Doped Laser Materials," American Physical Society Meeting, New York City, March 1980. Bull. Am. Phys. Soc. 25, 519 (1980).

8. R.C. Powell, "Laser Spectroscopy Studies of Energy Transfer in Solids," Physics Department Colloquium, University of Arkansas, January 1980.

9. R.C. Powell, "Laser Spectroscopy Studies of Energy Transfer in Solids," Physics Department Colloquium, University of Missouri-Rolla, January 1980.

10. R.C. Powell, Laser Spectroscopy Studies of Energy Transfer in Solids," Physics Department Colloquium, University of Missouri-Columbia, January 1980.

11. R.C. Powell, "Laser Spectroscopy Studies of Energy Transfer in Solids," Physics Department Colloquium, Iowa State University, Ames, Iowa, January 1980.

12. R.C. Powell, "Laser Spectroscopy Studies of Energy Transfer in Solids," Physics Department Colloquium, University of Nebraska, January 1980.

13. R.C. Powell, "Laser Spectroscopy Studies of Energy Transfer in Solids," Research Colloquium, Philips Research Laboratory, March 1980.

14. R.C. Powell, "Energy Transfer in Laser Materials," Physical Chemistry Research Colloquium, University of Utrecht, The Netherlands, June 1980.

15. R.C. Powell, "Energy Transfer in Solids," Physics Colloquium, Universidad Autonoma de Madrid, Spain, June 1980.

16. R.C. Powell, "Energy Transfer in Laser Materials," Physics Colloquium, Universidad Nacional Autonoma de Mexico, Mexico, August 1980.

17. R.C. Powell and W.K. Zwicker "Spectroscopic Properties of Nd-Laser Materials," Intl. Conf. on Lasers, '80, New Orleans, Dec. 1980.

18. D.K. Sardar and R.C. Powell, "Energy Transfer Processes in $YVO_4:Nd^{3+}$," American Physical Society Meeting, New York City, March 1980. Bull. Am. Phys. Soc. 25, 519 (1980).

19. W.B. Smith and R.C. Powell, "Energy Transfer in $CaWO_4:Sm^{3+}$," American Physical Society Meeting, Phoenix, March 1981. Bull Am. Phys. Soc. 26, 278 (1981).

20. C.M. Lawson, R.C. Powell and W.K. Zwicker, "Energy Transfer in $Nd_xLa_{1-x}P_5O_{14}$," American Physical Society Meeting, Phoenix, March 1981. Bull. Am. Phys. Soc. 26, 279 (1981).

21. C.M. Lawson, R.C. Powell and W.K. Zwicker, "Four-Wave Mixing in $Nd_xLa_{1-x}P_5O_{14}$, Crystals," Third Conf. on Dynamical Processes in the Excited States of Ions and Molecules in Solids, Regensburg, July (1981).

22. L.D. Merkle, R.C. Powell, E.E. Freed, and M.J. Weber, "Energy Transfer Among Neodymium Ions in Glass Hosts," Int. Conf. on Luminescence, Berlin, July, 1981.

23. R.C. Powell, "Optical Spectroscopy of Laser Materials," Topical Meeting on Tunable Lasers, Keystone, Colorado, April, 1981.

24. R.C. Powell, "Energy Transfer in Laser Materials," Physics Colloquium, Czechoslovakian Academy of Sciences, Prague, July, 1981.

25. R.C. Powell and W.K. Zwicker, "Energy Transfer in Stoichiometric Rare-Earth Crystals", Intl. Conf. on Lasers, '81, New Orleans, Dec. 1981.

II. THEORY AND COMPUTER MODELING

This section is divided into three parts. In the first section the manuscript describes a Monte Carlo technique for treating energy migration on a random lattice, and a new theoretical model for treating energy transfer in the case in which weak direct sensitizer-activator interaction acts as a small perturbation on energy transfer by diffusion among sensitizers. In the second section the model outlines the treatment of energy transfer among ions on a discrete lattice and shows the importance of using this theory in describing energy transfer among ions in heavily doped solids. The third section describes the development of the theory of four-wave mixing in the configuration which is useful for studying exciton dynamics in solids. Appendix A reproduces some theoretical aspects of this problem that are important in developing the final analytical expressions.

PHYSICAL REVIEW B VOLUME 21, NUMBER 9 1 MAY 1980

Models for energy transfer in solids

H. C. Chow and Richard C. Powell
Department of Physics, Oklahoma State University, Stillwater, Oklahoma 74078
(Received 16 October 1979)

Two new approaches for describing the dynamics of energy transfer in solids have been developed and are described here. The first is a method for treating the case in which weak direct sensitizer-activator interaction acts as a small perturbation on energy transfer by diffusion among sensitizers. A technique involving a propagator expansion and the Born approximation in the interaction strength is used to solve this problem. The second approach is a Monte Carlo technique to simulate the migration of energy on a random distribution of sensitizers. The predictions of both these models are compared to experimental results and to the predictions of other theoretical models. In their regions of validity they predict significantly different results than those of the models commonly used. The models developed here are applicable to many important materials such as those used for rare-earth lasers.

I. INTRODUCTION

The transfer of electronic excitation energy between ions or molecules in a solid has been the subject of many investigations for over forty years. Recently there has been increased interest in characterizing this process in materials used for laser and phosphor applications. Energy transfer can be used to increase the pumping efficiency of the active ions or molecules in these materials but it can also cause decreased fluorescence emission through concentration quenching interactions. Despite the significant amount of interest and research activity in this area there are still some important aspects to the problem of energy transfer which are not well characterized and understood. The work described here treats two aspects of this problem which have not been satisfactorily accounted for in previous developments.

Energy transfer is generally treated in one of two limiting cases. The first is a direct transfer from an excited "sensitizer" to an unexcited "activator." The theory describing this "single-step process" has been developed in the classic papers of Förster[1] and Dexter[2] with problems such as the effect of random disorder being attacked recently.[3-5] The second case is that of energy transfer to activators after multistep diffusion among sensitizers. The description of this "exciton" diffusion energy transfer was first developed by Frenkel,[6] Trlifaj,[7] and Förster.[1] A major problem in studying diffusional energy transfer is how to separate the properties of diffusion among sensitizers and the properties of trapping at an activator site from the total energy-transfer properties which are measured. Several theories have been proposed to account for simultaneous sensitizer energy diffusion and sensitizer-activator interaction[8-10] but the final solutions of each of these theories involve assumptions which limit their validity to specific cases. One important case to which the currently available theories do not apply is one in which the direct sensitizer-activator interaction is smaller than the diffusional term but not small enough to be negligible. A theoretical description of this case is developed in Sec. II of this paper and several cases where it may apply are discussed.

A second problem involving multistep migration of energy concerns the spatial distribution of sensitizers. All the standard theories assume a uniformly distributed lattice of sensitizers so that the random walk of the exciton can be described by a single average hopping time. This picture should be valid for "host-sensitized" energy transfer or other situations involving high concentrations of sensitizers but it is certainly a poor approximation if the sensitizers are randomly distributed impurities with low concentrations. In Sec. III of this paper we describe a Monte Carlo treatment of this problem and compare the results to the predictions of existing theories and experimental results.

II. EFFECTS OF DIRECT SENSITIZER-ACTIVATOR INTERACTION ON DIFFUSIONAL ENERGY TRANSFER

In this section we consider the situation in which energy transfer includes both diffusion among sensitizers and single-step resonant transfer between sensitizer-activator pairs. Yokota and Tanimoto[8] treated the limiting case in which the one-step transfer is dominant and the diffusive contribution is a small perturbation. They developed an interpolation scheme for the time dependence of the excited sensitizer concentration in this limit. On the other hand, if diffusion is the more important of the two transfer processes, the usual treatment[10,11] is to as-

sume some finite trapping radius for the activators outside of which diffusion takes place, while neglecting any direct, single-step sensitizer-activator interaction. Here we will consider the fast-diffusion regime and specifically examine what effects the single-step transfer might have on the time development of the excited sensitizer concentration otherwise depleted by diffusion.

The equation governing the excited sensitizer concentration $n(\vec{r},t)$ including both diffusion and single-step transfer is

$$\partial n(\vec{r},t)/\partial t = -\beta n(\vec{r},t) + D\nabla^2 n(\vec{r},t) - \sum_i v(\vec{r}-\vec{R}_i)n(\vec{r},t) \quad . \tag{1}$$

Here β is the intrinsic decay rate of the sensitizers, D is the diffusion coefficient, $\vec{R}_i$ is the position vector for a given activator, and $v(\vec{r}-\vec{R}_i)$ is the interaction strength for a given sensitizer-activator pair. In this development the interaction is taken to be of the common electric dipole-dipole type, and thus $v(\vec{r}-\vec{R}_i)$ varies inversely as the sixth power of $|\vec{r}-\vec{R}_i|$. The solution to Eq. (1) must eventually be averaged over the configuration of activator distributions, which is a difficult task. With the assumption of a uniform activator distribution, however, Yokota and Tanimoto[8] have shown that the problem is reduced to averaging the solution of a single-center problem, in which an activator acting as an absorber is located at $\vec{r}=0$. For this case

$$\partial n(r,t)/\partial t = -\beta n(r,t) + D\nabla_r^2 n(r,t) - v(r)n(r,t) \quad , \tag{2}$$

where

$$\nabla_r^2 = \frac{1}{r^2}\frac{\partial}{\partial r}\left(r^2\frac{\partial}{\partial r}\right)$$

is the isotropic Laplacian operator. The general solution to Eq. (2) can be written as

$$n(r,t) = \sum_k \exp(-\beta t - Dk^2 t)\phi_k(r) \tag{3}$$

with $\phi_k(r)$ obeying the eigenvalue equation

$$[\nabla_r^2 + k^2 - D^{-1}v(r)]\phi_k(r) = 0 \quad . \tag{4}$$

Because of the assumed r^{-6} dependence of $v(r)$, no solution to Eq. (4) can be found that is regular at $r=0$. Nevertheless, it is possible[12] to employ the Fermi pseudopotential method to find the lowest eigenvalue and eigenfunction, k^2 and $\phi_k(r)$, respectively, which according to Eq. (3) determine the asymptotic behavior of the excited sensitizer concentration. In this approach $\phi_k(r)$ thus determined is identically zero for a finite distance, $0 \le r \le a$, the so-called scattering length.

The above remarks serve to justify the use of an approximate potential in lieu of the exact dipole-dipole interaction. Namely, we let

$$v(r) \cong v_0(r) + u(r) \tag{5}$$

in which

$$v_0(r) = \begin{cases} 0, & r > a \\ \infty, & r \le a \end{cases} \quad ,$$
$$u(r) = \begin{cases} 0, & r \le a \\ a/r^6, & r > a \end{cases} \quad . \tag{6}$$

With the use of this approximate potential, the kinetic Eq. (2) is solved exactly except for $u(r)$ which is treated in the Born approximation. Such a solution clearly corresponds to the case in which energy transfer via diffusive migration is stronger than transfer by single-step electric dipole-dipole resonant transfer.

The method of solution is based on the well-known propagator expansion.[13] Upon writing $n(r,t) = e^{-\beta t}\psi(r,t)$, it is seen because of the linearity of the operations in Eq. (2) that the temporal and spatial development of $\psi(r,t)$ is governed by

$$\psi(r,t) = \int G(r,t|r_0,t_0)\psi(r_0,t_0)\,dr_0 \tag{7}$$

in which the propagator or Green's function $G(r,t|r_0,t_0)$ obeys the equation

$$[-\partial/\partial t + D\nabla_r^2 - v(r)]G(r,t|r_0,t_0) = \delta(r-r_0)\delta(t-t_0) \quad , \tag{8}$$

where $\delta(x)$ is the Dirac δ function. If instead of the full electric dipole-dipole interaction, one solves for the Green's function for the approximate potential $v_0(r)$

$$[-\partial/\partial t + D\nabla_r^2 - v_0(r)]G_0(r,t|r_0,t_0) = \delta(r-r_0)\delta(t-t_0) \tag{9}$$

then the objective enunciated in the preceding paragraph is accomplished by obtaining

$$\psi(r,t) \cong \psi_0(r,t) + \psi_1(r,t) = \int G_0(r,t|r_0,t_0)\psi(r_0,t_0)\,dr_0 - \int G_0(r,t|r_1,t_1)u(r_1)G_0(r_1,t_1|r_0,t_0)\psi(r_0,t_0)\,dr_1\,dt_1\,dr_0 \quad . \tag{10}$$

We determine $G_0(r,t|r_0,t_0)$ by the method of image. Upon writing

$$G_0(r,t|r_0,t_0) = r^{-1}\tilde{G}(r,t|r_0,t_0)$$

Eq. (8) reads

$$[-\partial/\partial t + D(\partial^2/\partial r^2) - v_0(r)]\tilde{G}(r,t|r_0,t_0) = r_0\delta(r-r_0)\delta(t-t_0) \tag{11}$$

The effect of $v_0(r)$ is accounted for if it is required that $\tilde{G}(r,t|r_0,t_0)$ vanishes for $r \leq a$. This may be accomplished by introducing a source of strength r_0 at $r = r_0$ and an image source at $r = 2a - r_0$, leading to

$$G_0(r,t|r_0,t_0) = \frac{r_0}{r}\frac{\theta(t-t_0)}{[4\pi D(t-t_0)]^{1/2}}\{\exp[-(r-r_0)^2/4D(t-t_0)]$$

$$-\exp[-(r+r_0-2a)^2/4D(t-t_0)]\}, \quad r, r_0 \geq a \tag{12}$$

where $\theta(t)$ is a unit Heaviside step function. For uniform initial excitation of sensitizers, $\psi(r,t_0) = n_0$ at $t_0 = 0$, the result is

$$\psi_0(r,t) = n_0\left\{1 - \frac{a}{r} + \frac{a}{r}\operatorname{erf}\left[\frac{r-a}{(4Dt)^{1/2}}\right]\right\} \tag{13}$$

which is identical to the result[12] describing the diffusive migration of excited sensitizers in the presence of a trap of radius a.

The effect of concurrent single-step electric dipole-dipole resonant transfer from sensitizer to activator is contained in the next term in the Born approximation

$$\psi_1(r,t) = \int dr_1 u(r_1) K(r,t|r_1), \tag{14}$$

where

$$K(r,t|r_1) = \frac{n_0}{(4\pi D)^{1/2}}\frac{r_1}{r}\int_0^t \frac{d\tau}{(t-\tau)^{3/2}}\{\exp[-(r-r_1)^2/4D(t-\tau)] - \exp[-(r+r_1-2a)^2/4D(t-\tau)]\}$$

$$\times\left\{1 - \frac{a}{r_1} + \frac{a}{r_1}\operatorname{erf}\left[\frac{r_1-a}{(4D\tau)^{1/2}}\right]\right\} \tag{15}$$

Further progress can be made with the aid of the following integrals (which are derivable from the results in the appendix of Ref. 13):

$$\int_0^t \frac{d\tau}{(t-\tau)^{3/2}}\exp[-\beta^2/4D(t-\tau)] = 2\sqrt{\pi}\exp(-\beta^2/4Dt) - \left(\frac{\pi}{D}\right)^{1/2}\beta\operatorname{erfc}\left[\frac{\beta^2}{(4Dt)^{1/2}}\right]$$

$$\int_0^t \frac{d\tau}{(t-\tau)^{3/2}}\exp[-\beta^2/4D(t-\tau)]\operatorname{erf}\left[\frac{r-a}{(4D\tau)^{1/2}}\right]$$

$$= \operatorname{erf}\left[\frac{r-a}{(4Dt)^{1/2}}\right]\left\{2\sqrt{\pi}\exp(-\beta^2/4Dt) - \left(\frac{\pi}{D}\right)^{1/2}\beta\operatorname{erfc}\left[\frac{\beta}{(4Dt)^{1/2}}\right]\right\}$$

$$-\frac{(r-a)}{(\pi D)^{1/2}}E_1\left[\frac{(r-a)^2+\beta^2}{4Dt}\right]$$

$$-\frac{4|\beta|}{(\pi D)^{1/2}}\int_{(r-a)^2/4Dt}^{\infty} dx\, e^{-x^2}\int_{|\beta|/(4Dt)^{1/2}}^{\infty} dx\, e^{-x^2}$$

in which $E_1(x) = \int_x^\infty e^{-t}t^{-1}\,dt$ is an exponential integral. Then Eq. (15) can be written as

$$K(r,t|r_1,t) = \frac{n_0}{(4\pi D)^{1/2}}\frac{r_1}{r}\left\{\frac{2}{r}\sum_{n=0}^{\infty}[I(r-r_1) - I(r+r_1-2a)]\right. \tag{16}$$

where

$$F_1(x) = \left[\frac{r_1}{a} - 1 + \operatorname{erf}\left(\frac{r_1 - a}{(4Dt)^{1/2}}\right)\right]\left[2\sqrt{t}\,e^{-x^2/4Dt} - (\pi/D)^{1/2}|x|\operatorname{erf}\left(\frac{|x|}{(4Dt)^{1/2}}\right)\right],$$

$$F_2(x) = \frac{r_1 - a}{(\pi D)^{1/2}} E_1\left(\frac{x^2 + (r_1 - a)^2}{4Dt}\right),$$

$$F_3(x) = \frac{-4|x|}{(\pi D)^{1/2}} \int_{r_1 - a/(4Dt)^{1/2}}^{\infty} dy\, e^{-y^2} \int_{(|x|/|r_1 - a|)y}^{\infty} dz\, e^{-z^2}.$$

Rather than finding the explicit space and time dependence of the excited sensitizer concentration which entails a further integration in Eq. (14), it is expedient to obtain the time-dependent energy-transfer rate $k(t)$ which is also accessible experimentally. The latter is related to the total amount of excitation $\tilde{N}(t)$ via[14]

$$\tilde{N}(t) = N(t)e^{\beta t} = N_0 \exp\left[-\int_0^t k(t')\,dt'\right] \tag{17}$$

It is also customarily treated as the quantity that appears in the rate equation

$$d\tilde{N}(t)/dt = -k(t)N_0. \tag{18}$$

It is clear that the two definitions are equivalent only in the limit that $\int_0^t k(t')dt'$ is much less than unity.

To proceed further, Eq. (2) is integrated over the volume of the sample Ω and the first identity of Green invoked to obtain

$$\partial\tilde{N}(t)/\partial t = -4\pi a^2 D\left[\frac{\partial\psi}{\partial r}\right]_{r=a} - \int u(r)\psi(r,t)\,d\Omega. \tag{19}$$

Comparison between Eqs. (18) and (19) leads to the expression for the time-dependent energy-transfer rate for the case of N_a activators per unit volume, correct to the first Born approximation

$$k(t) = \frac{N_a\Omega}{N_0}\left[4\pi a^2 D\left[\frac{\partial\psi_0}{\partial r} + \frac{\partial\psi_1}{\partial r}\right]_{r=a} + \int u(r)\psi_0(r,t)\,d\Omega\right] \tag{20}$$

The three factors that appear in Eq. (20) have rather obvious physical interpretations. The first factor has the explicit form

$$k_0(t) = 4\pi DaN_a[1 + a(\pi Dt)^{-1/2}] \tag{21}$$

and is simply the rate at which excitations arrive diffusively at the surfaces of the activator traps. It has been used as the standard result[11-14] for the time-dependent energy transfer in the fast diffusion regime. The generalized random-walk model[10] which includes an extended trapping region yields the same time dependence with a somewhat different interpretation of the physical parameters involved. The last factor in Eq. (20) is the integrated amount of excitations weighted with the probability per unit time of making a single-step transfer to an activator. This represents the rate of energy transfer by a single-step resonant process. The presence of such single-step transfer has the consequence of diminishing the amount of excitations available for transfer by diffusive migration. This is accounted for by the second factor in Eq. (20) which is intrinsically negative by virtue of the fact that

$$\left[\frac{\partial\psi_1}{\partial r}\right]_{r=a} = -\frac{n_0}{D}\int_a^{\infty} dr\, u(r)\operatorname{erfc}\left[\frac{r-a}{(4Dt)^{1/2}}\right] \times\left[\frac{r}{a} - \frac{1}{2}\operatorname{erfc}\left[\frac{r-a}{(4Dt)^{1/2}}\right]\right]. \tag{22}$$

Thus the time-dependent energy-transfer rate for the case considered here may be written as $k(t) = k_0(t) + k_1(t)$ with k_0 being the usual diffusion expression given in Eq. (21) and k_1 accounting for the two effects of direct sensitizer-activator interaction discussed above. For electric dipole-dipole interaction the latter term becomes

$$k_1(t) = \frac{4\pi N_a\alpha}{3a^3} + 2\pi N_a a^2\int_a^{\infty} dr\frac{\alpha}{r^6}\left[\operatorname{erfc}\left[\frac{r-a}{(4Dt)^{1/2}}\right]\right]^2 - 8\pi N_a a\int_a^{\infty} dr\frac{\alpha}{r^5}\left[\operatorname{erfc}\left[\frac{r-a}{(4Dt)^{1/2}}\right]\right] \tag{23}$$

At this point it is necessary to use numerical integration to extract the explicit time dependence of this additional contribution to the energy-transfer rate. However, since it is readily seen that the magnitude of $k_1(t)$ varies from $4\pi N_a\alpha/(3a^3)$ at $t = 0$ to $-4\pi N_a\alpha/(15a^3)$ as $t \to \infty$, a measure of the optimal significance of the effects of single-step transfer in the fast-diffusion regime may conveniently be chosen as the ratio $k_1(t=0)/k_0(t\to\infty) = \alpha'/(3Da^4)$. Table I[15-17] lists values of this ratio for a number of systems for which fast diffusion has been identified.

It should be pointed out that in the absence of any other theoretical considerations, the values of α, a,

TABLE I. Estimated importance of direct sensitizer-activator interaction on energy transfer in the fast-diffusion regime.

System	α (cm^6/sec)	D (cm^2/sec)	a (cm)	$\frac{k_1(t=0)}{k_0(t=\infty)}$
$Tb_3Al_5O_{12}$[a]	1.2×10^{-35}	1.25×10^{-11}	2.1×10^{-7}	1.65×10^{2}
$Y_{0.84}Yb_{0.1}Ho_{0.05}F_3$[b]	1.8×10^{-41}	2.2×10^{-11}	2.03×10^{-8}[c]	1.61
Eu, Cr: Glass[d]	5.0×10^{-38}	6.0×10^{-10}	1.2×10^{-7}	0.134
Anthracene in fluorene[e]	1.74×10^{-32}	3.4×10^{-7}	3.69×10^{-8}	9.2×10^{3}
Tetracene in anthracene[e]	1.78×10^{-32}	3.1×10^{-5}	1.84×10^{-6}	1.67×10^{-5}
Tetracene in naphthalene[e]	3.52×10^{-35}	3.1×10^{-6}	1.37×10^{-6}	1.07×10^{-6}

[a]Reference 16.
[b]Reference 17
[c]Estimated using $a=0.676(\alpha/D)^{1/4}$ from Ref. 8.
[d]Reference 15.
[e]Reference 14.

and D listed in Table I have been determined by fitting the experimental data with the standard diffusion theory and are therefore not totally reliable for establishing or dismissing the importance of single-step transfer in the fast-diffusion regime. [Note the inconsistency indicated by the fact that the parameter $\alpha/(3D\alpha^4)$ is larger than unity in several cases.] The present calculation hopefully can provide some criteria for assigning the values of these physical quantities and for assessing the significance of resonant transfer either by using an independently determined set of parameters or by comparing the full time dependence of the energy-transfer rate to the experimental results.

III. HOPPING ON A RANDOM LATTICE

Another phenomenological approach to the treatment of energy transfer which also enjoys rather frequent use is based on the physical picture of excitations hopping among sensitizers and from sensitizers to activators. In the limit of many steps the results of this random-walk approach are equivalent to those of the diffusion approach. The basic premises of random-walk treatments will now be briefly reviewed.[9,18] Let $p_j(t)$ denote the probability that an excited sensitizer is located at $\vec{R}_j$ at time t, the equation for excitation migration is

$$\frac{dp_j(t)}{dt}=-\beta p_j(t)-\sum_i \nu(\vec{R}_i-\vec{R}_j)p_j(t) \quad . \tag{24}$$

The meanings of the other symbols are the same as those encountered in the last section except that $\vec{R}_j$ now denotes the position vector for either an activator or a sensitizer. The solution to Eq. (24) must be averaged over the configuration of activator-sensitizer distributions and the result designated by $\phi(t)$ may be correlated to, for example, the luminescence emitted by the sensitizer. It should be noted that Eq. (24) neglects the effects of back transfer from activator to sensitizer ions. This is justified for systems in which relaxation processes on the activator take the excitation out of resonance with the sensitizer which is true for many cases that have been investigated. For systems where back transfer is not a negligible process an additional term is present in Eq. (24).

If the excitations are incapable of migration among the sensitizers themselves, it is possible to solve Eq. (24) and carry out an ensemble average over the uniform distribution of activators and the result, $\bar{\rho}(t)$, for electric dipole-dipole interaction is[1]

$$\bar{\rho}(t)=\exp[-\beta t-(C_a/C_0)(\pi\beta t)^{1/2}] \quad , \tag{25}$$

where C_a is the activator concentration and the "critical concentration" is $C_0=(\frac{4}{3}\pi R_0^3)^{-1}$. Here R_0 is defined as the distance between sensitizer and activator at which the rate of energy transfer is equal to the intrinsic decay rate; i.e., $\nu(\vec{R})=\beta(R_0/R)^6$. If, however, the excitations may hop among sensitizers, the interaction strength $\nu(\vec{R})$ that appears in Eq. (24) abruptly changes each time a hopping takes place and is therefore a random variable. By assuming that the duration over which the interaction strength $\nu(\vec{R})$ does not change is distributed according to $\tau_0^{-1}\exp(-t/\tau_0)$, and thus identifying τ_0 as the mean hopping time, Burshtein[9] was able to arrive at an equation governing $\phi(t)$

$$\phi(t)=\bar{\rho}(t)e^{-t/\tau_0}+\tau_0^{-1}\int_0^t \phi(t')\bar{\rho}(t-t')e^{-(t-t')/\tau_0}\,dt' \tag{26}$$

The solution for Eq. (26) can be obtained by numerical methods[19] and gives results equivalent to those of the Yokota-Tanimoto[8] theory in the appropriate limit. On the other hand, if Eq. (24) is to be augmented

with an additional term to account for the back transfer from activator to sensitizer ions, the problem is significantly more complicated[4] and indeed no analytic solution has yet been found.

The merit of Burshtein's approach lies in its simplicity and its relative ease for numerical solution. It remains, however, an approximation. For example, it is easily seen from the probability distribution for dipole-dipole interaction in a random system[20] that the corresponding hopping time distribution is proportional to $t^{-1/2}\exp(-\lambda t)$, where λ is a constant for a given concentration of sensitizers. For a small or moderately large concentration of sensitizers this function falls off much slower than the approximation used by Burshtein. The underlying difficulty in studying hopping motion on a random lattice as described above is this possible wide distribution of hopping times. In the absence of better theoretical techniques to handle such situations, we have resorted to Monte Carlo methods to study this problem. As will be seen, our study leads to rather different results from those predicted by Eq. (26).

The essence of the Monte Carlo calculation will now be described. We generate a finite number of excited sensitizers, allow the excitations to hop around on a matrix of prespecified concentrations of sensitizer and activator sites, and count the fractional excitations that survive at various times. Intrinsic decay of the excitations is easily accounted for and thus is not explicitly considered in this treatment. The disappearance of excitations therefore occurs solely as the result of a jump onto an activator site which has a jump probability dependent upon the fractional occupation of sites by activators. The physical nature of the random distributions of the sensitizers and activators and the ion-ion interaction mechanism can be simulated by the generation of a weighted set of random numbers to be used for hopping times. The standard set of random numbers generated by the computer are uniformly distributed and must be transformed to have the desired characteristics. For example, the sensitizers must obey the law of distribution of the nearest neighbor in a random distribution of available sites (the Hertzian distribution).[11] This law, in the representation of the number of available sites, y, in a sphere centered on a sensitizer site and interior to the nearest-neighboring sensitizer, is $c\exp(-cy)$, where c is the fractional sensitizer occupancy of sites. The sequence of numbers having such a feature is obtained from a sequence of uniformly distributed random numbers r via the expression $y = c^{-1}\ln(1-r)$. (The last relation follows from equating the cumulative distributions of the two sequences.) In a similar manner, we require that the sequence of numbers reflects the nature of an electric dipole-dipole interaction (which falls off as r^{-6}) in addition to that of a random distribution of sensitizers of a given concentration. The set of weighted random numbers constructed in this way are then used as hopping times for the simulated random walk.

A computer simulation is thus constructed which "observes" the hopping of each generated excitation having first insured that the excitation was not created on an activator site. The time for each hop is selected from the weighted set of random numbers generated by the method described above. This allows the excited sensitizer on each step of the random walk to interact with any of the other randomly distributed sensitizer and activator ions which reflects the electric dipole-dipole nature of the interaction. In this manner any spatial correlation is accounted for. Hopping is allowed to continue until either of the following two events takes place: an activator site is encountered or a particular hop takes a longer time than the time of interest (in the present study, about ten times the intrinsic lifetime). The survival time of each excitation is determined by calculating the sum of all its previous hopping times before being terminated by one of the two criteria mentioned previously. In the end, a bin sort is performed to determine the fractional number of excited sensitizers that have succeeded in avoiding any activator site at various times. To ensure that correct random-number sequences are used in the calculation, the sequences are tested and seen to obey the Hertzian distribution. Furthermore, the results are compared to test whether they are insensitive to different arbitrary cutoffs in the random numbers used in the calculation, as they should be if the proper distribution characteristics are built into the hopping time and sensitizer position distributions.

The results of some typical Monte Carlo calculations of this type are shown in Fig. 1. For each run an average hopping time is determined and is used as an input in Watts's program[19] for integrating Burshtein's equation. The predictions of the Burshtein approach, after being multiplied by $\exp(\beta t)$, are also shown in Fig. 1 for comparison. In general, for the same interaction strength, the Burshtein approach predicts a faster decrease in the excited sensitizer population than does the Monte Carlo simulation. Note that the concentrations used in curve (a) are those of a typical case of energy transfer among Nd^{3+} ions in yttrium gallium garnet crystals which has been investigated recently.[21] The data shown in Fig. 7 of Ref. 21 consist of the time evolution of the intensity ratios of emission centers at two different crystal-field sites. Ions in one type of site are selectively excited by the specific laser frequency used, and energy transfer occurs to ions in the other type of site. The intensity ratios for the three different sets of spectral transition shown in the figure are fitted with the same theoretical parameters. A good fit to experimental data under discussion occurs for either the Monte Carlo simulation with an interaction distance of 20 Å or the

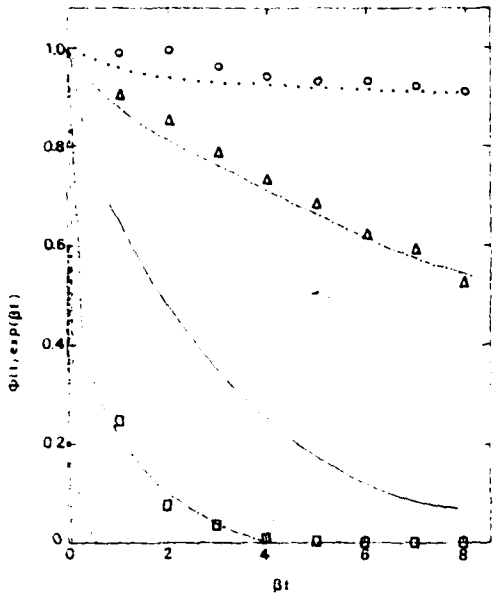

FIG. 1. Comparison of Monte Carlo predictions of excitation survival probability, $\phi(0)e^{\beta t}$ with the predictions of Burshtein's theory. (a) For $C_s = 8.33 \times 10^{-3}$, $C_a = 1.67 \times 10^{-3}$, $\beta^{-1} = 2.5 \times 10^{-4}$ sec, and $R_0 = 20$ Å. ○ gives the Monte Carlo predictions and —— gives the Burshtein-theory prediction. ---- gives the Burshtein theoretical prediction for the same concentrations but with $R_0 = 11$ Å. (b) For $C_s = 8.33 \times 10^{-2}$, $C_a = 1.67 \times 10^{-3}$, $\beta^{-1} = 2.5 \times 10^{-4}$ sec, and $R_0 = 20$ Å. Δ gives the Monte Carlo predictions and − − − is the prediction of the Burshtein theory. For the same concentrations but $R_0 = 12$ Å the Burshtein-theory prediction is given by −·−·. (c) For $C_s = 8.33 \times 10^{-2}$, $C_a = 1.7 \times 10^{-2}$, $\beta^{-1} = 2.5 \times 10^{-4}$ sec, and $R_0 = 20$ Å. □ represents the Monte Carlo results and −·· gives the Burshtein results. −−· gives the prediction of the Burshtein theory for the same concentrations but with $R_0 = 12$ Å.

Burshtein theory with a critical interaction distance of 11 Å. Theoretical estimates for R_0 for this system are closer to the larger value but this must be considered as only a rough approximation because of the complicated nature of the phonon-assisted diffusion enhanced energy transfer in this system.[21]

IV. DISCUSSION AND CONCLUSIONS

A rigorous, complete solution to the problem of energy transfer among randomly distributed sensitizers and activators is still lacking. This is especially true if the additional complications of back transfer from activators to sensitizers and random distributions of transition energies are included. Recently there have appeared a significant number of theoretical works on these and related subjects, among which may be mentioned the papers of Haan and Zwanzig,[5] Huber,[4] and Holstein, Lyo, and Orbach.[3] These generally use more powerful mathematical techniques and starting with the elemental interactions among sensitizers and activators, they seek to elucidate the connection between the behavior on the microscopic scale and the somewhat more phenomenological diffusion and random-walk models. The final exact solution to this complicated physical problem has not yet been obtained. In the preceding sections we have concerned ourselves with several aspects of both the diffusion and random-walk models of the energy problem with the objective to supplement and clarify some aspects of these existing models. The virtue of these models has been their capability of being brought into direct comparison with experimental results and the more fundamental theories[4,5] by and large confirm in the appropriate limits the validity of these phenomenological models. This provides the justification and possible usefulness of the present work.

We have developed here two important aspects of the energy-transfer problem. The first is a theoretical expression for treating the case: The direct sensitizer-activator interaction is a small perturbation on the transfer of energy by diffusion among the sensitizers. The second is a Monte Carlo approach to simulate the migration of excitations on a random distribution of sensitizers. It should be pointed out that the approach to the Monte Carlo simulation used here is similar to the continuous-time random-walk model developed to explain anomalous transit-time dispersion for charge carriers in amorphous solids.[22,23] It attempts to account for the possibility of transfer from an excited sensitizer to any other sensitizer in the system at each step in the random walk by using the configuration-averaged distribution of hopping times at each site. This is different from the Monte Carlo procedure used previously[3] which generates a specific lattice topology, assumes only first nearest-neighbor steps and then forms a configuration average of the results. In that study[3] which correlates the decrease in fluorescence emission from ions in selective excited sites due to energy migration to ions in different types of neighboring sites, care must be exercised in dealing with excitations hopping back to the original site since this offsets the time-dependent line-narrowing effect. This clearly presents no particular problem in the present study, a return to the original site has no distinguishable effects from hopping to a fresh sensitizer site.

Table II compares the commonly used phenomenological models of energy transfer and indicates the physical situation in which each model is valid. This shows the important areas of usefulness for the two theoretical treatments developed here. It should be stressed that each of these models should be applied only to the physical situations in which they are valid.

TABLE II. Phenomenological models for the dynamics of energy transfer.

Model	Region of applicability	Ref.
Förster-Dexter	Direct s-a interaction; no sensitizer energy diffusion	1, 2
Yokota-Tanimota	Strong s-a interaction; weak sensitizer energy diffusion	8, 1
Chow-Powell	Weak s-a interaction; strong sensitizer energy diffusion	This paper
Burshtein	Equivalent to Yokota-Tanimota model and diffusion/random-walk model in the appropriate limits	9
Soos-Powell	Strong sensitizer energy diffusion with the effects of extended trapping regions	10, 14
Diffusion-random walk	No direct s-a interaction; energy transfer by hopping onto an activator site	7, 11
Monte Carlo	No direct s-a interaction; transfer by energy diffusion on a random lattice	3, this paper

this has not generally been true in the past. For example, the results of the preceding section show that, if data involving energy migration on a random distribution of sensitizers are analyzed with the Burshtein model, the interaction strength one obtains is approximately a factor of 2 smaller than the value found from the Monte Carlo treatment which accounts for the random distribution of hopping times. Note that the Burshtein model is equivalent to the Yokota-Tanimota model in the weak-diffusion limit and equivalent to the standard diffusion result in the strong-diffusion limit. However, it does not correctly account for the effects of direct sensitizer-activator interaction when it is not negligible in the fast-diffusion regime and it does not correctly account for the distribution of hopping times when hopping takes place on a random lattice. The models developed here are most applicable in these regions where the Burshtein approach fails. Also, of course, there are special situations where none of the models in Table II apply. An example of this is when high-resolution laser experimental techniques, such as fluorescence line narrowing are used and theories accounting for differences in transition energies must be employed.

In summary, we have developed two new approaches to the problem of energy transfer of solids which allow for the treatment of physical situations involving strong diffusion with weak direct sensitizer-activator interaction and migration of energy on a random distribution of sensitizers. Both of these situations have important applications to impurity-doped laser materials and many of the previous results on these materials should be reinterpreted using the new models described here.

ACKNOWLEDGMENTS

This work was sponsored by the U.S. Army Research Office. The authors gratefully acknowledge the help of D. D. Smith in developing the Monte Carlo program and express their thanks to R. K. Watts for supplying us with a copy of his computer program for integrating the Burshtein equation.

[1]T. Förster, Ann. Phys. (Leipzig) 2, 55 (1948); Z. Naturforsch 4a, 321 (1949).
[2]D. L. Dexter, J. Chem. Phys. 21, 836 (1953).
[3]T. Holstein, S. K. Lyo, and R. Orbach, Phys. Rev. Lett. 36, 891 (1976); R. M. Rich, S. Alexander, J. Bernasconi, T. Holstein, S. K. Lyo, and R. Orbach, Phys. Rev. 18, 3048 (1979); S. K. Lyo, T. Holstein, and R. Orbach, Phys. Rev. B 18, 1637 (1978).
[4]W. Y. Ching, D. L. Huber, and B. Barnett, Phys. Rev. B 17, 5025 (1978); D. L. Huber, Phys. Rev. B (in press); D. L. Huber and W. Y. Ching (unpublished).
[5]S. W. Haan and R. Zwanzig, J. Chem. Phys. 68, 1879 (1978).
[6]J. Frenkel, Phys. Z. Sowjetunion 9, 158 (1936).
[7]M. Trlifaj, Czech. J. Phys. 6, 533 (1956); 8, 510 (1958).
[8]M. Yokota and O. Tanimoto, J. Phys. Soc. Jpn. 22, 779 (1967).
[9]A. I. Burshtein, Sov. Phys. JETP 35, 882 (1972).
[10]Z. G. Soos and R. C. Powell, Phys. Rev. B 6, 4035 (1972).
[11]S. Chandrasekhar, Rev. Mod. Phys. 15, 1 (1943).
[12]J. M. Blatt and V. F. Weisskopf, *Theoretical Nuclear Physics* (Wiley, New York, 1952), p. 72.
[13]R. P. Feynman and A. R. Hibbs, *Quantum Mechanics and Path Integrals* (McGraw-Hill, New York, 1965), Chap. 6.
[14]R. C. Powell and Z. G. Soos, J. Lumin. 11, 1 (1975).
[15]M. J. Weber, Phys. Rev. B 4, 2932 (1971).
[16]J. P. Van der Ziel, L. Kopf, and L. G. Van Uitert, Phys. Rev. B 6, 615 (1972).
[17]R. K. Watts and H. J. Richter, Phys. Rev. B 6, 1584 (1972).
[18]R. K. Watts, in *Optical Properties of Ions in Solids*, edited by B. DiBartolo (Plenum, New York, 1974), p. 307.
[19]R. K. Watts, J. Chem. Phys. 64, 902 (1976).
[20]S. K. Lyo, J. Phys. C 12, L83 (1979).
[21]L. D. Merkle and R. C. Powell, Phys. Rev. B 20, 75 (1979).
[22]H. Scher and E. W. Montroll, Phys. Rev. B 12, 2455 (1975).
[23]M. Silver and L. Cohen, Phys. Rev. B 15, 3276 (1977).

II.2

ENERGY TRANSFER IN STOICHIOMETRIC RARE-EARTH CRYSTALS

Richard C. Powell
Oklahoma State University, Stillwater, OK 74078
and
Walter K. Zwicker
Philips Laboratories, Briarcliff Manor, NY 10510

Abstract

Recent results are presented on the growth of rare earth pentaphosphate crystals and on the characteristics of energy transfer in these materials. For EuP_5O_{14} it is shown that a discrete lattice model must be used to account for the observed results.

I. Introduction

During the past two years we have been studying the spectroscopic properties of stoichiometric laser materials and especially rare-earth pentaphosphates. One aspect of these materials of significant importance in determining the concentration quenching properties is understanding the basic physical mechanism of energy transfer among the high concentrations of rare earth ions. At last year's Lasers '80 Meeting we reported on the spatial diffusion of energy without spectral transfer in $Nd_xLa_{1-x}P_5O_{14}$ crystals.[1] Since that time the major portion of our work on this system has centered around the development of the crystal growth of higher quality, larger size samples. An example of the results of this effort are shown in Fig. 1 which pictures NdP_5O_{14} and PrP_5O_{14} crystals grown in the Philips Laboratories. These were grown by the previously described flux technique from hot polyphosphoric acid. The crystals are greater than 4 cm in cross section. The solubility of rare earth pentaphosphates changes as the decreasing effective ionic radius of the rare earth ion. By increasing the growth temperature with decreasing ionic size, crystals of other rare earth pentaphosphates can be grown in similar quality and size. Since past problems with crystal growth have been an important limitation to the commercial application of stoichiometric laser materials, this ability to grow such large size, high quality crystals represents a significant advance in the field.

During the past year our major experimental effort has centered on the study of the optical properties of mixed EuP_5O_{14} and PrP_5O_{14} mixed crystals. Unlike the NdP_5O_{14} system, spectral energy diffusion is quite prominent in each of these types of samples. Results of studies of energy transfer in mixed $Eu_xY_{1-x}P_5O_{14}$ crystals done in collaboration with J. Tuminski are presented below.

Table I. Energy Transfer Characteristics Of Rare Earth Pentaphosphates

$Nd_xLa_{1-x}P_5O_{14}$	no spectral transfer
$Pr_xLa_{1-x}P_5O_{14}$	weak spectral transfer
$Eu_xY_{1-x}P_5O_{14}$	strong spectral transfer

Time resolved site-selection spectroscopy techniques were used to study energy transfer in pure EuP_5O_{14} and mixed $Eu_xY_{1-x}P_5O_{14}$ samples containing 100% and 1% Eu^{3+} ions. A nitrogen pumped tunable dye laser provides excitation pulses of about 6 ns in duration and less than 0.1 $Å$ in half width. These pulses excite the sample mounted in a cryogenic refrigerator and the signal is detected with a 1-meter monochrometer, a cooled phototube, and a boxcar integrator set to observe the spectrum at a specific time after the laser pulse. The spectra are recorded and analyzed with an LSI-11 computer system.

II. Energy Transfer in $Eu_xY_{1-x}P_5O_{14}$ Crystals.

Figure 2 shows the fluorescence spectrum at 12 K for the 100% sample at short times and long times after the laser pulse. Here we show an expanded region of one of the sets of transitions between the $^5D_0$ and $^7F_2$ levels. The two peaks in the spectra represent the same transition for ions in slightly different crystal field sites. The narrow laser excitation line selectively excites a higher percentage of the ions in the site with the lower transition energy and as time evolves this energy is tranferred to ions in the other type of site. Similar results are obtained at high temperatures and the fluorescent lifetimes for the 100% and 10% samples change only slightly as a function of temperature. The weak temperature dependence of these results indicates that the energy transfer characteristics are associated with resonant interactions and not strongly dependent on phonon assisted processes.

By monitoring the relative integrated fluorescence intensities of the activator and sensitizer, the characteristics of the energy transfer process can be determined. Figure ? shows the time dependence of these fluorescence intensity ratios for the 100% and 10% samples at low temperature. The dashed and dotted lines in the figure represent the best fit to the data with theoretical models discussed below.

A simple rate equation model can be used to interpret these data, the rate equations describing the time evolution of the concentration of excited states of sensitizers n_S and activators n_A are given by

$$dn_S/dt = W_S - \beta_S n_S - k n_S \quad (1)$$

$$dn_A/dt = W_A - \beta_A n_A + k n_S . \quad (2)$$

W_S and W_A represent the excitation rates which are treated as δ-functions while β_S and β_A represent the intrinsic decay rates of the sensitizer and activator ions and k is the energy transfer rate. Here it has been assumed that no back transfer is taking place. By solving Eqs. (1) and (2) the ratio of the concentrations of excited states of activators and sensitizers is obtained as

$$\frac{n_A(t)}{n_S(t)} = \frac{n_A(0)/n_S(0) + \int_0^t k(t') e^{\Delta t - \int_0^{t'} k(t'')dt''} dt'}{e^{\Delta t - \int_0^t k(t')dt'}} \quad ?$$

where $\Delta = \beta_S - \beta_A$. This is proportional to the measured ratio of fluorescence intensities. Several different expressions for the energy transfer rate were used in Eq. ? in attempting to fit the data. However, it was found that the best fit to the data is obtained using an energy transfer rate that varies as t^{-3} power. This is indicative of a single step electric dipole-dipole interaction with the energy rate given by

$$k^3(t) = \frac{3}{2} \pi^{3/2} (R_0^3)^3 N_A \left(\frac{R_0}{t}\right)^6 .$$

Here R_0^3 represents the critical interaction distance. The dashed lines in Fig. ? represent the best fits to the data using Eqs. (3) and (4) and treating R_0^3 and $n_A(0)/n_S(0)$ as adjustable parameters.

Table II: R_0^3 for $Eu_xY_{1-x}P_5O_{14}$

x	r'/x	R_0^3(Å)	R_0^3(Å)	R_0^3 Å
[illegible]	[illegible]	2.5	5.?	?.?
1.0	12	2.5	47.5	6.3

Table II lists the values of R_0^3 obtained as a best fit to the data using this model. For the 10% sample the results are approximately a factor of two larger than the value for R_0^3 determined theoretically from spectral overlap considerations. This discrepancy is probably due simply to the inaccuracies inherent in both the theoretically predicted value and the fitting procedure, and the good fit between theory and experiment shown in Fig. ? indicates that this model is adequate for explaining energy transfer in the 10% sample.

On the other hand a problem arose using this same model to fit the data obtained on the 100% sample. The values for R_0^3 necessary to obtain the best fit are a factor of 20 larger than the theoretically predicted values and are in fact unphysically large for describing interactions between Eu^{3+} ions. Thus, it is necessary to develop a different model for explaining energy transfer in the heavily concentrated sample.

The problem is associated with the fact in deriving the expression for $k^3(t)$ in Eq. ? a lattice continuum approximation is made. While this may be valid in samples with low concentrations of activator ions where most transfer takes place over distances of several lattice constants, it is not appropriate for a sample with 100% active ion occupancy where the discrete structure of the lattice can be quite important. Equation ?) shows the

appropriate expression for the energy transfer rate, taking into account the discrete nature of the lattice

$$W_D(t) = N_a(K) \frac{\sum_{\ell=1}^{K} w(R_\ell) \frac{(R_0^1)^6}{R_\ell^6} e^{-(t/\tau_s^0)(R_0^1/R_\ell)^6}}{\sum_{\ell=1}^{K} w(R_\ell) e^{-(t/\tau_s^0)(R_0^1/R_\ell)^6}} \quad (5)$$

The summations run over the number of lattice spheres considered K and $w(R_\ell)$ represents the probability of occupancy of an activator ion on a given sphere. The expression for this is

$$w(R_\ell) = \sum_{m=0}^{n_\ell} (1-x_a)^{n_\ell - m} x_a^m \frac{n_\ell!}{m!(n_\ell - m)!} \quad (6)$$

where n_ℓ represents the total number of sites on sphere ℓ, and m is the number of sites occupied by an activator ion on the ℓ sphere. x_a is the fractional probability of site occupancy by an activator ion.

We have developed a program which can be run on a microcomputer system such as an LSI-11 on which the actual lattice structure of a given crystal can be entered and the appropriate summation in Eq. (5) performed. The sum is carried out through distances where any additional contribution to the energy transfer rate outside the last lattice sphere considered is less than 1% of the overall transfer rate. The results of this calculation are then used in Eq. (5) and the dotted lines in Fig. 3 represent the best fits to the data, again treating R_0^1 and n_a ($=x_a n_0$) as adjustable parameters. It was necessary to go out to 200 lattice spheres to properly account for the energy transfer in these samples.

The values of R_0^1 obtained from fitting the data with the discrete energy transfer model are shown in Table II. For the lightly doped sample they are only slightly smaller than the values obtained using the continuum lattice model. However, for the 100% sample the values of R_0^1 using this discrete lattice model are significantly smaller than those obtained from fitting the data with the continuum model and are approximately a factor of two larger than the theoretically determined values. This latter discrepancy is again probably simply due to the inherent inaccuracies in both the theoretical estimates and fitting procedures.

III. Summary and Conclusion

In summary we have shown that energy transfer among Eu^{3+} ions in $Eu_xY_{1-x}P_5O_{14}$ crystals is dominated by a single step, electric dipole-dipole interaction. However, a very important observation is that for heavily doped samples it is necessary to account for the discrete structure of the lattice and using the normal continuum approximation leads to unphysical values for the critical interaction distance. Two other attempts have been made to develop energy transfer models accounting for the discrete nature of the lattice. Blasse and van den Eijk[3] derived expressions for luminescence efficiency but not the energy transfer rate and they included only a few lattice spheres in their summation. This is far too small to be useful in treating concentrated materials such as those investigated here. The second approach was by Reber and coworkers[4] and they derived an expression for the energy transfer rate as done here. However, for their probability of occupancy they simply used the fractional probability of a site being an activator, which is a useful approximation only for extremely low concentration of activators, thus, their approach also does not apply to heavily doped materials such as those investigated here.

Acknowledgements

The part of this work carried out at Oklahoma State University was jointly sponsored by the U.S. Army Research Office and the National Science Foundation under Grant No. DMR-8115150.

References

1. R.C. Powell and W.K. Zwicker, Proc. Int. Conf. on LASERS '81, ed. C.B. Collins (STS Press, McLean, VA 1981), p. 359.
2. Th. Förster, Z. Naturforschung 4a, 321 (1949).
3. A.L.W. Stevels and J.A.W. van der Does De Bye, J. Luminescence 18/19, 909 (1979).
4. H. Dornauf and J. Heber, J. Luminescence 22, 1 (1980).

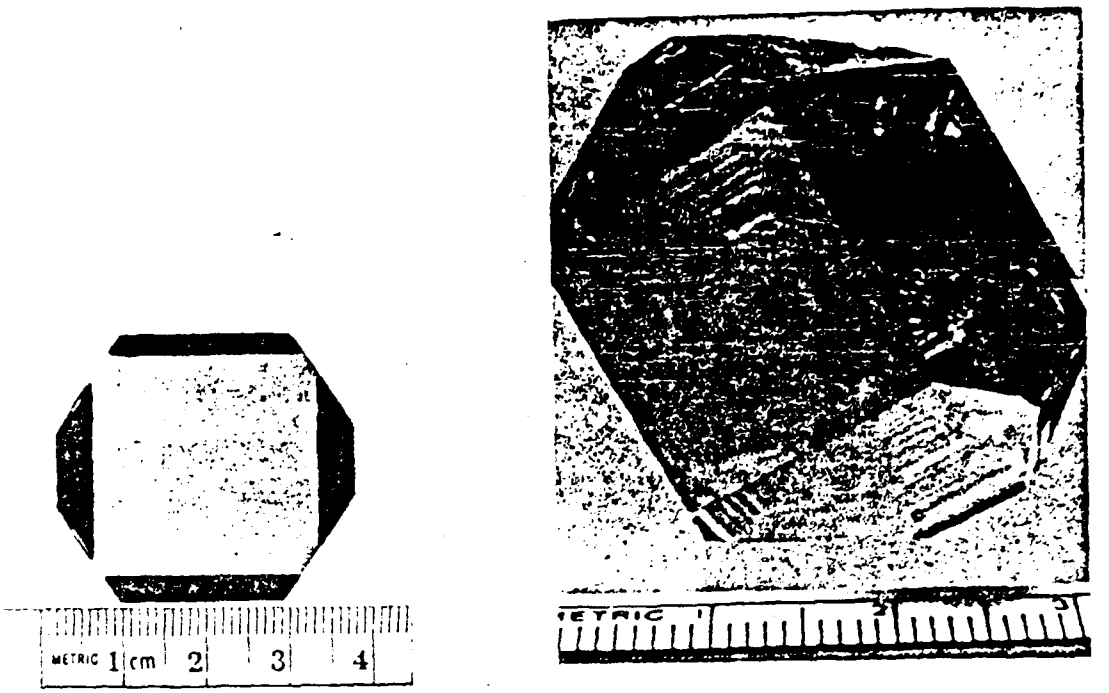

(A) (B)

Fig. 1. (A) NdP_5O_{14} single crystal. (B) PrP_5O_{14} single crystal.

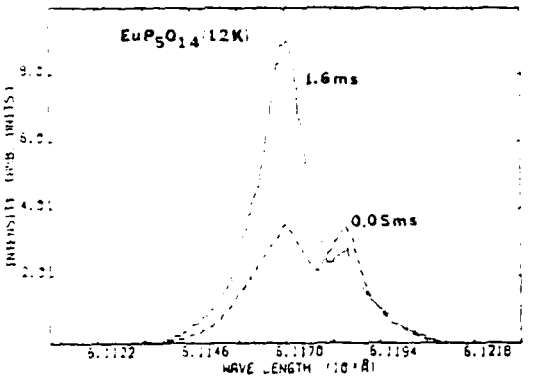

Fig. 2. Fluorescence of one set of $^5D_0 \rightarrow {}^7F_2$ transitions of EuP_5O_{14} at 12K for two times after the excitation pulse.

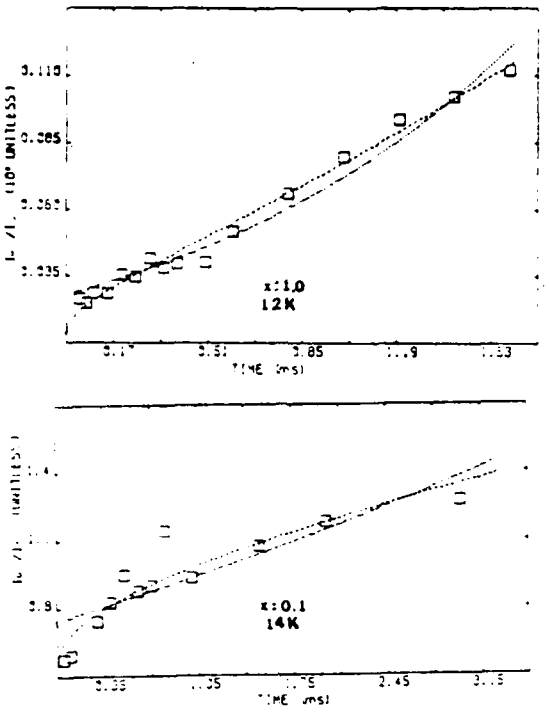

Fig. . Time dependences of the ratios of the integrated fluorescence intensities of the activator and sensitizer transitions for the 100% and 10% samples of $Eu_xY_{1-x}P_5O_{14}$ at low temperatures. (See text for explanation of theoretical lines.)

II.3

Theory of Four Wave Mixing

The four wave mixing process can be thought of as the production and reading out of a holographic index of refraction grating in a non-linear medium. In the four wave mixing configuration generally used to study energy migration, a laser beam is split into two strong "pump" beams of wave vectors $\underset{\sim}{k}_a$ and $\underset{\sim}{k}_b$, and a weaker "probe" beam of wavevector $\underset{\sim}{k}_p$ which counterpropagates against one of the pump beams. The two pump beams establish or "write" the grating and the probe beam "reads" the grating (see Figure IV-1).

The two pump beams interfere in the medium and optical absorption by the active ions creates a spatial distribution of excited states with a sinusoidal pattern of wavevector $\underset{\sim}{k}_g = \underset{\sim}{k}_b - \underset{\sim}{k}_a$. Corresponding to the grating wavevector $\underset{\sim}{k}_g$ is the grating wavelength Λ given by

$$\Lambda = \frac{\lambda}{2 \sin \theta/2}$$

where λ is the laser wavelength and θ is the crossing angle of the two pump beams.

The depth of the grating can then be probed by Bragg diffraction of the probe beam off of the grating. With the probe beam counterpropagating against the second write beam which has wavevector $\underset{\sim}{k}_b$, the Bragg condition requires the Bragg scattered signal beam to have wave vector $\underset{\sim}{k}_s = \underset{\sim}{k}_p + \underset{\sim}{k}_g = - \underset{\sim}{k}_a$, which implies that the signal beam counterpropagate back against the first pump beam.

The theory of FWM has recently been addressed in several papers (36,40-43). Two fundamentally different approaches have been used to model the FWM process.

References (40-42) explicitly consider the non-linear wave equations

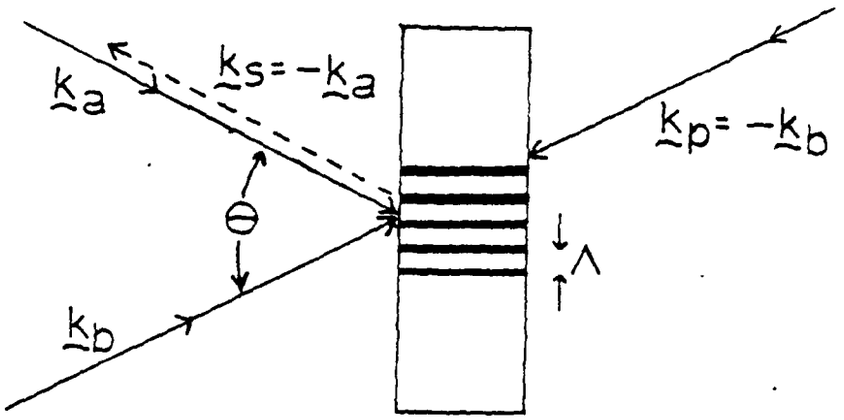

Bragg Condition $\underset{\sim}{k}_s = \underset{\sim}{k}_p + \underset{\sim}{k}_g = -\underset{\sim}{k}_a$

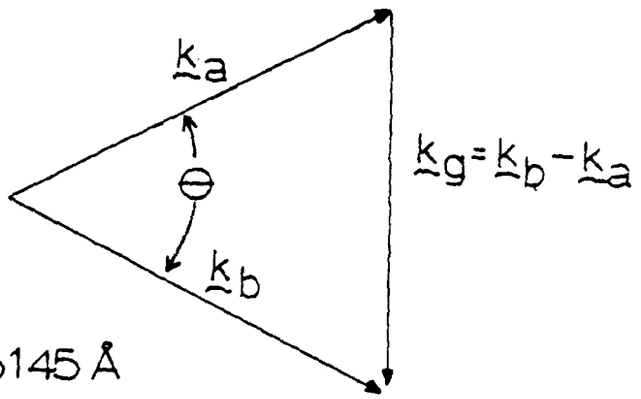

$\lambda = 5145\ \text{Å}$

$$\Lambda = \frac{\lambda}{2\sin(\Theta/2)} \approx \frac{\lambda}{\Theta}$$

Figure IV-1. Four Wave Mixing Wavevector Configuration

where the electric fields are coupled by the non-linear susceptibility in the material. Furthermore, (41) and (42) consider the mechanisms creating this non-linear susceptibility by modeling the system as an ensemble of two and three level atoms, respectively.

References (36,43) model the system in a very different way, where the probe beam Bragg diffracts off of a sinusoidally varying complex index of refraction grating. In this type of development, one assumes a spatially varying susceptibility $\chi(x,y,z)$ which forms a spatially varying holographic grating in the material. This is similar to the approach used by Kogelnik (53). The emphasis in this development is in understanding how the spatial properties (43) or temporal properties (36) of the grating affect the Bragg diffracted signal. However, this approach completely ignores the mechanisms creating the non-linear susceptibility which causes the spatially varying grating.

The approach used by References (41-42) yields important information about how the intrinsic properties of the material affect the steady state scattering efficiency. However, References (41-42) assume that the pump beams are counterpropagating and that the pump beams are exactly phase matched. In the first part of this chapter, the FWM scattering efficiency will be derived when the media is modeled as a two-level system as in Reference (41) but important extensions to the theory will be made. Instead of assuming counterpropagating pump beams, the assumption will be made that the pump beams intersect at crossing angle θ (a more common configuration in FWM energy migration studies). Furthermore, effects arising whenever the pump beams are not exactly phase matched will be explored. Thus the first part of this chapter will give information about how the pump beam properties and intrinsic properties of the material affect the steady state scattering efficiency.

The approach used in Reference (36) is much more useful in studying the temporal properties of the grating decay. In the second part of this chapter, the time evolution of the decay of the signal beam intensity is derived in a manner similar to Reference (36).

The last part of this chapter describes FWM data taken on $Nd_xLa_{1-x}P_5O_{14}$ crystals.

Derivation of Scattering Efficiency

The assumptions will be made that all beams are linearly polarized in the same direction, with the pump beam electric fields given by $E_2(\underline{r},t)$ and $E_4(\underline{r},t)$, the probe beam field as $E_1(\underline{r},t)$, and the Bragg diffracted signal beam field as $E_3(\underline{r},t)$.

If the z axis is taken to be along the pump beam with electric field E_4, then the configuration will be as shown in Figure IV-2.

If one makes the "parametric approximation" that the pump beams are undepleted in the media, then the four electric fields are given as

$$E_1(\underline{r},t) = A_1(z)\ell^{i\omega t - i\underline{k}_1\cdot\underline{r}} \ell^{i\omega t} = \ell^{i\omega t} E_1(\underline{r})$$

$$E_2(\underline{r},t) = A_2\ell^{i\omega t\ i\underline{k}_2\cdot\underline{r}} \ell^{i\omega t} = \ell^{i\omega t} E_2(\underline{r})$$

$$E_3(\underline{r},t) = A_3(z)\ell^{i\omega t - i\underline{k}_3\cdot\underline{r}} \ell^{i\omega t} = \ell^{i\omega t} E_3(\underline{r})$$

$$E_4(\underline{r},t) = A_4\ell^{i\omega t\ i\underline{k}_3\cdot\underline{r}} \ell^{i\omega t} = \ell^{i\omega t} E_4(\underline{r}) .$$

In the configuration used, there is no incident signal beam (i.e., $A_3(L) = 0$) and the signal beam will be much weaker than the probe beam

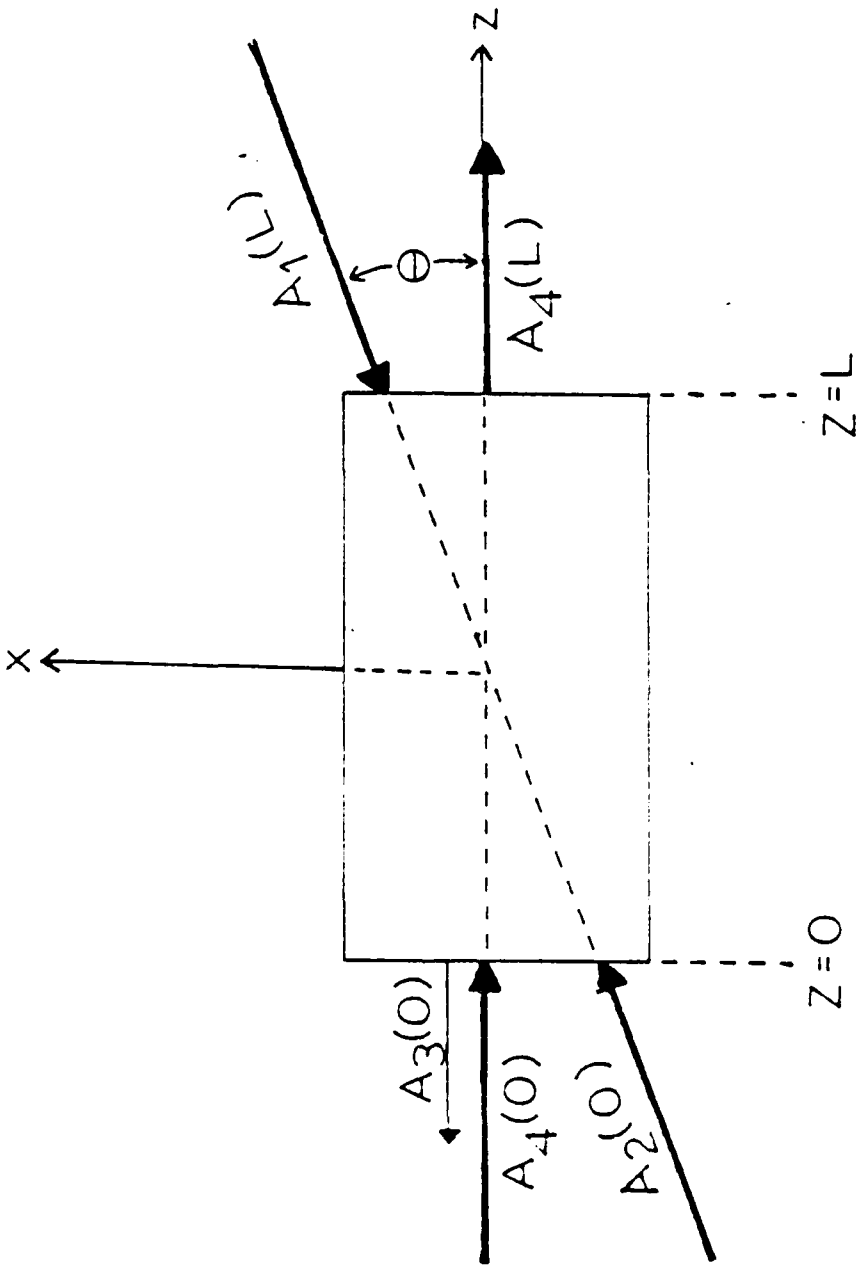

Figure IV-2. Four Wave Mixing Geometry

throughout the material. Since the probe beam is also much weaker than the pump beams,

$$|A_2|^2,\ |A_4|^2 >> |A_1|^2 >> |A_3|^2$$

and thus $|\frac{\Delta E}{E_o}| << 1$ where $E_o = E_2(\underline{r}) + E_4(\underline{r})$ and $\Delta E = E_1(\underline{r}) + E_3(\underline{r})$. The total electric field is then $E(\underline{r},t) = \ell^{i\omega t}(E_o+\Delta E)$.

The wave equation that these fields must obey in the material is

$$\nabla^2 E - \varepsilon_o \mu_o \partial_t^2 E = \mu_o \partial_t^2 P \qquad \text{(IV-1)}$$

where ε_o is the permitivity constant, μ_o is the permeability constant, and P is the polarization. The polarization P may be expressed in terms of the susceptibility χ as

$$P(E) = \varepsilon_o \chi(E) E \ . \qquad \text{(IV-2)}$$

The media can now be modeled as a two-level system. As is shown in Appendix A, the susceptibility for a two-level system is given by

$$\chi(E) = -\frac{2\alpha_o}{k}\left(\frac{i+\delta}{1+\delta^2+|E/E_s|^2}\right) \qquad \text{(IV-3)}$$

where δ is the normalized detuning from line center, $|E_s|^2$ is the saturation intensity, and α_o is the line center small-signal field attenuation coefficient.

Using $|\frac{\Delta E}{E_o}| << 1$, one can expand $\chi(E)$ and P(E) about E_o to first order in $|\frac{\Delta E}{E_o}|$ to obtain

$$\chi(E_o+\Delta E) = \chi(E_o)\left\{1 - \frac{(E_o \Delta E^* + E_o^* \Delta E)}{|E_s|^2(1+\delta^2)+|E_o|^2}\right\} \qquad \text{(IV-4)}$$

The polarization is given by (IV-2), and if one defines $I_s \equiv |E_s|^2(1+\delta^2)$, then to first order in $|\Delta E/E_o|$,

$$P(E_o+\Delta E) = \ell^{i\omega t}\varepsilon_o\chi(E_o)\left\{E_o+\Delta E - \frac{(E_o^2\Delta E^* + |E_o|^2\Delta E)}{I_s + |E_o|^2}\right\} . \qquad \text{(IV-5)}$$

Since $k^2 = |\underset{\sim}{k}_1|^2 = |\underset{\sim}{k}_3|^2$, the driving term $\mu_o\partial_t^2 P$ for Equation (IV-1) can be written as

$$\mu_o\partial_t^2 P = -k^2\ell^{i\omega t}\chi(E_o)\left\{E_o+\Delta E - \frac{(E_o^2\Delta E^* + |E_o|^2\Delta E)}{I_s + |E_o|^2}\right\} . \qquad \text{(IV-6)}$$

The left hand side of Equation (IV-1) now must be calculated.

The slowly varying envelope approximation,

$$\left|\frac{d^2A_i}{dz^2}\right| << \left|k\frac{dA_i}{dz}\right| \quad i = 1,3$$

implies that the field amplitude variation due to non-linear coupling is small over a wavelength.

E_1 and E_3 can be expressed as $E_1 = A_1(z)\ell^{i(k\cos\theta z + k\sin\theta z)}$

$$E_3 = A_3(z)\ell^{ikz}$$

so using the slowly varying envelope approximation,

$$\nabla^2 E - \varepsilon_o\mu_o\partial_t^2 E = 2ik\ell^{i\omega t}\left(\cos\theta\,\ell^{-ik_1\cdot\xi}\,\partial_z A_1(z) + \ell^{-ik_3\cdot\xi}\,\partial_z A_3(z)\right) . \qquad \text{(IV-7)}$$

Combining (IV-6) and (IV-7), the wave Equation (IV-1) becomes

$$2i\left(\cos\theta\,\ell^{-ik_1\cdot\xi}\,\partial_z A_1(z) + \ell^{-ik_3\cdot\xi}\,\partial_z A_3(z)\right) = -k\chi(E_o)$$

$$\{E_o + \Delta E - \frac{[E_o^2 \Delta E^* + |E_o|^2 \Delta E]}{I_s + |E_o|^2}\} . \qquad \text{(IV-8)}$$

One may write out $|E_o|^2$ as

$$|E_o|^2 = |A_2|^2 + |A_4|^2 + A_2 A_4^* e^{i(k_1 - k_3)\cdot r} + A_2^* A_4 e^{-i(k_1 - k_3)\cdot r} .$$

The intensities of the pump beams are given by $I_2 = |A_2|^2$ and $I_4 = |A_4|^2$, so if one defines

$$\zeta \equiv A_2 A_4^* e^{i(k_1 - k_3)\cdot r} ,$$

then

$$|E_o|^2 = I_2 + I_4 + \zeta + \zeta^* .$$

Along the z axis, ζ is given by $\zeta(z) = A_2 A_4^* e^{ik(1-\cos\theta)z}$, so $\zeta(z)$ oscillates with z with oscillation wavelength $\lambda_{os} = \frac{\lambda}{1-\cos\theta}$, and thus $E_o|^2$ has an interference term that oscillates with z with oscillation wavelength λ_{os}.

The only terms of interest on the right hand side of (IV-8) are those that satisfy the phase matching condition; i.e., those terms that synchronously drive $\nabla^2 E - \varepsilon_o \mu_o \partial_t^2 E$ as either $e^{i(\omega t - k_3 \cdot r)}$ or $e^{i(\omega t - k_1 \cdot r)}$.

Rewriting (IV-8) and numbering the terms, (IV-8) becomes

$$[\cos\theta e^{-ik_1 \cdot r} \partial_z A_1(z) + e^{-ik_3 \cdot r} \partial_z A_3(z)] = \qquad \text{(IV-9)}$$

$$\kappa_o |E_o|^2 (1-i\delta) \{ \underbrace{\frac{E_o}{I_s + |E_o|^2}}_{\text{term (i)}} + \underbrace{\frac{\Delta E}{I_s + |E_o|^2}}_{\text{term (ii)}}$$

$$- \frac{E_o^2 \Delta E^*}{(I_s + |E_o|^2)^2} - \frac{|E_o|^2 \Delta E}{(I_s + |E_o|^2)^2} \Big\} . \qquad \text{(IV-9)}$$

term (iii) term (iv)

Terms (i), (ii), (iii), and (iv) must now each in turn be examined to determine which of these satisfy the phase matching condition.

Since $E_o = A_2 e^{ik_1 \cdot r} + A_4 e^{ik_3 \cdot r}$, term (i) is clearly not synchronous with the left hand side of (IV-9) and thus term (i) is not phase matched.

Since $\Delta E = A_1(z) e^{-ik_1 \cdot r} + A_3(z) e^{-ik_3 \cdot r}$, term (ii) clearly is phase matched although the amplitude of this term will be modulated by the oscillatory behavior of $|E_o|^2$ which appears in the denominator.

E_o^2 may be written explicitly as

$$E_o^2 = A_2^2 e^{2ik_1 \cdot r} + A_4^2 e^{2ik_3 \cdot r} + 2A_2A_4 e^{i(k_1+k_3) \cdot r}$$

and ΔE^* may be written out explicitly as $\Delta E^* = A_1^*(z) e^{-ik_1 \cdot r} + A_3^* e^{-ik_3 \cdot r}$ thus

$$E_o^2 \Delta E^* = \{A_1^* A_2^2 e^{3ik_1 \cdot r} + A_3^* A_2^2 e^{i(2k_1+k_3) \cdot r}$$

$$+ A_1^* A_4^2 e^{i(2k_3-k_1) \cdot r} + A_3^* A_4^2 e^{3ik_3 \cdot r}$$

$$+ 2A_1^* A_2 A_4 e^{i(2k_1+k_3) \cdot r} + 2A_3^* A_2 A_4 e^{i(2k_3+k_1) \cdot r} \} .$$

Since none of these terms are synchronous with the left hand side of (IV-9), term (iii) is not phase matched.

Term (iv) may be explicitly written out as

$$- \frac{|E_o|^2 \Delta E}{(I_s + |E_o|^2)^2} = - (I_s + |E_o|^2)^{-2} \{(I_2 + I_4)\Delta E$$

$$+ A_1 A_2 A_4^* \ell^{-i\underline{k}_3 \cdot \underline{r}} + A_3 A_2^* A_4 \ell^{-i\underline{k}_1 \cdot \underline{r}}$$

$$+ [(A_2^* A_4 \ell^{-i(\underline{k}_1 - \underline{k}_3)\cdot \underline{r}}) A_1 \ell^{-i\underline{k}_1 \cdot \underline{r}}]$$

$$+ [(A_2 A_4^* \ell^{i(\underline{k}_1 - \underline{k}_3)\cdot \underline{r}}) A_3 \ell^{-i\underline{k}_3 \cdot \underline{r}}]\} .$$

The first three terms in this expression are obviously phase matched although they are modulated by $(I_s + |E_o|^2)^{-2}$.

The last 2 terms in square brackets must be looked at more closely. The fourth term is

$$- [\frac{(A_2^* A_4 \ell^{-i(\underline{k}_1 - \underline{k}_3)\cdot \underline{r}})}{(I_s + |E_o|^2)^2}] A_1 \ell^{-i\underline{k}_1 \cdot \underline{r}}$$

The quantity above in the square bracket can be thought of as modulating the phase matched term $A_1 \ell^{-i\underline{k}_1 \cdot \underline{r}}$.

Notice that since the exponent in the square bracket above has the same fourier component as the oscillatory part of $|E_o|^2$, this term will not necessarily average to zero.

Similarly, the last term on the right hand side of the expression for

$$- \frac{|E_o|^2 \Delta E}{(I_s + |E_o|^2)^2}$$

is

$$- \left[\frac{(A_2A_4^* e^{i(k_1-k_3)\cdot r}}{(I_s + |E_o|^2)^2}\right]A_3 e^{-ik_3\cdot r} .$$

The quantity in this square bracket modulates the phase matched term $A_3 e^{-ik_3\cdot r}$, and the exponent in the square bracket has the same fourier component as the oscillatory portion of $|E_o|^2$, so this term also will not necessarily average to zero.

Equation (IV-9) may therefore be rewritten as

$$[\cos\theta e^{-ik_1\cdot r} \partial_z A_1(z) + e^{-ik_3\cdot r} \partial_z A_3(z)] =$$

$$\frac{\alpha_o |E_s|^2 (1-i\delta)}{(I_s + |E_o|^2)^2} \{(I_s + |E_o|^2)(A_1 e^{-ik_1\cdot r} + A_3 e^{-ik_3\cdot r})$$

$$- (I_2 + I_4) A_1 e^{-ik_1\cdot r} + A_3 e^{-ik_3\cdot r}) \qquad \text{(IV-10)}$$

$$- A_1 A_2 A_4^* e^{-ik_3\cdot r} - A_3 A_2^* A_4 e^{-ik_1\cdot r}$$

$$- A^* A_1 e^{-ik_1\cdot r} - A A_3 e^{-ik_3\cdot r}) .$$

The terms with $e^{-ik_1\cdot r}$ behavior are

$$\cos\theta\, \partial_z A_1(z) = \frac{\alpha_o |E_s|^2 (1-i\delta)}{(I_s + |E_o|^2)^2} \{[I_s + I(z)] A_1(z) - A_2^* A_4 A_3(z)\}. \qquad \text{(IV-11)}$$

But the signal beam $A_3(z)$ will be much weaker than the probe beam $A_1(z)$, and since

$$\frac{|A_2^* A_4|}{|I_s + \zeta|} \leq 1,$$

one can neglect the last term in (IV-11) to obtain

$$\cos\theta \, \partial_z A_1(z) = \frac{\alpha_o |E_s|^2 (1-i\delta)}{(I_s + |E_o|^2)^2} \{(I_s + \zeta(z)) A_1(z)\} \qquad \text{(IV-12)}$$

and the terms from (IV-10) with $e^{-ik_3 \cdot \xi}$ dependence are

$$\partial_z A_3(z) = \frac{\alpha_o |E_s|^2 (1-i\delta)}{(I_s + |E_o|^2)^2} \{(I_s + \zeta^*(z)) A_3(z) - A_2 A_4^* A_1(z)\}. \qquad \text{(IV-13)}$$

Equations (IV-12) and (IV-13) describe the non-linear interactions in the media.

Along the z axis, $\zeta(z)$ and $\zeta^*(z)$ may be written

$$\zeta(z) = A_2 A_4^* e^{ik(1-\cos\theta)z}$$

$$\zeta^*(z) = A_2^* A_4 e^{-ik(1-\cos\theta)z}.$$

Now define phases ϕ_2 and ϕ_4 as

$$\phi_2 \equiv \arctan\left(\frac{\mathrm{Im}(A_2)}{\mathrm{Re}\, A_2}\right) \qquad \text{(IV-14)}$$

$$\phi_4 \equiv \arctan\left(\frac{\mathrm{Im}(A_4)}{\mathrm{Re}\, A_4}\right) \qquad \text{(IV-15)}$$

where $\mathrm{Re}(x) = \frac{x+x^*}{2}$, $\mathrm{Im}(x) = \frac{x-x^*}{2i}$; then

$$A_2 = |A_2| e^{i\phi_2}$$

$$A_4 = |A_4| e^{i\phi_4} .$$

The phase mismatch of the two pump beams Δ is given as $\Delta = \phi_2 - \phi_4$ and $\zeta(z)$ and $\zeta^*(z)$ become

$$\zeta(z) = |A_2 A_4| e^{i(k(1-\cos\theta)z+\Delta)} \qquad \text{(IV-16)}$$

$$\zeta^*(z) = |A_2 A_4| e^{-i(k(1-\cos\theta)z+\Delta)} . \qquad \text{(IV-17)}$$

The oscillatory behavior of $|E_o|^2$ can be shown more explicitly by defining the parameters

$$D_o \equiv I_s + I_2 + I_4$$

and

$$a \equiv |A_2 A_4| .$$

Equations (IV-12) and (IV-13) can then be expressed as

$$\partial_z A_3(z) = \alpha_o |E_s|^2 (1-i\delta) \left\{ \frac{[I_s + a e^{-i[k(1-\cos\theta)z+\Delta]}] A_3(z)}{[D_o + 2a\cos(k(1-\cos\theta)z+\Delta)]^2} - \frac{(a e^{i\Delta}) A_1(z)}{[D_o + 2a\cos(k(1-\cos\theta)z+\Delta)]^2} \right\} \qquad \text{(IV-18)}$$

$$\partial_z A_1(z) = \frac{\alpha_o |E_s|^2 (1-i\delta)}{\cos\theta} \left\{ \frac{[I_s + a e^{i[k(1-\cos\theta)z+\Delta]}] A_1(z)}{[D_o + 2a\cos(k(1-\cos\theta)z+\Delta)]^2} \right\} . \qquad \text{(IV-19)}$$

These equations can be simplified somewhat by defining β as

$$\beta = k(1-\cos\theta) .$$

Equations (IV-18) and (IV-19) may then be expressed as

$$\partial_z A_1(z) + P(z)A_1(z) = 0 \qquad \text{(IV-20)}$$

and

$$\partial_z A_3(z) + P(z)A_3(z) = Q(z) \qquad \text{(IV-21)}$$

where

$$P(z) = -\frac{\alpha_o |E_s|^2 (1-i\delta)}{\cos\theta} \left\{\frac{\left[I_s + a\ell^{i(\beta z+\Delta)}\right]}{\left[D_o+2a\cos(\beta z+\Delta)\right]^2}\right\} \qquad \text{(IV-22)}$$

and

$$P(z) = -\alpha_o |E_s|^2 (1-i\delta) \left\{\frac{I_s - a\ell^{-i(\beta z+\Delta)}}{\left[D_o+2a\cos(\beta z+\Delta)\right]^2}\right\} \qquad \text{(IV-23)}$$

and

$$Q(z) = -\frac{\alpha_o |E_s|^2 (1-i\delta) a\ell^{i\Delta} A_1(z)}{\left[D_o+2a\cos(\beta z+\Delta)\right]^2} . \qquad \text{(IV-24)}$$

The solutions to (IV-20) and (IV-21) fall into 2 categories, depending on whether or not $\zeta(z)$ and $\zeta^*(z)$ oscillate very rapidly over distances where $A_1(z)$ and $A_3(z)$ change appreciably.

Case I (θ is Not Small)

If θ is not small then $A_1(z)$ and $A_3(z)$ do not change appreciably over

$$\lambda_{os} = \frac{\lambda}{1-\cos\vartheta} .$$

Since for Case I $\zeta(z)$ and $\zeta^*(z)$ oscillate many times over distances where $A_1(z)$ and $A_3(z)$ change significantly, the quantities $P(z)$, $\bar{P}(z)$, and $\zeta(z)$ can be averaged over an oscillation wavelength λ_{os}.

$$\langle P(z)\rangle = -\frac{\alpha_o|E_s|^2(1-i\delta)}{\cos\vartheta}\left(\frac{1}{\lambda_{os}}\right)\int_o^{\lambda_{os}} dz\left\{\frac{I_s+a\cos\beta z+ia\sin\beta z}{(D_o+2a\cos\beta z)^2}\right\}$$

$$\langle P(z)\rangle = -\frac{\alpha_o|E_s|^2(1-i\delta)}{2\pi\cos\vartheta}\int_o^{2\pi} du\left\{\frac{I_s+a\cos u+ia\sin u}{(D_o+2a\cos u)^2}\right\}$$

$$\langle P(z)\rangle = -\frac{\alpha_o|E_s|^2(1-i\delta)}{\pi\cos\vartheta}\left\{I_s\int_o^{\pi}\frac{du}{(D_o+2a\cos u)^2} + a\int_o^{\pi}\frac{\cos u\,du}{(D_o+2a\cos u)^2}\right\}$$

$$\langle P(z)\rangle = -\frac{\alpha_o|E_s|^2(1-i\delta)}{\cos\vartheta}\left\{\frac{D_o I_s-2a^2}{(D_o^2-4a^2)^{3/2}}\right\} .$$

The complex absorption coefficient ξ can be defined as

$$\xi \equiv -\cos\theta\,\langle P(z)\rangle$$

or

$$\xi = \alpha_o|E_s|^2(1-i\delta)\left\{\frac{D_o I_s-2a^2}{(D_o^2-4a^2)^{3/2}}\right\} . \qquad \text{(IV-25)}$$

Equation (IV-20) can then be approximated as

$$\partial_z A_1(z) + \langle P(z)\rangle A_1(z) = 0$$

or

$$\partial_z A_1(z) - \xi \sec\theta A_1(z) = 0$$

which has solution

$$A_1(z) = A_1(L)e^{\xi\sec\theta(z-L)} \qquad (IV-26)$$

where $A_1(L)$ is the incident probe beam amplitude.

One sees from comparing (IV-22) to (IV-23) that

$$\langle P(z)\rangle = \cos\theta \langle P'(z)\rangle$$

$$\langle P(z)\rangle = -\xi \qquad (IV-27)$$

and (IV-21) may be approximated as

$$\partial_z A_3(z) - \xi A_3(z) = \langle Q(z)\rangle . \qquad (IV-28)$$

Remembering that $A_1(z)$ varies slowly over a distance ℓ_{ss}, one can use (IV-24) to obtain

$$\langle Q(z)\rangle = -\chi_0|E_s|^2(1-i\delta)a^2\ell^{2\xi}A_1(z)\int_0^\pi (D_0+2a\cos u)^{-2}du$$

$$\langle Q(z)\rangle = -\frac{\chi_0|E_s|^2(1-i\delta)a^2\ell^{2\xi}A_1(z)}{\pi}\int_0^\pi (D_0+2a\cos u)^{-2}du$$

$$\langle Q(z)\rangle = -\chi_0|E_s|^2(1-i\delta)a^2\ell^{2\xi}A_1(z)\left(\frac{D_0}{(D_0^2-4a^2)^{3/2}}\right).$$

One can simplify (IV-28) by defining

$$\gamma \equiv -\chi_0|E_s|^2(1-i\delta)a^2\ell^{2\xi}\left(\frac{D_0}{(D_0^2-4a^2)^{3/2}}\right)$$

so (IV-28) becomes

$$\partial_z A_3(z) - \xi A_3(z) = \rho A_1(L) e^{\xi \sec\theta (z-L)} . \qquad \text{(IV-29)}$$

Using the boundary condition that there is no incident signal beam, i.e., $A_3(0) = 0$, the solution to (IV-29) is

$$A_3(z) = \frac{\rho A_1(L)}{\xi(\sec\theta - 1)} \left\{ e^{\xi \sec\theta (z-L)} - e^{\xi (z-L)} \right\} . \qquad \text{(IV-30)}$$

One quantity of interest is the signal beam intensity as it exists the media $|A_3(0)|^2$, since this is an experimentally measurable quantity.

$$|A_3(0)|^2 = |\rho/\xi|^2 \frac{|A_1(L)|^2}{(\sec\theta - 1)^2} \left\{ e^{-2\xi_R L} + e^{-2\xi_R \sec\theta L} \right.$$

$$\left. - 2e^{-\xi_R (1+\sec\theta) L} \cos[\xi_i (1-\sec\theta) L] \right\} \qquad \text{(IV-31)}$$

where $\xi_R = \frac{\xi + \xi^*}{2}$, or

$$\xi_R = \frac{a_o}{(1+\delta^2)} \left\{ \frac{(1 + \frac{I_2}{I_s} + \frac{I_4}{I_s}) - \frac{2I_2 I_4}{I_s^2}}{\left[(1 + \frac{I_2}{I_s} + \frac{I_4}{I_s})^2 - \frac{4I_2 I_4}{I_s^2}\right]^{3/2}} \right\} \qquad \text{(IV-32)}$$

and

$$\xi_i = \frac{\xi - \xi^*}{2i} = -\delta \xi_R \qquad \text{(IV-33)}$$

and

$$|\frac{\rho}{\xi}|^2 = \frac{D_o^2 a^2}{(D_o I_s - 2a^2)^2}$$

or

$$\left|\frac{\beta}{\xi}\right|^2 = \frac{\left(\frac{I_2 I_4}{I_s^2}\right)\left(1 + \frac{I_2}{I_s} + \frac{I_4}{I_s}\right)^2}{\left[\left(1 + \frac{I_2}{I_s} + \frac{I_4}{I_s}\right) - \frac{2I_2 I_4}{I_s^2}\right]^2} \quad . \tag{IV-34}$$

Thus (IV-31) may be written as

$$|A_3(0)|^2 = \left\{\frac{\left(\frac{I_2 I_4}{I_s^2}\right)\left(1 + \frac{I_2}{I_s} + \frac{I_4}{I_s}\right)^2}{\left[\left(1 + \frac{I_2}{I_s} + \frac{I_4}{I_s}\right) - \frac{2I_2 I_4}{I_s^2}\right]^2}\right\} \times \left\{\frac{|A_1(L)|^2}{(\sec\theta - 1)^2}\right\} \tag{IV-35}$$

$$\times \left\{e^{-2\xi_R L} + e^{-2\xi_R \sec\theta L} - 2e^{-\xi_R(1+\sec\theta)L} \cos[\xi_i(1-\sec\theta)L]\right\}$$

where ξ_R and ξ_i are given explicitly by (IV-32) and (IV-33). Normally in a degenerate FWM experiment the two pump beams and the probe beam are obtained by splitting one laser beam into three parts. When this is the case, one sees from (IV-35) that the output Bragg diffracted signal beam intensity will vary as the cube of the laser power.

A good measure of the "scattering efficiency" η of the four wave mixing process is the ratio of the exiting signal beam $|A_3(0)|^2$ to the exiting probe beam in the absence of the pump beam interactions.

Using (IV-25) and (IV-26), one obtains

$$|A_1(0)|^2_{E_0=0} = |A_1(I)|^2 e^{-\left|\frac{2\alpha_0}{1+\delta^2}\right|L} \quad .$$

So the scattering efficiency η is given by

$$\eta = \left\{ \frac{(\frac{I_2 I_4}{I_s^2})(1 + \frac{I_2}{I_s} + \frac{I_4}{I_s})^2}{[(1 + \frac{I_2}{I_s} + \frac{I_4}{I_s}) - \frac{2I_2 I_4}{I_s^2}]^2} \right\} \left[\frac{2\alpha_o L}{\ell^{1+\delta^2}} \right] \frac{1}{(\sec\vartheta - 1)^2} \left\{ \ell^{-2\xi_R L} + \ell^{-2\xi_R \sec\vartheta L} \right.$$

$$\left. - 2\ell^{-\xi_R(1+\sec\vartheta)L} \cos[\xi_I(1-\sec\vartheta)L] \right) . \qquad \text{(IV-36)}$$

The dependence of the scattering efficiency η on crossing angle ϑ can be clarified somewhat whenever $|\xi L(1-\sec\vartheta)|$ is small.

This will usually be true since the experiment does not work well if:

(i) $|\xi L|$ is large since if $|\xi L|$ is large the beams are essentially extinguished in the crystal.

(ii) ϑ is very large since the output Bragg diffracted signal beam intensity decreases with increasing ϑ.

Thus if $|\xi L(1-\sec\vartheta)|$ is small, then to first order in $|\xi L(1-\sec\vartheta)|$, (IV-36) becomes

$$\eta = |\rho|^2 L^2 \ell^{-2\xi_R L} \frac{2\alpha_o L}{\ell 1+\delta^2} (1 + \xi_R L(1-\sec\vartheta)) \qquad \text{(IV-37)}$$

where

$$|\rho|^2 = (\frac{\alpha_o^2 I_s^2}{1+\delta^2}) \{\frac{a^2 D_o^2}{(D_o^2 - 4a^2)^3}\}$$

or

$$|\rho|^2 = \frac{\alpha_o^2}{1+\delta^2} \left\{ \frac{(\frac{I_2 I_4}{I_s^2})(1 + \frac{I_2+I_4}{I_s})^2}{[(1 + \frac{I_2+I_4}{I_s})^2 - \frac{4I_2I_4}{I_s^2}]^3} \right\} .$$

Equation (IV-37) shows that the scattering efficiency η decreases with increasing crossing angle θ.*

It is now of interest to calculate the scattering efficiency η when the pump intensity is well below saturation intensity, i.e., when $|\frac{I_1 + I_2}{I_s}| << 1$.

Assuming that $|\frac{I_2 + I_4}{I_s}| << 1$, then to first order in $\frac{(I_2 - I_4)}{I_s}$, $|\rho|^2$ and ξ_R become

$$|\rho|^2 = \frac{\alpha_o^2}{1+\delta^2} (\frac{I_2 I_4}{I_s^2})(1 - \frac{4(I_2+I_4)}{I_s})$$

and

$$\xi_R = \frac{\alpha_o}{1+\delta^2} (1 - 2 \frac{(I_2 + I_4)}{I_s})$$

so that (IV-37) becomes

$$\eta = (\frac{\alpha_o^2 L^2}{1+\delta^2})(\frac{I_2 I_4}{I_s^2})[1 + \frac{4(I_2+I_4)}{I_s} (\frac{\alpha_o L}{1+\delta^2} - 1)] \qquad \text{(IV-38)}$$

---

*In thick samples, there will be another effect that will decrease the output signal intensity with increasing crossing angle θ. In thick samples, as θ is increased, the beam overlap volume in the sample may decrease, which is not taken into account in this development.

$$\times \left[1 + \frac{\alpha_o L}{1+\delta^2}\left(1 - \frac{2(I_2+I_4)}{I_s}\right)\right.$$

$$\left. \times \quad (1-\sec\theta)\right]\}. \qquad \text{(IV-38)}$$

To lowest order in $\frac{(I_2 + I_4)}{I_s}$, (IV-38) becomes

$$\eta_{\substack{\text{well below} \\ \text{saturation}}} = \frac{\alpha_o^2 L^2}{1+\delta^2}\left(\frac{I_2 I_4}{I_s^2}\right)\left(1 + \frac{\alpha_o L}{1+\delta^2}(1-\sec\theta)\right) . \qquad \text{(IV-39)}$$

Experimentally, one usually works with crossing angles large enough that Case I applies and Equation (IV-36), (IV-37), or (IV-39) will be applicable. However, it is of interest to derive the scattering efficiency for very small angles in certain limiting cases to discover what new effects should be expected at very small crossing angles.

Case II (θ is Small)

If θ is very small, then $A_1(z)$ and $A_3(z)$ do change appreciably over $\lambda_{os} = \frac{\lambda}{1-\cos\theta}$; and thus $P(z)$, $\bar{P}(z)$, and $Q(z)$ cannot be averaged over λ_{os}.

Equations (IV-20) and (IV-21) cannot be solved for exactly in this case, since $P(z)$, $\bar{P}(z)$, and $Q(z)$ cannot be averaged.

Equations (IV-20) and (IV-21) will be approximately solved for in the case where the pump beams are well below saturation intensity, i.e., for the case that $\frac{a}{I_s}$ is small.

One can now define α as

$$\alpha = \frac{\alpha_o(1-i\delta)}{(1+\delta^2)}\left(1 + \frac{I_2 + I_4}{I_s}\right)^{-2}$$

and to first order in $\frac{a}{I_s}$; (IV-22) becomes

$$P(z) = -\alpha\{1 - \frac{3a}{I_s}\cos(\beta z+\Delta) + \frac{ia}{I_s}\sin(\beta z+\Delta)\} . \qquad (IV-40)$$

The solution to Equation (IV-20) is then

$$A_1(z) = C_1 \exp\{\alpha z - \frac{3a}{\beta I_s}\sin(\beta z+\Delta) - \frac{ia}{\beta I_s}\cos(\beta z+\Delta)\} \qquad (IV-41)$$

C_1 is a constant which is determined from boundary conditions to be given by

$$C_1 = A_1(L)\exp\{-\alpha[L - \frac{3a}{\beta I_s}\sin(\beta L+\Delta) - \frac{ia}{\beta I_s}\cos(\beta L+\Delta)]\} . \qquad (IV-42)$$

Equation (IV-41) then becomes

$$A_1(z) = A_1(L)\exp\{\alpha(z-L) - \frac{2\alpha a}{\beta I_s}[3\sin(\frac{\beta(z-L)}{2})\cos(\frac{\beta(z+L)}{2}+\Delta) - i\sin(\frac{\beta(z+L)}{2}+\Delta)\sin(\frac{\beta(z-L)}{2})]\} . \qquad (IV-43)$$

To first order in a/I_s, Equation (IV-24) becomes

$$P(z) = -\alpha^{1/3}(\frac{a}{I_s})A_1(z)(1 - \frac{4a}{I_s}\cos(\beta z+\Delta)) \qquad (IV-44)$$

and since $|A_3(z)| \ll |A_1(z)|$, $P(z)$ may be approximated as $P(z) = -\alpha$ so that Equation (IV-21) may be approximated as

$$\frac{1}{2}A_3(z) - \alpha A_3(z) = P(z) \qquad (IV-45)$$

with solution

$$A_3(z) = e^{\alpha z} C_2 + \int \beta(z) e^{-\alpha z} dz)$$

or

$$A_3(z) = C_2 e^{\alpha z} - \frac{\alpha \beta^{1/2} e^{\alpha z} C_1}{I_s} \int dz' \left(1 - \frac{4a}{I_s} \cos(\delta z + \phi)\right)$$

$$\times \exp\left[-\frac{4a}{\delta I_s}(\beta \sin(\delta z+\phi) + \alpha \cos(\delta z+\phi))\right] \qquad \text{IV-47}$$

where C_1 is given by (IV-42) and C_2 is a constant that remains to be determined using boundary conditions.

To perform the integration indicated in Equation (IV-46), one needs to expand the exponent inside the integral in powers of a/I_s. Since the factor a/I_s in the exponent is multiplied by a factor of α/β, it is important to briefly examine magnitude of α/β to be sure that it is not large. This parameter can be rewritten as

$$\frac{\alpha}{\beta} = \frac{\alpha L}{\beta L} = \frac{\alpha L}{k(1-\cos\theta)L} .$$

The beams are approximately attenuated as $e^{-\alpha L}$ as they pass through the crystal, so $|\alpha L|$ must be of order unity or smaller or else the beams are so severely attenuated through the crystal that the Bragg diffracted signal beam will be negligible.

Furthermore, $|k(1-\cos\theta)L|$ will be ≥ 1 for typical sample dimensions unless than angle is too small to be experimentally realizable.

Thus taking $|\alpha/\beta| \leq 1$ will be a good assumption for almost any meaningful experimental configuration.

Expanding the exponent inside the integral from Equation (IV-46) and keeping terms first order in a/I_s, (IV-46) becomes

$$A_3(z) = C_2 e^{\alpha z} - \frac{\alpha e^{i\Delta} e^{\alpha z} a C_1}{I_s} \int dz \{1 - \frac{3a\alpha}{\beta I_s} \sin(\beta z+\Delta)$$

$$- \frac{a}{I_s} (4 + \frac{i\alpha}{\beta}) \cos(\beta z+\Delta) \}. \qquad \text{(IV-47)}$$

Performing the integration, this becomes

$$A_3(z) = C_2 e^{\alpha z} - \frac{\alpha e^{i\Delta} e^{\alpha z} a C_1}{I_s} \{z + \frac{3a\alpha}{\beta^2 I_s} \cos(\beta z+\Delta) - \frac{a}{\beta I_s} (4 + \frac{i\alpha}{\beta}) \sin(\beta z+\Delta) \}.$$

(IV-48)

One can use the boundary condition $A_3(L) = 0$ to obtain

$$C_2 = \frac{\alpha e^{i\Delta} a C_1}{I_s} [L + \frac{3a\alpha}{\beta^2 I_s} \cos(\beta L+\Delta) - \frac{a}{\beta I_s} (4 + \frac{i\alpha}{\beta}) \sin(\beta L+\Delta)] . \qquad \text{(IV-49)}$$

One can then substitute (IV-49) into (IV-48) to obtain

$$A_3(z) = \frac{\alpha a C_1 e^{i\Delta} e^{\alpha z}}{I_s} \{(L-z) - \frac{3a\alpha}{\beta^2 I_s} [\sin(\frac{\beta(L+z)}{2} + \Delta) \sin(\frac{\beta(L-z)}{2})]$$

$$- \frac{2a}{\beta I_s} (4 + \frac{i\alpha}{\beta}) [\sin(\frac{\beta(L-z)}{2}) \cos(\frac{\beta(L+z)}{2} + \Delta)] \}. \qquad \text{(IV-50)}$$

One can expand (IV-42) to first order in a/I_s to obtain

$$C_2 = A_1(L) e^{-\alpha L} (1 + \frac{a\alpha}{\beta I_s} [3\sin(\beta L+\Delta) + i\cos(\beta L+\Delta)]) \qquad \text{(IV-51)}$$

One can now substitute (IV-51) into (IV-50) to obtain to first order in a/I_s

$$A_3(z) = \frac{\alpha a A_1(L) e^{i\Delta} e^{\alpha(z-L)}}{I_s} \{(L-z) [1 + \frac{a\alpha}{\beta I_s} (3\sin(\beta L+\Delta) + i\cos(\beta L+\Delta)]$$

(IV-52)

$$- \frac{6a\alpha}{\beta^2 I_s}\left[\sin\left(\frac{\beta(L+z)}{2}+\Delta\right)\sin\left(\frac{\beta(L-z)}{2}\right)\right] \qquad \text{(IV-52)}$$

$$- \frac{2a}{\beta I_s}\left(4+\frac{i\alpha}{\beta}\right)\left[\sin\left(\frac{\beta(L-z)}{2}\right)\cos\left(\frac{\beta(L+z)}{2}+\Delta\right)\right]\Big\} .$$

At the output face z = o,

$$A_3(0) = \frac{i\alpha A_1(L)\, e^{\frac{i\alpha}{2}L-\alpha L}}{I_s}\left\{L+\frac{i\alpha L}{\beta I_s}\left(3\sin(\beta L+\Delta)+i\cos(\beta L-\Delta)\right)-\frac{6a\alpha}{\beta^2 I_s}\right.$$

$$\times\left[\sin\left(\frac{\beta L}{2}+\Delta\right)\times\sin\left(\frac{\beta L}{2}\right)\right]-\frac{2a}{\beta I_s}\left(4+\frac{i\alpha}{\beta}\right)\sin\left(\frac{\beta L}{2}\right)\cos\left(\frac{\beta L}{2}+\Delta\right)\Big]\Big\} . \qquad \text{(IV-53)}$$

The output intensity of the Bragg scattered signal beam will be equal to $|A_3(0)|^2$, and to first order in $|a/I_s|$, this is given by

$$|A_3(0)|^2 = L|\alpha_1|^2\left(\frac{I_2 I_4}{I_s^2}\right)|A_1(L)|^2 e^{-2\alpha_R L}\left\{L+\frac{2aL}{\beta I_s}\left[3\alpha_R\sin(\beta L+\Delta)-\alpha_1\cos(\beta L+\Delta)\right]\right.$$

$$- \frac{12a\alpha_R}{\beta^2 I_s}\sin\left(\frac{\beta L}{2}+\Delta\right)\sin\left(\frac{\beta L}{2}\right) \qquad \text{(IV-54)}$$

$$\left.- \frac{4a}{\beta I_s}\left(4-\frac{\alpha_i}{\beta}\right)\left[\sin\left(\frac{\beta L}{2}\right)\cos\left(\frac{\beta L}{2}+\Delta\right)\right]\right\}$$

where

$$\alpha_R = \frac{\alpha+\alpha^*}{2} = \left(\frac{\alpha_o}{1+\delta^2}\right)\left(1+\frac{I_2+I_4}{I_s}\right)^{-2}$$

and

$$\alpha_i = \frac{\alpha-\alpha^*}{2i} = -\delta\alpha_R .$$

Equation (IV-54) is the expression for the output Bragg scattered signal beam to first order in $\frac{|A_2 A_4|}{I_s}$ for CASE II (small angles).

Examining this result more closely, one can see from Equation (IV-54) that all of the terms in (IV-54) that are first order in $\frac{|A_2 A_4|}{I_s}$ all vary sinusoidally with the phase mismatch Δ of the two pump beams.

If the 2 pump beams are within the coherence length of each other, then the phase mismatch Δ will be given by

$$\Delta = \frac{2\pi}{\lambda}(\Delta L)$$

where ΔL is the difference in path length between the two pump beams. Thus the component of $|A_2(0)|^2$ which is first order in $\frac{|A_2 A_4|}{I_s}$ will be exceptionally sensitive to vibration and to the precise alignment of the pump beams. Thus at very small angles, Equation (IV-54) predicts the observed Bragg scattered signal beam to have a component that oscillates very rapidly due to vibrations or minor adjustments superimposed on an "envelope signal" that is insensitive to vibrations and precise alignments.

Remembering that the "scattering efficiency" η of the four wave mixing process is the ratio of the exiting signal beam $|A_2(0)|^2$ to the exiting probe beam in the absence of the pump interactions $|A_1(0)|^2_{E_3=0}$, one obtains from (IV-43) that

$$|A_1(0)|^2_{E_3=0} = |A_1(L)|^2 e^{-\frac{2\alpha_0 L}{1+\theta^2}}.$$

Using (IV-54), the scattering efficiency η for the small angles of CASE II to first order in $|A_2 A_4|/I_s$ is

$$\eta = L|\alpha_1|^2 \left(\frac{I_2 I_4}{I_s^2}\right) e^{\frac{2\alpha_o L}{1+\delta^2}} e^{-2\alpha_R L} \left\{L + \frac{2aL}{\beta I_s}\left[\beta\alpha_R \sin(\beta L+\Delta) - \alpha_i \cos(\beta L+\Delta)\right]\right.$$

(IV-55)

$$\left. - \frac{12a\alpha_R}{\beta^2 I_s} \sin\left(\frac{\beta L}{2} + \Delta\right)\sin\left(\frac{\beta L}{2}\right) - \frac{4a}{\beta I_s}\left(4 - \frac{\alpha_i}{\beta}\right)\left[\sin\left(\frac{\beta L}{2}\right)\cos\left(\frac{\beta L}{2} + \Delta\right)\right]\right\} .$$

Transient Behavior

When the pump beams are chopped, two processes can contribute to the decay of the sinusoidal excited state population grating. The grating can decay because of the decrease in the excited state population by normal fluorescence decay and because of exciton migration from the peak to the valley regions of the grating. Whenever the exciton motion is diffusive, the density of excited states is given by (36)

$$\partial_t n(x,t) = D\,\partial_x^2 n(x,t) - \frac{n(x,t)}{\tau} \qquad \text{(IV-56)}$$

where x is along the direction of the grating wavevector, D is the diffusion coefficient, and τ is the fluorescence decay time. If it is assumed that n(x,t) initially has a sinusoidal spatial distribution, the solution to (IV-56) is

$$n(x,t) = \frac{e^{-t/\tau}}{2}\left\{1 + e^{-k_g^2 Dt}\cos(k_g x)\right\} \qquad \text{(IV-57)}$$

where k_g is the magnitude of the grating wavevector. The depth of the grating Δn is given by

$$\Delta n = n(x=0,t) - n\left(x = \frac{\Lambda}{2}, t\right) = e^{-\frac{K}{2}t} \qquad \text{(IV-58)}$$

where K is the decay constant given by

$$K = 2(k_g^2 D + \frac{1}{\tau}) \quad . \qquad (IV-59)$$

The magnitude of the grating wavevector k_g is given by

$$k_g = \frac{2\pi}{\Lambda} = \pi/\sin(\theta/2) \quad .$$

For small θ, k_g may be approximated as

$$k_g = \frac{2\pi}{\theta} \quad .$$

Since the scattering efficiency is proportional to Δn (43), the Bragg scattered signal beam intensity $I_s(t)$ may be written as

$$I_s(t) \propto I_p[I_w \Delta n]^2$$

or

$$I_s(t) \propto I_p I_w^2 e^{-Kt} \qquad (IV-60)$$

where I_p is the incident probe beam intensity and I_w is the pump beam intensity. Thus the Bragg diffracted signal beam should decay exponentially with decay constant

$$K = 2(\frac{\pi^2}{\sin^2(\frac{\theta}{2})} D + \frac{1}{\tau}) \qquad (IV-61)$$

which for small angles becomes

$$K = \frac{2}{\tau} + \frac{8\pi^2}{\theta^2} D \quad . \qquad (IV-62)$$

REFERENCES

36. Salcedo, J. R., A. E. Siegman, D. D. Dlott, and M. D. Fayer, Phys. Rev. Letters 41, 131 (1978).

37. Eichler, H. J., J. Eichler, J. Knof, and Ch. Noack, Phys. Stat. Sol. (a) 52, 481 (1979).

38. Hamilton, D. S., D. Heiman, J. Feinberg, and R. W. Hellwarth, Optics Letters 4, 124 (1979).

39. Liao, P. F., L. M. Humphrey, D. M. Bloom, and S. Geschwind, Phys. Rev. B 20, 4145 (1979); P. F. Liao and D. M. Bloom, Optics Letters 3, 4 (1978).

40. Yariv, A. and D. M. Pepper, Opt. Lett. 1, 16 (1977).

41. Abrams, R. L., and R. C. Lind., Opt. Lett. 2, 94 (1978); R. L. Abrams and R. C. Lind., Opt. Lett. 3, 205 (1978).

42. Liao, P. F. and D. M. Bloom, Opt. Lett. 3, 4 (1978).

43. Siegman, A. E., J. Opt. Soc. Am., 67, 545 (1977).

III. PROPERTIES OF $Nd_xY_{1-x}P_5O_{14}$ AND $Nd_xLa_{1-x}P_5O_{14}$ CRYSTALS

A significant amount of time was spent characterizing the optical properties of stochiometric laser materials for possible use in minilaser applications. The most significant result of these investigations are summarized in the following three manuscripts. Additional information on the quantum efficiency of these materials is presented in Section V.I.

J. Phys. Chem. Solids Vol. 41, pp. 345–350
Pergamon Press Ltd. 1980. Printed in Great Britain

III.1

LIFETIME MEASUREMENTS, INFRARED AND PHOTOACOUSTIC SPECTROSCOPY OF NdP_5O_{14}

RICHARD C. POWELL, DEAN P. NEIKIRK, JOHN M. FLAHERTY
Department of Physics, Oklahoma State University, Stillwater, OK 74074, U.S.A.

and

JOHN G. GUALTIERI
Army Night Vision and Electro-Optics Laboratory, Fort Monmouth, NJ 07703, U.S.A.

(*Received* 11 *June* 1979; *accepted* 24 *August* 1979)

Abstract – We have made a series of spectroscopic measurements to better understand the optical properties and concentration quenching characteristics of the stoichiometric laser material NdP_5O_{14}. The results of fluorescence lifetime measurements in the presence of different surface environments indicates that the surface condition affects the concentration quenching whereas lifetime measurements under applied uniaxial stress show that the presence of internal strains in the crystal is not significantly effective in fluorescence quenching. A comparison of the internal reflection spectrum with the normal infrared spectrum did not reveal any significant differences in the Nd^{3+} energy levels. Photoacoustic spectroscopy results proved difficult to interpret but appear to be consistent with the presence of surface quenching of excitons and indicate that the intrinsic quantum efficiency of Nd^{3+} ions in the pentaphosphate host in the absence of concentration quenching is approximately 0.90.

1. INTRODUCTION

Understanding the optical properties of NdP_5O_{14} is of significant importance because of the use of this material in minilaser applications [1]. One of the most interesting properties of this material is the small amount of concentration quenching of the fluorescence compared to that of Nd^{3+} in other types of hosts. There appear to be two possibilities for explaining concentration quenching in NdP_5O_{14}. The first is energy migration to "sinks" which are defect sites at which the energy is dissipated radiationlessly [2]. The second is the quenching of excitons at the surface of the crystal [3]. We describe here the results of several different types of spectroscopic measurements which provide further information concerning the characteristics of fluorescence quenching in NdP_5O_{14}.

We recently published the results of an investigation of $Nd_xY_{1-x}P_5O_{14}$ crystals using time-resolved site-selection spectroscopy techniques [3, 4]. One of the conclusions drawn from this work was that spatial energy migration was taking place in this material without spectral diffusion. More recent fluorescence line narrowing experiments corroborate this conclusion at least at low temperatures [5]. The observation of no energy transfer between ions in nonequivalent crystal field sites casts some doubt on the possibility of a quenching transfer occurring to ions in randomly distributed sink sites. However, a consistent interpretation of the results can be provided by a model of trapping and quenching of excitons at a macroscopic defect region such as the sample surface.

We report here the results of measuring the fluorescence lifetime of NdP_5O_{14} crystals in the presence of different surface environments and the results of laser photoacoustic measurements. Although the results do not conclusively prove which model of concentration quenching is correct for this system, they are consistent with an interpretation based on surface quenching and cannot be easily explained by migration to randomly distributed sinks. In addition measurements of the fluorescence lifetime under conditions of uniaxial stress indicate that internal strains are not effective in producing increased quenching as would be expected for sink sites. IR and internal reflection spectra were obtained in an attempt to characterize quenching centers but the results were inconclusive.

2. LIFETIME MEASUREMENTS

The fluorescence lifetime of Nd^{3+} emission can be used as a measure of the rate of concentration quenching with the quenching rate defined as

$$W_Q = \tau^{-1} - \tau_0^{-1} \qquad (1)$$

where τ_0 is the intrinsic decay time and τ is the decay time measured in the presence of quenching. In lightly doped crystals of $Nd_xY_{1-x}P_5O_{14}$ at room temperature the value of τ_0 is measured to be about 220 μsec whereas for concentrated NdP_5O_{14} the measured values of τ range from about 100–120 μsec at room temperature depending on the exact wavelength of excitation [3]. We performed a series of measurements of the fluorescence lifetime of NdP_5O_{14} crystals with different types of perturbations affecting either the surface or interior environments of the Nd^{3+} ions to determine how such environmental changes affect the concentration quenching.

(a) *Effect of surface environments*

The first of these experiments consisted of measuring the fluorescence lifetime of the crystal immersed in various types of solutions which should perturb the environment of Nd^{3+} ions at the surface of the crystal. Measurements were made at room temperature using the same experimental equipment and procedure described previously [3] with the excitation laser tuned to give a value of $\tau \approx 120\,\mu$sec for an air or vacuum environment. We found that in a concentrated solution of hydrofluoric acid the decay time was decreased to about 104 μsec. In concentrated solutions of carbon tetrachloride or carbon disulfide the decrease in lifetime was about half this amount whereas when the sample was immersed in acetone, no change in lifetime was detectable.

To further check the effects of the surface concentration quenching a sample was grown which had an NdP_5O_{14} substrate and an epitaxial layer of $Gd_{0.54}La_{0.46}P_5O_{14}$. For the preparation of the epitaxial layer, the methods used for the growth of crystals were employed. The seed was lowered into the solution which was kept at a temperature in the range of 500–550°C. Epitaxial growth proceeded for three days until a 1 mm thick layer was grown. This corresponds to a relatively fast growth rate of 14 μm hr. A small region of the substrate at one end of the sample was left uncovered. To qualitatively evaluate the perfection of the overgrowth, Laue X-ray back reflection patterns were obtained. Sharp spot patterns with the same symmetry configurations were obtained from both the substrate and overgrowth indicating that both regions were single crystalline and there is no misalignment between them. No evidence of mosaic structure or lattice constant mismatch could be found.

A comparison was made of the fluorescence lifetimes measured when the sample was excited through the epitaxial layer and in the region of uncovered substrate material. At room temperature with the particular laser excitation wavelength which was used the lifetime measured with substrate excitation was 110 μsec whereas the lifetime measured after excitation through the epitaxial layer was 119 μsec.

The fact that the fluorescence lifetime can be altered by the surface environment of the crystal indicates that the surface plays some role in the concentration quenching of fluorescence in NdP_5O_{14}. However, it has not yet been possible to find the environment necessary for significantly reducing the quenching.

(b) *Uniaxial stress measurements*

Fluorescence lifetime measurements were made while samples were under uniaxial stress to determine the contribution to the fluorescence quenching due to energy migration to randomly distributed sinks. A sample of $Nd_{0.9}Y_{0.1}P_5O_{14}$ was mounted in a dewar containing an hydraulically driven piston and immersed in liquid nitrogen. The sample was compressed along the x-axis and excited by the nitrogen laser-pumped dye laser at 5825 Å. The fluorescence lifetime was monitored at various levels of applied stress. The results are shown in Fig. 1. The application of extremely high levels of stress (up to 2000 psi, results in only an additional 20% quenching of the fluorescence lifetime.

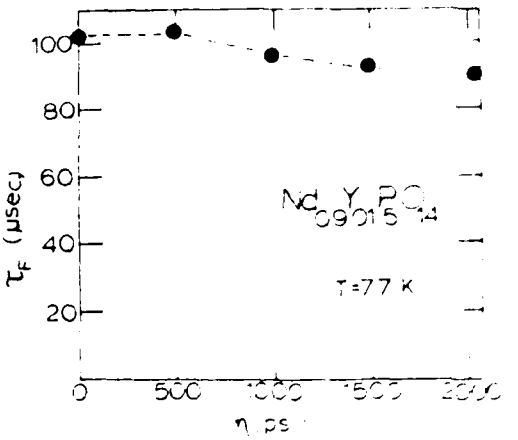

Fig. 1. Fluorescence lifetime of the $^4I_{3/2}$ level at 77 K as a function of uniaxial stress applied along the x-axis.

Sinks for radiationless quenching of energy are generally associated with Nd^{3+} ions located near crystal imperfections where local strains cause differences in the energy level structure allowing cross relaxation to occur. Thus, the application of external stress would be expected to introduce additional strains in the sample and, therefore, increase the number of sink sites resulting in enhanced quenching. It is well known that neodymium pentaphosphate is a ferroelastic crystal and twin boundaries can be introduced into the crystal by very small forces [4]. The fact that only a small change in quenching is observed even with a large magnitude of applied stress indicates that randomly distributed sinks are probably not the sites responsible for radiationless quenching in this case.

3. SPECTROSCOPIC MEASUREMENTS

(a) *IR spectra*

If radiationless quenching occurs at the surface of NdP_5O_{14} crystals but not in the bulk, it might be expected that the energy levels of Nd^{3+} ions in surface sites are shifted in position with respect to those of ions in normal sites in such a way that cross relaxation transitions are more favorable. One way for this to occur is the shifting of the $^4I_{13/2}$ level to lower energy. An attempt was made to detect such a shift by comparing the internal reflection spectrum to the ordinary transmission spectrum.

The internal reflection spectrum of NdP_5O_{14} was obtained in the region of the $^4I_{11/2}$, $^4I_{13/2}$ and $^4I_{15/2}$ levels using a Perkin Elmer model 21 spectrophotometer with the Wilks reflectance attachment. The cleaved samples were mounted on thallium bromoiodide (KRS-5) prisms with index matching fluid

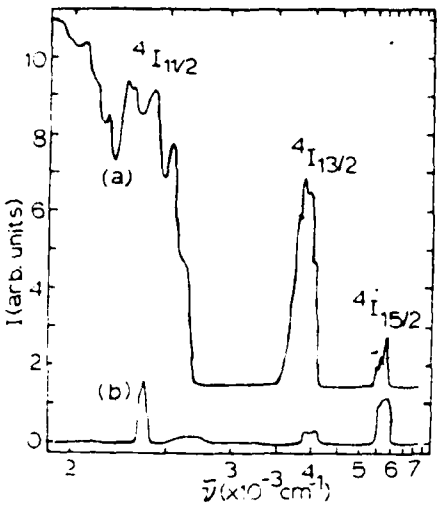

Fig. 2. IR (a) and internal reflection (b) spectra of NdP_5O_{14} crystals at room temperature.

$(n = 1.802)$. The b direction was chosen because NdP_5O_{14} can be cleaved perpendicular to the b axis. The flatness of the (010) cleaved surface is typically 10 nm over the total area of the sample. This eliminates polishing procedures and yields a surface free of contaminants. The Wilks micro-sampling transmission attachment was used to obtain a transmission spectrum under similar conditions to those used in the internal reflection measurement. The two spectra are shown in Fig. 2. Wide slits (400 μm) were used to improve the signal to noise ratio. Although this broadens the spectra, no shifts in the centroids of the ^4I multiplets can be detected.

The penetration depth of the evanescent wave in the rarer medium in internal reflection is typically on the order of 0.2λ. In the spectral region investigated the penetration depth would be approx. 0.3–0.9 μm which is about 300–500 times the lattice spacing in the b direction. The lack of observation of a spectral shift in the internal reflection results does not necessarily prove that the energy levels of Nd^{3+} ions in surface sites are not perturbed. It may be that the region sampled is so large that the majority of ions involved in transitions are located in bulk sites instead of surface sites.

Another point to note about the infrared spectrum in Fig. 2 is that no impurity bands can be observed in the region between 2800 and 3800 cm^{-1}. It is well known that phosphate materials can contain hydrogen impurities which can act as quenching centers for luminescence. This does not appear to be the case here since OH vibrational transitions would be easily visible in the near IR region of the spectrum investigated.

(b) *Photoacoustic spectroscopy*

Photoacoustic (PA) spectroscopy is a technique which directly monitors radiationless relaxation processes by detecting the sound produced in an acoustical cell when a sample is excited by a periodically varying light source [7]. We previously reported on the PA spectra of $Nd_xY_{1-x}P_5O_{14}$ crystals and the basic experimental apparatus is described in Ref. [3]. Two additional types of PA measurements have now been performed on this set of samples using the individual lines of an argon ion laser for excitation. This light was chopped at frequencies varying from 100–2700 Hz and the laser power was continuously monitored and stabilized at a level of 0.15 W. The PA signal intensities from the samples were more than two orders of magnitude greater than noise and empty cell signals.

The first experiment was to record the maximum PA signal from the various samples at twelve or more chopping frequencies ν_c after excitation with the 5145 Å argon laser line. The results are shown in Fig. 3 for the NdP_5O_{14} and $Nd_{0.1}Y_{0.9}P_5O_{14}$ samples. The lightly doped sample shows a PA signal intensity which varies as ν_c^{-1} throughout the whole range of frequencies investigated whereas the concentrated sample signal varies as ν_c^{-1} at frequencies up to about 450 Hz and then varies as $\nu_c^{-3/2}$ at higher frequencies. Samples with intermediate concentrations exhibit PA signal intensities which vary with chopping frequency between a ν_c^{-1} and $\nu_c^{-3/2}$.

The thickness of these samples is of the order of one millimeter and the optical penetration depth ($l_{op} = \alpha^{-1}$) varies between about 700 μm for the concentration sample and 7000 μm for the 10% sample at this excitation wavelength. According to the theory of Rosencwaig and Gersho (RG) the thermal diffusion length varies with chopping frequency as [8]

$$l_{th} = \left(\frac{\beta}{\pi\nu_c}\right)^{1/2} \tag{2}$$

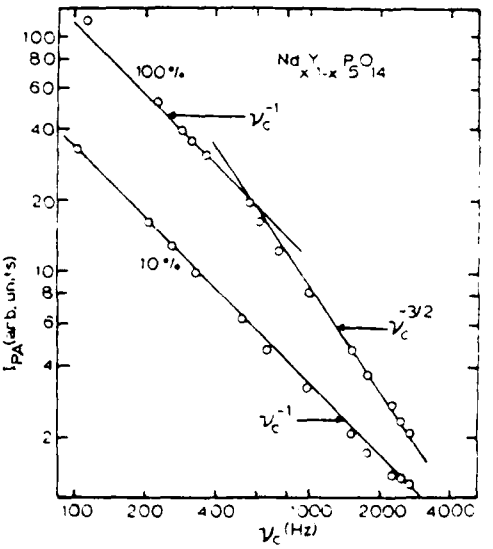

Fig. 3. PA signal intensity vs chopping frequency at room temperature for 5145 Å excitation.

where β is the thermal diffusivity. For NdP_5O_{14} the largest value of β is [9] $\sim 10^{-2}$ cm^2 sec^{-1} and, thus, l_{th} ranges from about 54 μm at ν_c = 110 Hz to 11 μm at ν_c = 2700 Hz. It is approximately 27 μm at 450 Hz where the change in slope occurs in the curve for the 100% sample as seen in Fig. 3.

From the above considerations the results of these experiments should be classified in terms of the special cases of the RG theory as an optically thin-thermally thick case for the 10% sample and an optically thick-thermally thick case for the 100% sample. Since $l_{th} \ll l_\beta$ in all cases the PA signal intensity is expected to vary as $\nu_c^{-3/2}$. The fact that this is not observed is probably due to the fact that the RG theory is based on a one-dimensional model where the thermal gradient at the excited surface causes uniform heat flow back into the cell. In these experiments a small area of the total sample surface is excited by the laser beam and the heat is generated in a cylindrical volume within the sample. The heat generated in a layer close to the front surface still is dominated by the temperature gradient at the surface and contributes to the PA signal as predicted by the one-dimensional theory. However, further into the sample, the heat flow is dominated by the temperature gradient radially out from the excited cylinder and most of it will never reach the surface within a duty cycle to contribute to the detected PA signal. Comparing these considerations withthe results obtained on the 10% sample indicate that the effective optical layer depth for heat contributing to the PA signal l_{eff} is $\gtrsim 10$ μm, the smallest value of l_{th}. For $l_{eff} < l_{th}$ the RG theory predicts a ν_c^{-1} variation of the PA signal intensity as observed. For the 100% sample applying the above considerations to the data shown in Fig. 3 indicate that the effective optical layer is two and a half times greater than that in the 10% sample. A possible explanation for this is the added contribution to the PA signal from the heat generated by the diffusion and surface quenching of excitons. Although these PA results are obviously too complicated to be considered proof of exciton migration and surface quenching, this interpretation is at least consistent with previous results indicating exciton migration lengths of the order of tens of microns and quenching at the surface.

The second PA experiment performed on these samples was an attempt to measure their absolute quantum efficiency. The maxima PA intensity and the phase at signal maximum was measured for two different wavelengths of excitation at two different chopping frequencies. The 4765 and 5145 Å lines of the argon laser were used for excitation and measurements were made with ν_c = 312 and 1000 Hz.

The Nd^{3+} energy level model used to interpret these data is shown in Fig. 4. After absorption into levels E_7 or E_6 heat is generated by radiationless relaxation to the metastable level E_5. This level has radiative transitions to the various multiplets of the ^4I_J term with branching ratios b_{5j}. There are also the possibilities of nonradiative decay and concentration

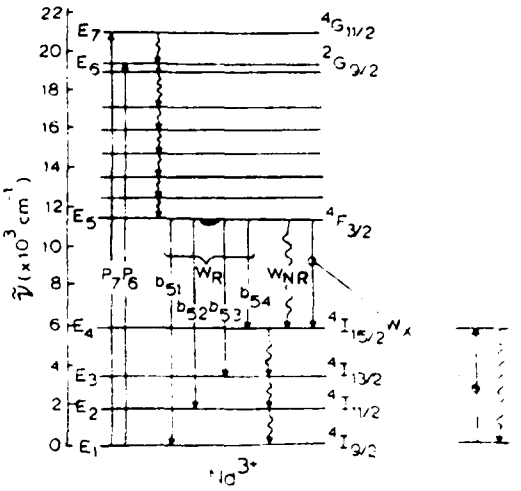

Fig. 4. Energy levels and transitions for Nd^{3+} ions.

quenching in which all of the energy in E_5 is lost to heat. After transitions to the higher lying ground term levels, heat is generated by radiationless relaxation to the lowest ground level. These levels and transition rates are labeled in Fig. 4. The quantum efficiency, probability of nonradiative relaxation, and probability of concentration quenching of the metastable state are given by

$$QE = W_R/(W_R + W_{NR} + W_X)$$
$$P_{NR} = W_{NR}/(W_R + W_{NR} + W_X)$$
$$P_X = W_X/(W_R + W_{NR} + W_X) \quad (13)$$

with the condition

$$QE + P_{NR} + P_X = 1. \quad (14)$$

The expression for the PA signal at phase angle θ after excitation in energy level E_a is

$$I_a(\theta) = C(P_a E_{a1}) \sum_{ij} \phi_{ij}^{nr} E_{ij} \cos[\psi - \tan^{-1}(2\pi\nu\tau_a) - \theta], \quad (15)$$

where P_a is the power absorbed, C is a factor accounting for properties of the cell and detection system, and the summation is over all transitions in which heat is produced. ϕ_{ij}^{nr} is the probability for the nonradiative transition to occur between levels i and j, E_{ij} is the energy of this transition, $\tan^{-1}(2\pi\nu\tau_a)$ is the phase shift of the signal due to the lifetime of the initial level and ψ is the phase shift due to the detection procedure. For NdP_5O_{14} all of the energy level positions and branching ratios are known [10]. Only the metastable level has a long enough lifetime to introduce a measurable phase shift into the signal. Evaluating the sum in eqn (15) explicitly leads to

$$I_a(\theta) = C(P_a E_{a1})[E_{a5}\cos(\psi - \theta) + (E_{a1} - kQE)\cos(\psi - \tan^{-1}(2\pi\nu\tau_a) - \theta)] \quad (16)$$

where τ_5 is the lifetime of the metastable level and

$$k = E_{51} - b_{54}E_{41} - b_{53}E_{31} - b_{52}E_{21} \qquad (7)$$

In order to eliminate the unknown experimental factor C, we took the ratio of PA signals at two different excitation wavelengths. Solving for QE gives

$$QE = \frac{AE_{65}\cos(\psi - \theta_5) + AE_{51}\cos(\psi + \tan^{-1}(2\pi\nu_c\tau_5) - \theta_5) - E_{65}\cos(\psi - \theta_6) - E_{61}\cos(\psi + \tan^{-1}(2\pi\nu_c\tau_5) - \theta_6)}{k'A\cos(\psi + \tan^{-1}(2\pi\nu_c\tau_5) - \theta_5)\cos(\psi + \tan^{-1}(2\pi\nu_c\tau_5) - \theta_6)} \qquad (8)$$

where the 6 and 5 subscripts refer to excitation at 5145 and 4765 Å, respectively and the factor A is

$$A = (I_{o5}I_{o6}(E_{65}E_{51})(P_5 - P_6)). \qquad (9)$$

Since the values to be used for ψ are still in question, a second equation was generated by maximizing eqn (6) with respect to ψ and solving for QE which gives

$$QE = \frac{E_{65}\sin(\psi - \theta_{65})}{k'A\sin(\psi + \tan^{-1}(2\pi\nu_c\tau_5) - \theta_{65})} + E_{61} \qquad (10)$$

Equation (8) and the two equations obtained from eqn (10) for two different excitation wavelengths can now be solved simultaneously in an iterative way to obtain a unique value for QE. To check the uniqueness of the result, the procedure was repeated for both chopping frequencies.

For the NdP_5O_{14} sample a quantum efficiency of 0.45 was found by the method described above. In this case the power absorbed in eqn (9) was assumed to be the total incident power for both wavelengths of excitation. The value of the quantum efficiency in the absence of concentration quenching can be found from the expression $QE(O) = QE(x)\tau_m/\tau_r$. The combined lifetime and $QE(x)$ results indicate that $QE(O)$ is approximately 0.90 for NdP_5O_{14}. Similar analysis of the $x = 0.20$ sample gives $QE(x) = 0.82$ and $QE(O) = 0.90$.

The above procedure for determining quantum efficiency by taking the ratio of two PA signals was first suggested by Rockley [11] and applied to a simpler case where phase angles for different transitions did not present a problem. Although the results obtained on NdP_5O_{14} appear to be reasonable, it should be pointed out that the value obtained for QE is extremely sensitive to the parameter A and even very small changes in factors such as the ratio of power absorbed can cause significant changes in the predicted QE. This is especially a problem when we are dealing with a situation having involvement with an effective thermal layer as discussed previously and, thus, the value obtained for $QE(O)$ must be considered as only a very rough estimate. Quimby and Yen [12] have reported measurements of the quantum efficiency of Nd^{3+} ions in a glass host using PA measurements. The model used in the interpretation of their data is similar to the one used here except that phase shifts for different transitions were not considered. Their results indicate a $QE(O)$ of between 0.65 and 0.75 for Nd^{3+} in glass.

4. SUMMARY AND CONCLUSIONS

The various results described here provide further information on the optical properties of NdP_5O_{14}. Both the lifetime and PA measurements indicate that the surface plays some role in the concentration quenching of this material but the results are not conclusive in identifying the quenching mechanism. Photoacoustic measurements made by Auzel [7] on powdered samples indicate that radiationless quenching is greater for powders of 50 μm grain size than for large single crystals which is also consistent with the predictions of surface quenching [13]. More direct measurements of exciton diffusion using transient grating techniques are presently being used to determine the possible contribution of long range exciton migration to the quenching.

Acknowledgements — This work was supported by the U.S. Army Research Office. The authors gratefully acknowledge the help of D. D. Smith and A. H. Zewail in making the low temperature FLN measurements.

REFERENCES

1. Chinn S. R., Hong H. Y-P. and Pierce J. W., *Laser Focus* **12**, 64 (1976); Danielmeyer H. G. and Weber H. P., *IEEE J. Quantum Elect.* **8**, 805 (1972); Danielmeyer H. G., In *Festkorperprobleme (Advances in Solid State Physics)* Vol. 15, p. 253 (Edited by H. J. Queisser) Pergamon Viewag, Braunschweig (1975); Weber H. P., *Opt. and Quantum Elect.* **7**, 431 (1975).
2. Lempicki A., *Optics Comm.* **23**, 376 (1977).
3. Flaherty J. M. and Powell R. C., *Phys. Rev.* **B19**, 32 (1979).
4. Flaherty J. M. and Powell R. C., *Solid State Commun.* **26**, 803 (1978).
5. Powell R. C., Smith D. D. and Zewail A. H., unpublished results.
6. Weber H. P., Tofield B. C. and Liao P. F., *Phys. Rev.* **B11**, 1152 (1975); Budin J. P., Milatos-Roulos A., Chirle N. D. and Le Roux G., *J. Appl. Phys.* **46**, 2867 (1975); Kobayashi T., Sawada T., Ikeo H., Muto K. and Kai J., *J. Phys. Soc. Japan* **40**, 595 (1976).
7. Rosencwaig A., In *Advances in Electronics and Electron Physics*, Vol. 46, p. 207. Academic Press, New York (1978).
8. Rosencwaig A. and Gersho A., *J. Appl. Phys.* **47**, 64 (1976).

9. Chinn S. R. and Zwicker W. K., *J. Appl. Phys.* **49**, 5892 (1978).
10. Lomheim T. S. and DeShazer L. G., *Opt. Comm.* **24**, 89 (1978).
11. Rockley M. G. and Waugh K. M., *Chem. Phys. Lett.* **54**, 597 (1978).
12. Quimby R. S. and Yen W. M., *Optics Lett.* **3**, 181 (1978).
13. Auzel F., Meichenin D. and Michel J. C., *J. Luminescence*, **18/19**, 97 (1979).

J. Phys. C: Solid State Phys., 14 (1981) 2027–2038. Printed in Great Britain

III.2

Effects of pressure on the spectra and lifetimes of $Nd_xY_{1-x}P_5O_{14}$

Larry D Merkle†§, Ian L Spain† and Richard C Powell‡

† Physics Department, Colorado State University, Fort Collins, Colorado 80523, USA
‡ Physics Department, Oklahoma State University, Stillwater, Oklahoma 74078, USA

Received 29 September 1980, in final form 9 December 1980

Abstract. Variations in the fluorescence line positions, linewidths, and lifetimes with hydrostatic pressure up to about 80 kbar are reported for samples of NdP_5O_{14} and $Nd_xY_{1-x}P_5O_{14}$. The results for the lightly doped sample are consistent with changes in the radiative decay rate while the very different results obtained on the heavily doped sample are interpreted in terms of increased radiationless quenching due to energy migration to trapping sites. Results are also reported on the variations in the fluorescence lifetimes of the R lines, and the positions of the N lines and vibronic peaks of ruby as a function of hydrostatic pressure.

1. Introduction

The study of the effects of pressure on the optical properties of impurity ions in solids can be useful in many regards. Changes in the widths, positions, and lifetimes of electronic transitions and their vibrational sidebands as a function of applied pressure can give important information concerning the interaction of the impurity ion with its surroundings (Drotning and Drickamer 1976, Tyner and Drickamer 1977, Klick *et al* 1977, Webster and Drickamer 1980). Diamond anvil high-pressure cells are convenient for such investigations, requiring the study of very small samples. In this regard, the light intensity and small size of the illuminated area available with lasers are valuable. The work reported here represents an exploratory application of the techniques of pulsed laser excitation and gated electronics for time-resolved fluorescence studies at high pressures in a diamond anvil cell.

The measurements reported here include studies of the effects of pressure on the absorption and fluorescence spectra and the lifetimes of $Nd_xY_{1-x}P_5O_{14}$ for $x = 0.1$ and 1.0. In recent years there has been significant interest in understanding the optical characteristics of NdP_5O_{14} because of its properties as a stoichiometric laser material for minilaser applications (Weber 1975). One of the most important properties of this material, which is still not understood, is the nature of the mechanism giving rise to the weak concentration quenching of the fluorescence. These pressure-dependent results give new information on the fluorescence quenching in this material which is consistent

§ Present address: Physics Department, Oklahoma State University, Stillwater, Oklahoma 74078, USA

0022-3719/81/142027 + 12 $01.50

with an energy migration model. In addition results are presented on the pressure dependence of the fluorescence spectra and lifetimes of heavily doped ruby crystals, see section V.2.

2. Experimental details

The diamond anvil high-pressure cells used for this study were designed by one of us (JLS) and are very similar to a cell described previously (Yu *et al* 1979). The major modification made in the cells used here is the opening of a conical hole of 16° included angle in the piston and driving screw, allowing optical access with approximately *f*/3.5 aperture. A fluid of approximately four parts methanol to one part ethanol served to maintain hydrostatic and homogeneous pressures.

Pressure was monitored by observation of the wavelength shift of the R_1 fluorescence line of ruby. For pressures in the range of interest to this work, this shift has been found to be $+0.365$ Å kbar^{-1} (Piermarini *et al* 1975). Also, a correction was made for the temperature shift of the line, which is $+0.067$ Å K^{-1} near room temperature (Paetzold 1951) due to small drifts in room temperature, at which all measurements were made. The ruby fluorescence was excited by about 10 mW of power from the 5145 Å line of an argon laser, which has been found empirically to be considerably less than the power required to measurably raise the temperature of the small chips of ruby typically used (10–30 μm on a side). The R-line spectra were measured with sufficient resolution that the accuracy of the pressure measurements was limited by noise and wavelength calibration to about ±1 kbar.

The lifetime and high-resolution fluorescence measurements of the $^4F_{3/2} \rightarrow {}^4I_{9/2}$ transitions in the $Nd_xY_{1-x}P_5O_{14}$ samples and of the ruby transitions were made with excitation by the 5145 Å line of the argon laser focused onto the sample through the driving screw end of the pressure cell. Fluorescence was collected from the opposite end of the cell, focused onto the entrance slit of a one-meter monochromator equipped with a grating blazed at 1 μm; and detected by a cooled RCA C31034 photomultiplier tube. For analysing the ruby vibronic spectra, a resolution of about 0.4 Å was used and for the pentaphosphate spectra the resolution was about 1.2 Å. To record steady-state spectra, the excitation power was about 10 mW, the beam was mechanically chopped at 100 Hz, and the signal analysed by a lock-in amplifier. For lifetime measurements an electro-optic shutter was used to generate 50 μs pulses with pulse heights chosen to keep the average power well below 10 mW. The decay times were analysed by a boxcar integrator.

Optical absorption measurements were made using a 100 W quartz–halogen lamp through a 1/4 M monochromator for the illumination source. The light was detected by a cooled RCA C31034 photomultiplier tube whose output was measured by a pico-ammeter. The observed shift in the ruby R_1 fluorescence line position indicates that the light source caused sample temperatures to be raised by about 5 to 10 K in these experiments.

For infrared fluorescence measurements, the sample was illuminated by up to 200 mW of power of the 5145 Å line of the argon laser, which caused less temperature rise than the transmission experiment, and the signal was chopped at 500 Hz. The fluorescence was detected by a cooled PbS detector whose output was analysed by a lock-in amplifier.

The samples used in these measurements were chips broken from single crystals. The ruby was analysed by atomic absorption and found to have about 0.03% Cr^{3+} ions replacing the aluminium. The $Nd_{0.1}Y_{0.9}P_5O_{14}$ and NdP_5O_{14} crystals cleave easily and it

was thus possible to choose flat pieces with parallel faces for the optical transmission experiments. However, it was difficult to measure the thicknesses of these small pieces accurately, so only relative absorption coefficients of a given piece are reported at the various pressures.

3. $Nd_xY_{1-x}P_5O_{14}$ results and interpretation

The fluorescence decay times of the Nd^{3+} emission in the two pentaphosphate samples were measured at several pressures up to about 90 kbar. The fluorescence decay rates are plotted in figure 1. The decay curves for NdP_5O_{14} were simple exponentials at all pressures. At low pressures, the decay curves for $Nd_{0.1}Y_{0.9}P_5O_{14}$ were also pure exponentials but at higher pressure a faster initial decay was observed to grow in. It was difficult to get a quantitative value for this initial decay time, since it was not greatly different from the asymptotic time and lasted for only about the first 60 μs of the decay.

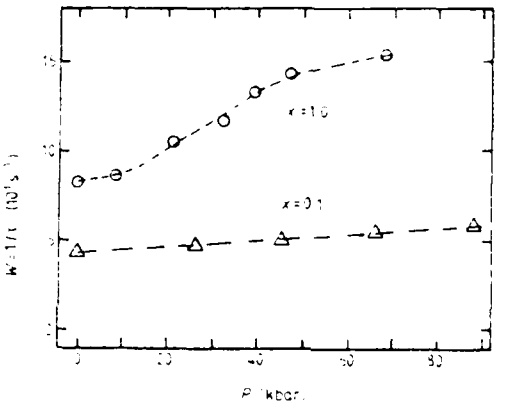

Figure 1. Total fluorescence decay rate of $^4F_{3/2}$ level in $Nd_xY_{1-x}P_5O_{14}$ for $x = 0.1$ and 1.0, as a function of pressure.

Figure 2 shows the fluorescence spectra of the $^4F_{3/2} \rightarrow {}^4I_{9/2}$ Nd^{3+} transitions at low and high pressures for both pentaphosphate samples. The shifts in positions, changes in relative intensities, and variations in lineshapes with pressure are different for the two samples. Figure 3 shows plots of the line positions versus pressure and the pressure-dependent widths of two of the transitions are shown in figure 4. These are the only two lines well enough resolved to allow their widths to be measured accurately. The labels for these transitions are R_1 and R_2 for the lower- and higher-energy crystal-field components of the $^4F_{3/2}$ metastable state and Z_1 refers to the ground state. The shape of the R_2–Z_1 transition in NdP_5O_{14} was analysed to determine the homogeneous (lorentzian) contribution to the linewidth and this is also shown in figure 4. All of the lines in the spectra of NdP_5O_{14} appeared to narrow at high pressures similarly to the data shown in figure 4. The equivalent transitions in $Nd_{0.1}Y_{0.9}P_5O_{14}$ all broadened considerably with pressure, but they were not well enough resolved to make quantitative measurements of the widths as can be seen in figure 2.

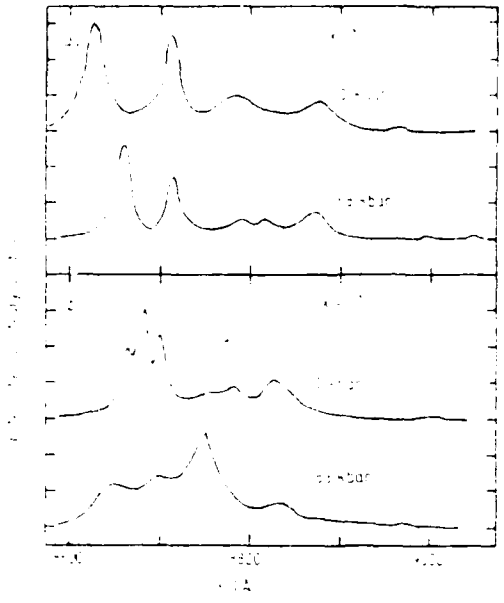

Figure 2. $Nd_xY_{1-x}P_5O_{14}$ $^4F_{3/2} \rightarrow {}^4I_{9/2}$ fluorescence spectra at two pressures: (*a*) $x = 1.0$ at 1 bar and 58 kbar; (*b*) $x = 0.1$ at 1 bar and 58 kbar. Spectra are not corrected for wavelength dependence of detector response.

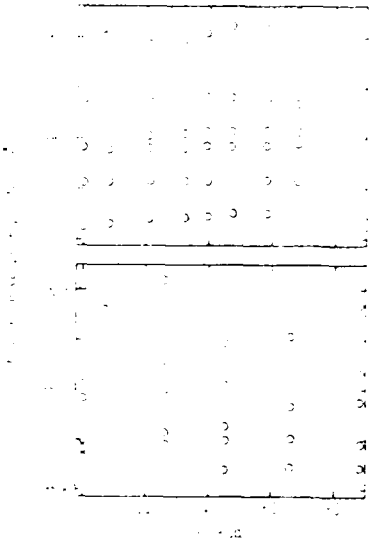

Figure 3. Pressure dependence of the $^4F_{3/2} \rightarrow {}^4I_{9/2}$ fluorescence peaks of (*a*) NdP_5O_{14} and (*b*) $Nd_{0.1}Y_{0.9}P_5O_{14}$.

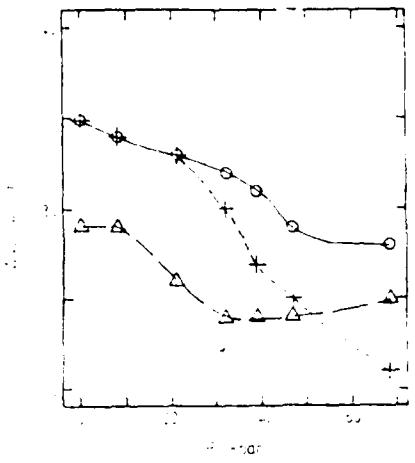

Figure 4. Pressure dependence of the $R_1 \rightarrow Z_{1,2,3,4}$, $R_2 \rightarrow Z_{1,2,3,4}$ (tot) (○) and $R_2 \rightarrow Z_1$ (50cm^{-1}) (×) linewidths of NdP_5O_{14}.

The line positions for NdP_5O_{14} are shown in table 1 at low and high pressures. These are compiled from visible absorption and fluorescence spectra and from infrared emission spectra. The fluorescences to the $^4I_{13/2}$ and $^4I_{11/2}$ manifolds were measured with very wide slits on the monochromator due to the poor sensitivity of the PbS detector and thus only the total breadths of these manifolds are given. Transitions to the $^4I_{15/2}$ levels were too weak to observe either in fluorescence or absorption for a sample small enough for diamond cell studies and the levels listed in table 1 are taken from Blatte *et al* (1973) and shown for completeness. Note that most of the levels move to lower energies with increasing pressure and some appear to be more sensitive to pressure than others.

The line broadening with pressure observed in the fluorescence spectrum of the lightly doped sample and the line narrowing reported in figure 4 for the heavily doped sample are difficult to interpret. In other materials, such as $Y_3Al_5O_{12}:Nd^{3+}$, the homogeneous contribution to the linewidths has been attributed to phonon absorption and emission transitions among the various levels of each manifold (Kushida 1969). These processes may change with pressure as the positions of the energy levels change, but exact calculation of such changes is not possible without data on the pressure variation of the vibrational properties of these crystals.

The observed increase in the fluorescence decay rate at high pressures could possibly be due to one of three effects: an increase in the radiative decay rate of each Nd^{3+} ion; an increase in the non-radiative decay rate of each Nd^{3+} ion; or an increase in the interaction between Nd^{3+} ions leading to fluorescence quenching. The third possibility appears to be the most likely, since single-ion effects should be independent of concentration and the observed pressure-dependent quenching properties are different for lightly doped and heavily doped samples. In addition, quantitative estimates of the non-radiative decay rate of the $^4F_{3/2}$ level give values of ≈30.2 of the total decay rate (Weber *et al* 1974, Powell *et al* 1980b) and it is doubtful that pressure would cause this to increase to the extent necessary to explain the NdP_5O_{14} data.

The radiative decay rates can be estimated from the absorption strength of the

Table 1. Absorption transition energies and energy levels in NdP_5O_{14} at two pressures.

Transition or level		P = 1 bar Energy (cm^{-1})	P = 68 kbar Energy (cm^{-1})
		19589 ± 5	19512 ± 5
		19376	—
$^4I_{9/2} \rightarrow {}^2G_{9/2} + {}^4G_{5/2}$		19212	19117
		19117	19015
		19044	18932
		18979	18850
		17550 ± 5	17528 ± 5
		17473	17422
		17382	17340
		17318	17215
$^4I_{9/2} \rightarrow {}^4G_{7/2} + {}^2G_{7/2}$		17256	17167
		17155	17085
		17120	—
		17050	16981
		16929	16895
$^4I_{9/2} \rightarrow {}^4F_{3/2}$		—	—
		13622 ± 5	13592 ± 5
		13581	13554
		13537	13480
$^4I_{9/2} \rightarrow {}^4S_{3/2} + {}^4F_{5/2}$		13443	13432
		13410	—
		13360	13328
		13177	—
		12587 ± 5	12545 ± 5
		12492	12477
$^4I_{9/2} \rightarrow {}^4H_{9/2} + {}^4F_{7/2}$		12412	12372
		12326	12329
		12271	12228
$^4F_{9/2}$	R_2	11592 ± 5	11546 ± 5
	R_1	11477	11474
		6289	
		6274	
		6210	
		6081	
$^4I_{9/2}$[a]		6072	—
		6011	
		5912	
		5872	
$^4I_{11/2}$		4260 ± 30	4290 ± 30
		3840	3870
$^4I_{13/2}$		2190 ± 30	2260 ± 30
		1930	1980
	Z_6	525 ± 5	427 ± 5
	Z_5	256[b]	—
$^4I_{9/2}$	Z_4	212	201
	Z_2	82	67
	Z	0	0

[a] at 77 K (Blatte *et al* 1973).
[b] at low temperature (Strek *et al* 1977).

$^4I_{9/2} \rightarrow {}^4F_{3/2}$ transitions and the relative fluorescence intensities. If the transition probabilities $W_{Z_1-R_1}$ and $W_{Z_1-R_2}$ are known, the emission rate is found from Einstein's relations to be

$$W_{R-Z_1} = n_{R_1}W_{R_1-Z_1} + n_{R_2}W_{R_2-Z_1} \propto n_{R_1}W_{Z_1-R_1} + n_{R_2}W_{Z_1-R_2} \tag{1}$$

where n_{R_1} and n_{R_2} are the thermal population factors for the two crystal-field components of the $^4F_{3/2}$ level. By working with the ratios of transition rates for high and low pressures, problems with accurately measuring sample thickness can be avoided in determining the changes in absorption cross sections. Correction must be made to account for the change in the number of ions in the path of the light beam. This can be accounted for by a factor of a^3(68 kbar)/a^3(0 kbar) where a represents the lattice constant. Table 2 lists the integrated absorption coefficients for the two transitions and pressures of interest.

Table 2. Relative radiative transition rate parameters for NdP_5O_{14} at atmospheric pressure and 68 kbar.

	P = 1 bar	P = 68 kbar
$W_{Z_1-R_1(\text{lines})}$ (arbitrary units)	0.37	0.57
$W_{Z_1-R_2(\text{lines})}$ (arbitrary units)	0.95	1.04
n_{R_1} (room temperature)	0.64	0.58
n_{R_2} (room temperature)	0.36	0.42
W_{R-Z_1} (arbitrary units)	0.58	0.72 a^3(68 kbar)/a^3(0 kbar)
$I[^4F_{3/2} \rightarrow {}^4I_{9/2}(1)]/I[^4F_{3/2} \rightarrow {}^4I_{9/2}(\text{all})]$	0.25	0.25
$I[^4F_{3/2} \rightarrow {}^4I_{9/2}]/I(\text{tot})$	0.37	0.35
$I[^4F_{3/2} \rightarrow {}^4I_{11/2}]/I(\text{tot})$	0.52	0.55
$I[^4F_{3/2} \rightarrow {}^4I_{13/2}]/I(\text{tot})$	0.11	0.10
$W_{\text{rad}}^{\text{tot}}$ (arbitrary units)	6.3	8.2 a^3(68 kbar)/a^3(0 kbar)

It also gives the relative thermal populations of two crystal-field components of the $^4F_{3/2}$ level and the computed radiative decay rate to the Z_1 level. Comparison of the relative fluorescence intensities of transitions to other components of the ^4I_J term and correction for the known branching ratios at 1 bar (Lomheim and DeShazer 1978), noting that the transitions to the $^4I_{15/2}$ levels make a negligible contribution to the decay rate, gives the results

$$\frac{W_{R-Z}(68\text{ kbar})}{W_{R-Z}(0\text{ kbar})} = \frac{a^3(68\text{ kbar})}{a^3(0\text{ kbar})}(1.2 \pm 0.3) \tag{2}$$

and

$$\frac{W_{\text{rad}}^{\text{tot}}(68\text{ kbar})}{W_{\text{rad}}^{\text{tot}}(0\text{ kbar})} = \frac{W^{\text{rad}}(68\text{ kbar})}{W^{\text{rad}}(0\text{ kbar})}{}_{^4F_{3/2}\rightarrow\text{all lower levels}} = \frac{a^3(68\text{ kbar})}{a^3(0\text{ kbar})}(1.3 \pm 0.4). \tag{3}$$

A recent paper by Asaumi *et al* (1980) gives the compressibility of NdP_5O_{14} along the a and c axes but not the b axis. Their data indicate that the compression factors in the above equations must be no smaller than about 0.95. The radiative decay rate at atmospheric pressure has been estimated to be about 3225 s^{-1} and thus the increase with

pressure predicted by equation (3) is far too small to account for the NdP_5O_{14} data shown in figure 1.

It has been shown that the oscillator strengths for Nd^{3+} transitions in $Nd_xLa_{1-x}P_5O_{14}$ are independent of Nd^{3+} concentration (Auzel 1976). Thus the change in the radiative decay rate with pressure should also depend little on concentration and the prediction of equation (3) should be applicable to the $Nd_{0.1}Y_{0.9}P_5O_{14}$ sample. Comparing equation (3) with the data for the lightly doped sample shown in figure 1 shows relatively good agreement.

The above considerations indicate that the pressure dependence of the fluorescence decay rate in NdP_5O_{14} is not due to changes in single-ion decay rates. Two multi-ion quenching processes are possible, cross-relaxation between pairs of Nd^{3+} ions (Strek *et al* 1977) and energy migration to sinks (Lempicki 1977, Flaherty and Powell 1979, Powell *et al* 1980a). For electric dipole–dipole interaction, both of these processes have an R^{-6} dependence on the separation between Nd^{3+} ions and this will vary only weakly with pressure because of the small compressibility of the material (Asauni *et al* 1980). The efficiency of cross-relaxation between pairs of Nd^{3+} ions is dependent upon the degree of resonance between the $^4F_{3/2} \rightarrow {}^4I_{15/2}$ transitions on one ion and the $^4I_{9/2} \rightarrow {}^4I_{15/2}$ transitions on the other ion. The branching ratio for fluorescence to the $^4I_{15/2}$ manifold is quite small at atmospheric pressure and the fact that these transitions are still not observed at high pressure suggests that the matrix elements for these transitions remain small. Since transitions to the $^4I_{15/2}$ levels could not be observed, the change in their positions with pressure is unknown. However, since the $^4F_{3/2}$ levels move to lower energy with increased pressure and the spectral lines become narrower, in order to have increased resonance for cross-relaxation transitions at high pressures the $^4I_{15/2}$ levels would have to move very strongly to lower energies and reach very specific positions favourable for energy matching. Thus the observed spectral properties do not appear to favour strongly increased cross-relaxation at the pressures attained in this study.

The final possibility is that the increased decay rate at high pressures is due to the increased energy migration to traps. This process involves transitions between the $^4F_{3/2}$ and $^4I_{9/2}$ states for which the matrix elements were shown above to increase with pressure. Also, since the transfer involves ions whose relevant energy levels are in resonance, the narrowing of the fluorescence lines increases the interaction strength at high pressures. A simple diffusion model may be used to check the plausibility of this hypothesis quantitatively. In this case the rate of energy transfer to traps is proportional to the diffusion coefficient, D, and for resonant electric dipole–dipole interaction this is given by (Trlifaj 1958)

$$W^{\text{mig}} \propto D \propto a^{-4} W_{\text{ion}}^{-1} \Delta\nu_{\text{hom}}^{-1} \tag{4}$$

where a is an average lattice spacing, W_{ion} is the single-ion transition rate and $\Delta\nu_{\text{hom}}$ is the homogeneous linewidth which is used to approximate the spectral overlap integral between the two interacting ions. Using equation (2), and the homogeneous linewidths measured for the R_2–Z_1 line, the ratio of the rates of energy migration and trapping at high and low pressures is

$$\frac{W^{\text{mig}}(68\text{ kbar})}{W^{\text{mig}}(0\text{ kbar})} = \frac{a^4(0\text{ kbar})}{a^4(68\text{ kbar})}\left\{\frac{a^2(68\text{ kbar})}{a^2(0\text{ kbar})}(1.2 \pm 0.31)\right\}^2\left(\frac{35}{21}\right) = 2.4 \pm 1. \tag{5}$$

This prediction can be compared with the ratio of the radiationless quenching rates found from the experimental data shown in figure 1 and corrected for the change in

radiative decay rate using equation (3)

$$\frac{W^{NR}(68\text{ kbar})}{W^{NR}(0\text{ kbar})} = \frac{W^{obs}(68\text{ kbar}) - W^{rad}_{vac}(68\text{ kbar})}{W^{obs}(0\text{ kbar}) - W^{rad}_{vac}(0\text{ kbar})} = 3.0 - (0.8 \pm 0.3)\frac{a^3(68\text{ kbar})}{a^3(0\text{ kbar})} \qquad (6)$$

where the radiative decay rate at atmospheric pressure has been estimated to be 3225 s^{-1}. As noted earlier, the compression factor is nearly unity, so that the observed ratio of the radiationless quenching rates is about 2.2 ± 0.3, which is in close agreement with the prediction of equation (5).

5. Discussion and conclusions

The physical mechanisms leading to the observed changes in the energy level positions and transition strengths with increased pressure in the neodymium pentaphosphate samples are probably due to changes in the symmetry of the crystal field and the amount of configuration mixing due to the strength of the odd crystal-field components. Further studies are necessary to clarify the details of these changes. Different transition energies have been associated with several types of site symmetries in $Nd_xY_{1-x}P_5O_{14}$ crystals (Kruhler *et al* 1975) but no consistent trend toward one type of symmetry can be seen in our high-pressure results. Some work on crystal-field changes with pressure has been reported by Huber *et al* (1977) on europium pentaphosphate.

For the lightly doped mixed pentaphosphate sample the decreased lifetime with pressure is consistent with the increased radiative decay rate whereas the stronger variation observed in the heavily doped sample can only be explained by increased concentration quenching. The variations of the quenching rate and transition linewidths with hydrostatic pressure are more consistent with a model of energy migration quenching than one of cross-relaxation. However, they do not help to distinguish between randomly distributed quenching sites and surface quenching.

Acknowledgments

The part of this work performed at Oklahoma State University was sponsored by a grant from the US Army Research Office, and that done at Colorado State University by a grant from NASA Lewis Research Center.

References

Asaumi K, Kojima S and Nakamura T 1980 *J. Phys. Soc. Japan* **48** 1298
Auzel F 1976 *IEEE J. Quantum Electron.* QE-12 258
Blatte M, Danielmeyer H G and Ulrich R 1973 *Appl. Phys.* **1** 275
Drotning W D and Drickamer H G 1976 *Phys. Rev.* B **13** 4568, 4576, 4586, 4592
Flaherty J M and Powell R C 1979 *Phys. Rev.* B **19** 32
Huber G, Svassen K and Holzapfel W B 1977 *Phys. Rev.* B **15** 5123
Klick D I, Bieg K W and Drickamer H G 1977 *Phys. Rev.* B **16** 4599
Kruhler W W, Huber G and Danielmeyer H G 1975 *Appl. Phys.* **8** 261
Kushida T 1969 *Phys. Rev.* **185** 500
Lempicki A 1977 *Opt. Commun.* **23** 376
Lomheim T S and DeShazer L G 1978 *Opt. Commun.* **24** 89
Paetzold H K 1951 *Z. Phys.* **129** 123
Piermarini G J, Block S, Barnett J D and Forman R A 1975 *J. Appl. Phys.* **46** 2774
Powell R C, Neikirk D P, Flaherty J M and Gualtieri J G 1980a *J. Phys. Chem. Solids* **41** 345
Powell R C, Neikirk D P and Sardar D 1980b *J. Opt. Soc. Am.* **70** 486
Strek W, Szafranski C, Lukowiak E, Mazurak Z and Jezowska-Trzebiatowska B 1977 *Phys. Stat. Solidi* (a) **41** 547
Trlifaj M 1958 *J. Physique* **8** 510
Tyner C E and Drickamer H G 1977 *J. Chem. Phys.* **67** 4116
Weber H P 1975 *Opt. Quantum Electron.* **7** 431
Weber H P, Liao P F and Tofield B C 1974 *IEEE J. Quantum Electron.* QE-10 563
Webster G A and Drickamer H G 1980 *J. Chem. Phys.* **72** 3730, 4661
Yu S C, Liu C Y, Spain I L and Skelton E F 1979 in *High-Pressure Science and Technology* vol 1, ed K D Timmerhaus and M S Barber (New York: Plenum) p 274

VOLUME 46, NUMBER 15 PHYSICAL REVIEW LETTERS 13 APRIL 1981

[6]J. C. Bruyère, A. Deneuville, A. Mini, J. Fontenille, and R. Danielou, J. Appl. Phys. 51, 2199 (1980).
[7]F. K. Zellama, P. Germain, S. Squelard, B. Bourdon, J. Fontenille, and R. Danielou, to be published.
[8]J. C. Knights and R. A. Lujan, Appl. Phys. Lett. 35, 244 (1979).
[9]T. Shimada, Y. Katayama, and K. F. Komatsubara, J. Appl. Phys. 50, 5530 (1979).
[10]A. Madan, S. R. Ovshinsky, and E. Benn, Philos. Mag. 40, 259 (1979).

Measurement of Exciton Diffusion Lengths in $Nd_xLa_{1-x}P_5O_{14}$ by Four-Wave Mixing Techniques

Christopher M. Lawson and Richard C. Powell
Physics Department, Oklahoma State University, Stillwater, Oklahoma 74078
and
Walter K. Zwicker
Philips Laboratories, Briarcliff Manor, New York 10510
(Received 21 November 1980)

Transient four-wave mixing techniques have been used to measure the decay rate of the excited-state population grating in $Nd_xLa_{1-x}P_5O_{14}$ samples as a function of grating spacing. The results show that at room temperature there is diffusive energy migration over distances of the order of 0.36 μm in the highly concentrated samples.

PACS numbers: 78.20.-e

Degenerate four-wave mixing (FWM) spectroscopy has been shown recently to be a powerful method for studying spatial migration without spectral transfer of electronic excitation energy in solids.[1-4] This technique has been used to determine the diffusion coefficient of molecular excitons in organic solids,[1] but attempts to make similar measurements on Frenkel excitons in inorganic materials have resulted only in placing an upper bound on the diffusion coefficient because the migration is too short to observe in the samples which have been studied.[2-4] We report here the results of FWM measurements on single crystals of $Nd_xLa_{1-x}P_5O_{14}$ at room temperature. The presence of energy migration is easily observed and it is found to be diffusive with a migration distance of the order of 0.36 μm. These results are of significant importance since they represent an unambiguous determination of the range of energy migration in this class of stoichiometric materials used as "minilasers" for low-threshold, high-gain applications.[5,6] The mechanism causing concentration quenching of the fluorescence in these materials is not understood but it is known to have quite different properties from other neodymium laser materials.[5] This is not only an interesting fundamental physics question, but it is also important in material development for laser applications. The contribution of energy migration to concentration quenching in neodymium pentaphosphate has been the subject of significant interest and some controversy, with estimates of migration lengths ranging from a few angstroms to a few microns.[7-10] These FWM results provide an answer to one of the fundamental questions surrounding this controversy.

The samples used for this investigation were cleaved from high-quality single crystals grown by the technique described recently.[16] Several different experimental arrangements have been used to establish and probe population gratings of excited states. A schematic diagram of the setup used for this work is shown in Fig. 1. The 5145-Å line of an argon laser was used since it falls on one edge of a Nd^{3+} absorption line. The absorption of this light by the Nd^{3+} ions in the sample creates a spatial distribution of excited states with a sinusoidal pattern of wavelength $\Lambda = \lambda/\theta$, where θ is the crossing angle of the write beams and λ is the wavelength of the light in the sample. This "population grating" can cause the probe beam to be scattered with the maximum scattering efficiency occurring when the Bragg condition is satisfied.

Figure 2 shows the results from measuring the decay rate K of the scattered probe beam as a function of the square of the crossing angle of the write beams for single crystals of NdP_5O_{14} and

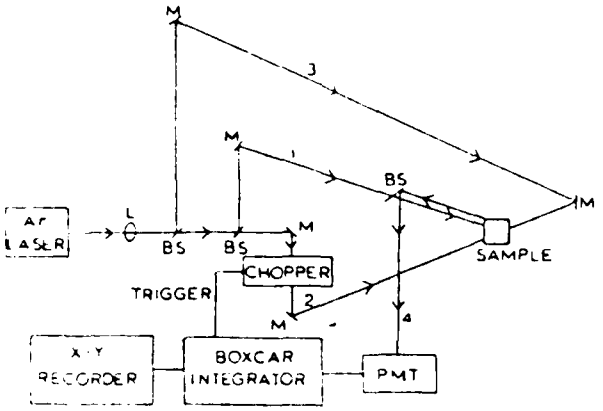

FIG. 1. Experimental setup for transient four-wave mixing measurements. 1 and 2, the write beams; 3, the incident probe beam; and 4, the scattered probe beam.

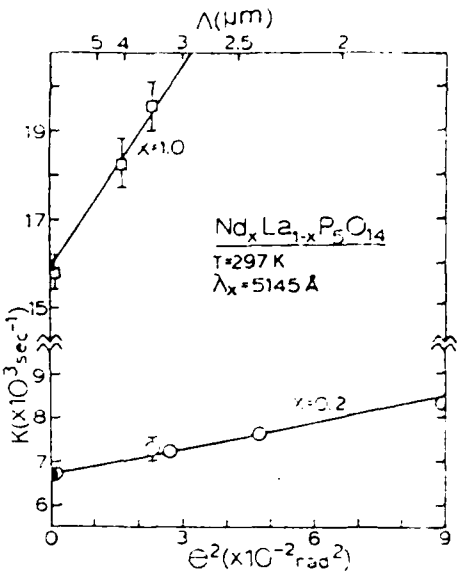

FIG. 2. Measured decay rates of the scattered probe beam for NdP_5O_{14} and $Nd_{0.2}La_{0.8}P_5O_{14}$ crystals at room temperature for various values of the crossing angle of the write beams. The filled points are twice the measured fluorescence decay rates and the straight lines represent the predictions of Eq. (4).

$Nd_{0.2}La_{0.8}P_5O_{14}$ at room temperature. The decay curves were found to be exponential and the data points shown in the figure represent the average obtained from repeating the measurements numerous times at the same crossing angle. The error bars represent the spread in the data acquired at each point. The increase in background "noise" due to extraneous light scattering and the decrease in probe beam transmission caused the data obtained on the heavily concentrated sample to be less accurate than that obtained on the 20% Nd sample.

For both of the samples investigated, the probe beam decay rate increases approximately linearly with increasing values of θ^2. This can be related directly to the mechanisms responsible for the destruction of the population grating. This grating can be destroyed both by the decrease in the excited-state population by normal fluorescence decay and by the migration of excited states (excitons) from the peak to the valley regions of the grating. If the exciton motion is diffusive the time evolution of the spatial distribution of the excited-state population $n(x, t)$ is given by the one-dimensional diffusion equation[1]

$$\partial n(x, t)/\partial t = D\partial^2 n(x, t)/\partial x^2 - \tau^{-1} n(x, t), \qquad (1)$$

where D is the diffusion coefficient and τ is the fluorescence decay time. For the initial condition of a sinusoidal spatial distribution of $n(x, 0)$ in the x direction, the solution of Eq. (1) is

$$n(x, t) = \tfrac{1}{2} e^{-t/\tau}\{1 + \exp[-(2\pi/\Lambda)^2 Dt]\cos(2\pi x/\Lambda)\}. \qquad (2)$$

The scattering efficiency is proportional to the depth of the grating.[17,18] This leads to the expression for the diffracted probe-beam intensity

$$I_s(t) = I_p(I_e \Delta n)^2 = I_p I_e^2 e^{-Kt}, \qquad (3)$$

where

$$K = 2[(2\pi/\Lambda)^2 D + \tau^{-1}] = (8\pi^2 D/\lambda^2)\theta^2 + 2\tau^{-1}. \qquad (4)$$

Here I_p is the probe beam intensity in the absence of scattering and I_e is the write beam intensity. Both λ and θ have been corrected for the index of refraction of the sample.

The theory outlined above predicts that in the presence of diffusive exciton migration the measured scattered probe-beam intensity will decay exponentially with a decay rate which increases linearly with θ^2. These predictions are consistent with the experimental results obtained on the $Nd_xLa_{1-x}P_5O_{14}$ crystals. The solid lines in Fig. 2 represent the fit of the theoretical expression in Eq. (4) to the experimental data. The intercepts of these lines should be $2/\tau$ and their slopes can be used to determine values of D. Table I lists the measured fluorescence lifetimes for these samples and they are used to plot the solid points shown in Fig. 2 at $\theta^2 = 0$. The theoretical lines extrapolate nicely to these points. Table I also

TABLE I. *Exciton diffusion parameters for* $Nd_xLa_{1-x}P_5O_{14}$ *crystals.*

Sample (x)	τ (μsec)	D (cm^2/sec)	l_x (μm)
0.2	300	6.85×10^{-7}	0.20
1.0	125.3	5.09×10^{-6}	0.36

lists the calculated diffusion coefficients for these samples. The average displacement of an exciton along the grating directions in its lifetime is given by $l_x=(2D\tau)^{1/2}$. The values for this one-dimensional exciton diffusion length for the two pentaphosphate samples are listed in Table I.

The results reported here were all obtained with the laser beams incident on the *b* plane (cleavage plane) of the crystal and with the sample oriented to measure diffusion in approximately the *a* direction. Although some changes in the results were observed when the sample was rotated to different orientations, this experiment is so sensitive to precise alignment that it is not clear at this point whether the observed changes are due to anisotropy in the exciton diffusion or simply a slight misaligning of the experiment. The question of orientation dependence of D will be thoroughly investigated in the future. At high "probe-beam" intensities a double exponential decay was observed with a faster initial decay rate. At angles larger than those reported in Fig. 2 this fast-decay component dominated the detected signal even at smaller probe-beam intensities and thus limited the range of grating spacings available for study. The decay rate of the fast signal is independent of the crossing angle of the "write beams" and does not extrapolate to $2/\tau$ and thus is not directly associated with the "population grating." There are several other sources of refractive index gratings in crystals due to different types of nonlinear optical interactions and it is not surprising that other interference effects are present in a birefringent, ferroelastic crystal such as $Nd_xLa_{1-x}P_5O_{14}$. In this paper we focus our attention on the properties of the population grating and plan to study the characteristics of other types of gratings in future investigations. It should be pointed out that thermal gratings can also be studied by this technique and that the thermal diffusion coefficients are of the same order of magnitude as those reported here. We can be sure that the diffusion coefficients reported are not due to thermal diffusion since the observed decay rates extrapolate to twice the fluorescence decay rates and the value of D varies significantly with Nd concentration. Neither of these characteristics is true for thermal gratings.

One important aspect of characterizing energy migration is identifying the microscopic nature of the interaction causing the motion. A rough approximation for the diffusion coefficient of an exciton undergoing an incoherent random walk resulting from electric dipole-dipole interaction is[10]

$$D=\tfrac{1}{2}(\tfrac{4}{3}\pi N_s)^{4/3}R_0^{\,6}/\tau_0, \tag{5}$$

where N_s is the sensitizer concentration, τ_0 is the intrinsic fluorescence lifetime, and R_0 is the "critical interaction distance." For NdP_5O_{14}, $N_s=4\times10^{21}$ cm^{-3} and, if concentration quenching is attributed to energy migration, $\tau_0=350$ μs. Use of these values and the measured value of D in Eq. (5) gives $R_0=45$ Å. Although this is extremely high, compared with typical values for R_0 in lightly doped solids, it is consistent with the theoretically predicted value R_0 in a stoichiometric crystal such as NdP_5O_{14} if resonant interaction between ions in identical sites with small homogeneous linewidths is assumed.[12] Also, Eq. (5) predicts that the diffusion coefficient should vary as the $\frac{4}{3}$ power of the concentration, which is consistent with the results given in Table I. In addition, it should be noted that the electric dipole-dipole interaction has a long enough range to overcome any structural anisotropy.[5]

These FWM results show that at room temperature in NdP_5O_{14}, excitons diffuse over an average distance of 0.36 μm in a specific direction. The relatively long range of the exciton diffusion measured here disagrees strongly with several of the previously published results.[6, 11, 15] However, it should be noted that the authors of Ref. 15 have obtained more recent results in agreement with those reported here.[5] It is not clear why the results of Weber and co-workers[6, 11] are in contradiction to the present results, but one source of difference may be the greatly improved quality of the large-size crystals now available for study.[16] Although the results reported here do not give direct information concerning the mechanism of concentration quenching, they do show the presence of long-range energy migration and thus it is quite possible for exciton diffusion and trapping to play an important role in the quenching process. The complete theoretical characterization of energy transfer in $Nd_xLa_{1-x}P_5O_{14}$ must await further experimental results and this investigation is presently being extended to several other

samples with different Nd^{3+} concentrations in order to establish the concentration dependence of the diffusion parameters, which can then be compared to the variation of the quenching rate. Also, these experiments will be extended to low temperatures to see whether any coherent contribution to the exciton migration can be detected.[20]

This work was supported by the U. S. Army Research Office.

[1]J. R. Salcedo, A. E. Siegman, D. D. Dlott, and M. D. Fayer, Phys. Rev. Lett. 41, 131 (1978).
[2]H. J. Eichler, J. Eichler, J. Knof, and Ch. Noack, Phys. Status Solidi (a) 52, 481 (1979).
[3]D. S. Hamilton, D. Heiman, J. Feinberg, and R. W. Hellwarth, Opt. Lett. 4, 124 (1979).
[4]P. F. Liao, L. M. Humphrey, D. M. Bloom, and S. Geschwind, Phys. Rev. B 20, 4145 (1979); P. F. Liao and D. M. Bloom, Opt. Lett. 3, 4 (1978).
[5]H. G. Danielmeyer, in *Festkörperprobleme*, edited by H. J. Queisser (Pergamon, New York, 1975), Vol. 15, p. 253.
[6]H. P. Weber, Opt. Quantum Electron. 7, 431 (1975).
[7]S. Singh, D. C. Miller, J. R. Potopowicz, and L. K. Shick, J. Appl. Phys. 46, 1191 (1975).
[8]W. Strek, C. Szafranski, E. Lukowiak, Z. Mazurak, and B. Jezowska-Trzebiatowska, Phys. Status Solidi (a) 41, 547 (1977).
[9]B. C. Tofield, H. P. Weber, T. C. Damen, and P. F. Liao, J. Solid State Chem. 12, 207 (1975).
[10]M. Blätte, H. G. Danielmeyer, and R. Ulrich, Appl. Phys. 1, 275 (1973).
[11]P. F. Liao, H. P. Weber, and B. C. Tofield, Solid State Commun. 16, 861 (1973).
[12]J. M. Flaherty and R. C. Powell, Phys. Rev. B 19, 32 (1979).
[13]F. Auzel, D. Meichenin, and J. C. Michel, J. Lumin. 18/19, 97 (1979).
[14]S. J. Nettel and A. Lempicki, Optics Commun. 30, 387 (1979).
[15]G. Huber, J. P. Jeser, W. W. Krühler, and H. G. Danielmeyer, IEEE J. Quantum Electron. 10, 766 (1974).
[16]R. D. Plättner, W. W. Krühler, W. K. Zwicker, T. Kovats, and S. R. Chinn, J. Cryst. Growth 49, 274 (1980).
[17]H. Kogelnik, Bell System Tech. J. 48, 2909 (1969).
[18]A. E. Siegman, J. Opt. Soc. Am. 67, 545 (1977).
[19]Th. Förster, Ann. Phys. (Paris) 2, 55 (1948).
[20]Y. M. Wong and V. M. Kenkre, Phys. Rev. B 22, 3072 (1980); V. M. Kenkre, Phys. Rev. 13, 3064 (1976).

5*f*-Electron Localization in Uranium Compounds

Wolf-Dieter Schneider and Clemens Laubschat
Institut für Atom- und Festkörperphysik, Freie Universität Berlin, D-1000 Berlin 33, Germany
(Received 17 December 1980)

Observed 7-eV satellites in the x-ray–photoemission spectra of UGa_2 and other *B*-group compounds are shown to be due to two-hole final states as confirmed by existing Auger data. The presence of these satellites is an indication for a weak *fd* hybridization and, when compared to uranium–transition-metal compounds, increased 5*f* localization.

PACS numbers: 71.70.Ms, 79.60.Cn

The nature of the 5*f* electrons in the actinides has attracted much attention both from the experimental and the theoretical point of view. For α-U metal it has been shown recently that the 5*f* electrons have primarily itinerant character.[1] The degree of 5*f* localization depends on the overlap of the corresponding 5*f* wave functions on neighboring atoms and on the 5*f*-6*d* hybridization. Since in uranium compounds the interatomic U-U distance and the bonding properties are changed as compared to α-U, a change in the degree of the localization can be expected.

X-ray photoemission spectroscopic (XPS) investigations on uranium compounds with *B*-group elements have shown a characteristic satellite structure at 7 eV higher binding energy of the U 4*f* core-level spectra (see Table I). The only serious attempt to explain these structures has been made for UO_2 where this satellite has been attributed to a shakeup process from the oxide-derived *p* band to unoccupied 5*f* states.[2,3]

In this Letter we show that, in the XPS spectra of the intermetallic compound UGa_2, a similar structure exists for the U 4*f* as well as for the U 5*f* levels (we note that even the valence bands of UO_2 show such a structure, which has been interpreted as belonging to the O 2*p* band[3]). In UGa_2 this structure cannot be explained by a

IV. ENERGY TRANSFER IN SEVERAL NEODYMIUM DOPED LASER MATERIALS

The following three sections describe the results of studies of energy transfer in three different types of Nd^{3+} doped laser materials. Section IV.1 describes the work done on YVO_4 crystals including both host sensitized energy transfer and site-selection spectroscopy studies. The manuscript in Section IV.2 describes energy migration amoung Nd^{3+} ions in neodymium aluminum borate crystals using time-resolved site-selection spectroscopy techniques. The manuscript in Section IV.3 discusses the results obtained on energy migration among neodymium ions in four different types of glass hosts. Of special interest are the results obtained as a function of temperature in this latter study.

Energy transfer processes in $YVO_4:Nd^{3+}$

Dhiraj Sardar and Richard C. Powell
Physics Department, Oklahoma State University, Stillwater, Oklahoma 74074

(Received 11 January 1980; accepted for publication 31 January 1980)

Laser-excited, time-resolved spectroscopy techniques were used to investigate the characteristics of energy transfer in $YVO_4:Nd^{3+}$ crystals. The temperatuare and time dependencies of the energy transfer rates were determined for both host-sensitized and impurity ion interaction processes. The former process is found to have characteristics consistent with the migration and trapping of localized host excitons whereas the latter process is consistent with multistep energy migration via a two-phonon-assisted electric dipole-dipole interaction mechanism.

PACS numbers: 78.20. – e, 78.40. – q, 78.50.Ec

I. INTRODUCTION

Yttrium orthovanadate (YVO_4) is an important material for applications in various types of optical systems. It is useful as an infrared polarizer, and a host for rare-earth phosphors and lasers.[1-5] In fact, $YVO_4:Nd^{3+}$ laser crystals have been found to have some performance characteristics superior to those of standard YAlG:Nd^{3+} lasers.[5] Because of the significant potential of this material it is important to characterize and understand the fundamental physical processes underlying its optical properties. We describe here the results of an investigation of processes of energy transfer in $YVO_4:Nd^{3+}$ crystals.

The general spectroscopic properties of undoped YVO_4, and YVO_4 doped with Eu^{3+}, Er^{3+}, and Nd^{3+} ions have been investigated.[1-10] Host-sensitized energy transfer has been studied in samples doped with Eu^{3+} and Er^{3+} ions.[6] This process is especially important in applications as a rare-earth phosphor material but also can be useful in enhancing the pumping of a laser material. The process of energy transfer between impurity ions in YVO_4 has been investigated[7] for Eu^{3+}. This process can be important in concentration quenching in luminescent materials and in the operational characteristics of lasers. We have characterized both host-sensitized energy transfer and ion-ion interaction in $YVO_4:Nd^{3+}$ and the results are compared to those obtained previously on yttrium vanadate samples containing other trivalent rare-earth ions.

In addition to the practical importance of the information obtained in this work, the results enhance our general understanding of the fundamental proceses of energy transfer in optical materials. The model used to interpret the data obtained on host-sensitized energy transfer is one involving exciton migration and trapping which has recently been applied[6] to inorganic "molecular" crystals such as YVO_4. The model employed to explain energy transfer between Nd^{3+} ions in this host is based on one of the new two-photon-assisted interaction processes developed recently to interpret high-resolution laser spectroscopy data.[11] In both of these areas only a few experimental investigations have been carried out and further work is necessary to develop a complete understanding of these energy transfer processes.

The single crystal samples of $YVO_4:Nd^{3+}$ were investigated. One had a doping concentration of 2% (2.55×10^{20} cm^{-3}) and the other 3% (3.82×10^{20} cm^{-3}).

The experimental technique of laser time-resolved spectroscopy was employed for investigating the properties of energy transfer. A block diagram of the experimental apparatus is shown in Fig. 1. The samples were mounted in a cryogenic refrigerator for controlling the temperature. For studying host-sensitized energy transfer a pulsed nitrogen laser was used to excite the sample whereas for direct excitation of the Nd^{3+} impurity ions a tunable dye laser containing rhodamine 6G and pumped by the nitrogen laser was used. In both cases the excitation pulses were less than 10 nsec in duration. The half width of the dye laser pulse was less than 0.4 Å. The sample fluorescence was analyzed by a 1-m spectrometer, detected by a cooled RCA C31034 photomultipler tube, averaged by a boxcar integrator triggered by the laser, and displayed on a strip-chart recorder.

II. HOST-SENSITIZED ENERGY TRANSFER

The absorption edge of YVO_4 crystals occurs at about 3400 Å and the fluorescence emission appears as a broad band peaked near 4500 Å. Although some thermal quench-

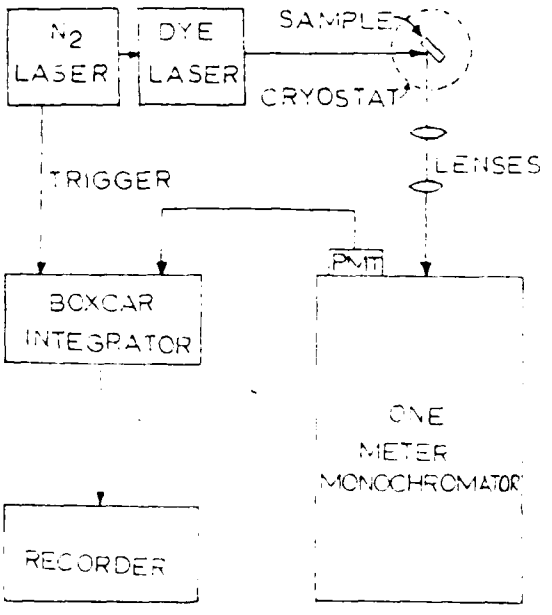

FIG. 1. Time-resolved spectroscopy apparatus

 0021-8979/80/052829-07$01.10

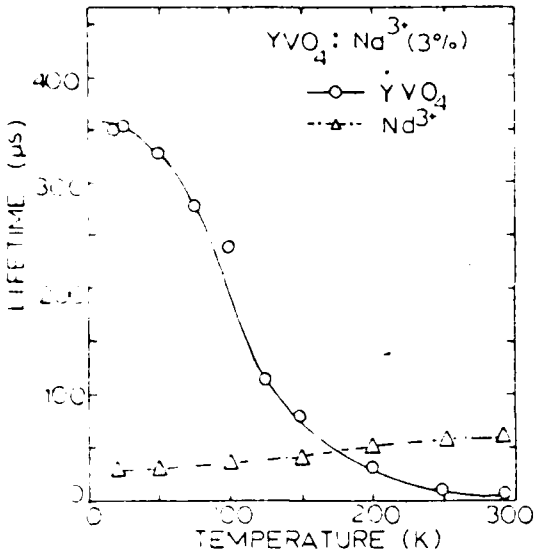

FIG. 2. Temperature dependences of fluorescence lifetime of $YVO_4:Nd^{3+}$ (3%) after excitation with a pulsed N_2 laser.

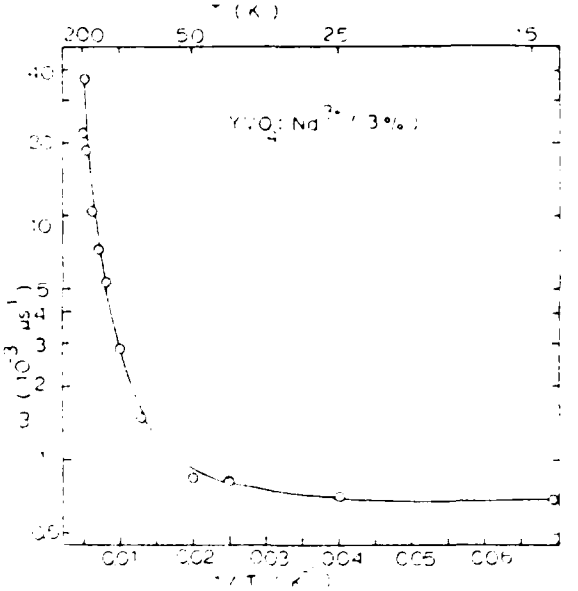

FIG. 3. Temperature dependence of the host-sensitized energy transfer rate for $YVO_4:Nd^{3+}$ (3%). (See text for explanation of the theoretical line.)

ing occurs in this material, it still fluoresces quite efficiently at room temperature. The yttrium vanadate host crystals were excited with pulses from the nitrogen laser at 3371 Å and energy transfer to Nd^{3+} impurity ions was studied by monitoring the fluorescence spectrum at different times after the excitation pulse and by measuring the fluorescence decay times as a function of temperature. The fluorescence decay times for the host and Nd^{3+} emissions are shown as a function of temperature in Fig. 2 for the 3% sample. The decay time of $^4F_{3/2}$ metastable state of Nd^{3+} shows very little temperature dependence. The values of the measured decay times are less than the radiative decay time[8] of 152 μs which indicates that some radiationless quenching is taking place. This is not surprizing at these relatively high levels of Nd^{3+} concentrations. The host fluorescence lifetime of the doped sample exhibits the same temperature dependence as the undoped sample but the magnitudes of the lifetimes are smaller at each temperature due to energy transfer.[6] The rate of energy transfer ω can be derived from this lifetime quenching as

$$\omega = \tau_H^{-1} - (\tau_H^0)^{-1}, \tag{1}$$

and this is shown plotted as a functionof $1/T$ in Fig. 3. As seen from Fig. 3, the transfer rate is approximately constant at low temperatures and increases exponentially above about 75 K. The activation energy for this increase in rate is about 250 cm^{-1}.

The fluorescence spectra at two different times after the laser pulse are shown in Fig. 4. The sharp line Nd^{3+} emission increases with respect to the broad band host fluorescence as a function of time after the laser pulse. Figure 5 shows plots of the ratios of the integrated fluorescence intensities of the Nd^{3+} and host fluorescence emissions at two temperatures. These time-resolved spectroscopy (TRS) data can be interpreted using the model shown in Fig. 6. n_H and n_I represent the concentration of excited states of the host and impurity ions, respectively, while B_H and B_I are their fluorescence decay rates. W is the rate of creation of host excited states and ω is the energy transfer rate. The rate equations describing the time evolution of the excited state populations are

$$dn_H/dt = W - B_H n_H - \omega n_H, \tag{2}$$

$$dn_I/dt = \omega n_H - B_I n_I. \tag{3}$$

These can be solved by assuming a delta function excitation pulse. The ratios of the excited state populations obtained in this way are proportional to the observed fluorescence intensity ratios with the proportionality constant involving the ratio of the radiative decay rates. Solutions to these equations were obtained for two cases: a time-independent energy transfer rate, and an energy transfer rate which varied as

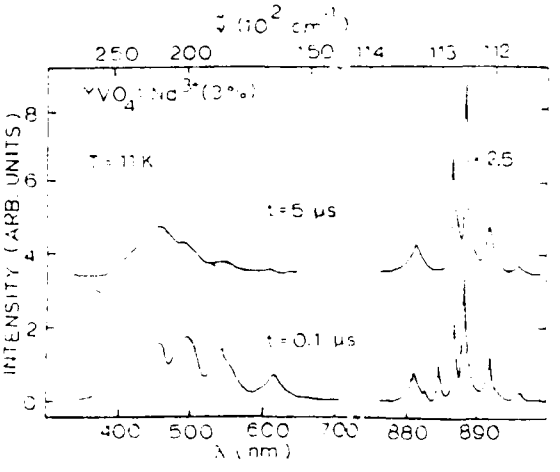

FIG. 4. Spectrum of $YVO_4:Nd^{3+}$ (3%) at two times after the laser excitation pulse.

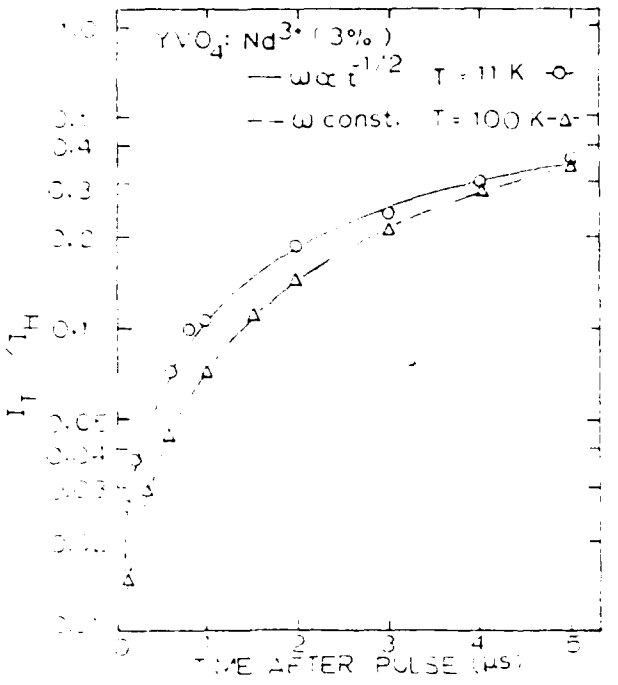

FIG. 5. Ratios of the integrated fluorescence intensities of the Nd^{3+} and immediate emissions as a function of time after the laser pulse for YVO_4:Nd^{3+} (3%). (See text for explanation of the theoretical lines.)

$t^{-1/2}$. Then the magnitude of the energy transfer rate and the proportionality constant K were treated as adjustable parameters and the theoretical solutions were fitted to the TRS data.

It was found that at low temperatures the theoretical predictions for a constant energy transfer rate could not give a good fit to the data whereas the solid line giving the good fit to the data shown in Fig. 5 was obtained using the time-dependent energy transfer rate. In this case the theoretical expression is given by

$$I_T/I_H = K\left[\exp\left((B_H - B_T)t + 2\omega t^{1/2} - \frac{\omega}{(B_H - B_T)t^{1/2} + \omega}\right)\right], \tag{4}$$

where

$$\omega = \tfrac{4}{3}\pi^{3/2} R_0^3 C_T (\tau_H^0 t)^{1/2}. \tag{5}$$

This expression describes the rate of energy transfer by a single-step electric dipole-dipole interaction where C_T is the concentration of Nd^{3+} ions and R_0 is the critical interaction distance. Using the measured value of the host fluorescence decay time in the undoped sample τ_H^0 and the value of ω obtained from fitting the experimental TRS data at 11 K gives a value of 14.6 Å for R_0. A theoretical prediction for R_0 can be obtained from the expression

$$R_0 = [5.86 \times 10^{-25} \Omega \phi_H^0/(n\bar{\nu}_a)^4]^{1/6}, \tag{6}$$

where ϕ_H^0 is the quantum efficiency of the sensitizer, Ω is the overlap integral of the absorption spectrum of the neodymium ions and the emission spectrum of the host, n is the index of refraction, $\bar{\nu}_a$ is the average wave number in the region of spectral overlap, and the numerical factor is for unit consistency and includes a factor of $\frac{2}{3}$ for the average angular dependence of randomly oriented dipoles. The overlap integral is found from spectral data to be $\Omega = 7.3 \times 10^{-21}$ l/mol cm. Using this value along with $\bar{\nu}_a = 2.0 \times 10^4$ cm^{-1}, $\phi_H^0 = 0.54$, and $n = 1.53$ predicts a value of 5.5 Å for R_0.

At high temperatures (about 100 K and above) it was found that Eq. (4) no longer gave a good fit to the time-resolved spectroscopy data. Instead the best fit to the data was found by assuming a time-independent energy transfer rate. In this case the solutions to Eqs. (2) and (3) lead to

$$I_T/I_H = K' \frac{\omega'}{(B_H + \omega' - B_T)} \cdot \{\exp[(B_H + \omega' - B_T)t] - 1\}. \tag{7}$$

The dashed line in Fig. 5 represents the best fit to the data obtained by treating ω' and K' as adjustable parameters.

A constant energy transfer rate is indicative of a multistep energy migration process. This can be treated through either the mathematics of diffusion or random walk with the resulting energy transfer rates expressed as

$$\omega' = 4\pi D R_0 C_T p \tag{8a}$$

or

$$\omega' = V_m C_T C(A) t_H^{-1} p, \tag{8b}$$

respectively. Here D is the diffusion coefficient, R_0 is the trapping radius at the activator site, V_m is the volume per molecule, t_H is the excitation energy hopping time, $C(A)$ is the capacity of the random walk which reflects the size and shape of the trapping region, and p represents the probability of the host excitation energy being transferred to an activator after migration has occurred to a host site next to an activator. Since only one primary experimental parameter is obtained, (ω'), it is very difficult to separately determine the characteristics of the migration process and the trapping processes. The best way to do this is to compare the results obtained from similar experiments on the same type of host crystal with different types of activator traps keeping in mind that the migration properties of energy transfer should be the same for all samples with any differences in the data

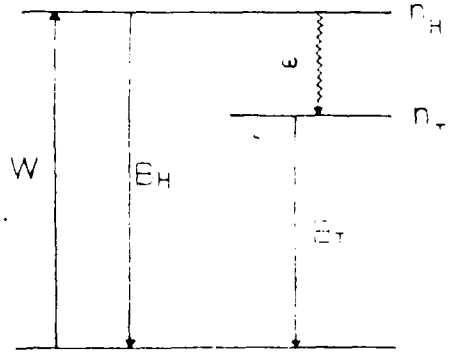

FIG. 6. Rate equation model for explaining host-sensitized energy transfer.

TABLE I. Comparison of the results obtained on YVO_4 samples containing Eu^{3+}, Er^{3+}, and Nd^{3+} ions as activators.

Parameters	$YVO_4:Nd^{3+}$ ($3.8\times10^{20}cm^{-3}$)	$YVO_4:Eu^{3+}$ ($1.27\times10^{19}cm^{-3}$)	$YVO_4:Er^{3+}$ ($1.27\times10^{20}cm^{-3}$)
R_0 (Å)	14	4	2
ΔE (cm^{-1})	250	156	1000
ω (sec^{-1})*	4.1×10^{4}	1.0×10^{4}	2.1×10^{5}
$C(4\pi r_0^3/3)$	2.40×10^{3}	1.75×10^{6}	3.68×10^{6}
DR_0/ρ	8.6×10^{-18}	6.27×10^{-17}	1.32×10^{-16}
ρ_0	1.0×10^{-3}	7.96×10^{-3}	1

*$T = 297$ K.

being attributable to different trapping characteristics of the various activators. Table I compares the results obtained on YVO_4 samples containing Eu^{3+}, Er^{3+}, and Nd^{3+} ions as activators.[6,7]

In order to compare the fundamental energy transfer properties in these three samples it is first necessary to adjust for the different thermal properties of the energy transfer rates. The same qualitative dependence as shown in Fig. 3 was observed in the other two samples but the measured activation energies are quite different as shown in Table I. This can be attributed to thermal effects being present in both the migration on trapping processes. Previous work on undoped YVO_4 crystals indicates that host energy migration occurs with the activation energy of about 625 cm^{-1} indicating that the differences between this number and the values of ΔE appearing in Table I are due to the need for absorbing or emitting phonons in the trapping process at the activator sites which can be accounted for as $\rho = \rho_0 \exp(+\Delta E/kT)$.

After adjusting the data to account for the different thermal characteristics of the trapping process there are two possible ways to interpret the results. The first is to assume that the trapping regions for the three types of activators are all the same size and the difference in the trapping characteristics is due to the factor ρ_0. Assuming a point trapping region[12] $C(4\pi r_0^3/3) = 0.659$ or assuming a trapping radius equal to the nearest neighbor Y-V distance of $R_0 = 3.15\times10^{-8}$ cm, the values obtained for ρ_0 are listed in Table I. In this case the random walk model predicts a hopping time of $t_h = 2.9\times10^{-8}$ sec and the diffusion model predicts that $D = 2.6\times10^{-8}$ cm^2 sec^{-1}. In the limit of many steps in the random walk the two models should predict the same results. This can be checked with the relationship

$$t_h = \alpha^2/(6D), \tag{9}$$

where α is the average stepping distance for the excitation energy. If this is taken to be the shortest V-V separation of 4.75 Å and the value of D obtained above is used, the hopping time is predicted to be 1.5×10^{-7} sec which is consistent with the value obtained from the random walk model. The number of steps in the random walk is given by

$$n = \tau_0/t_h, \tag{10}$$

which for the Nd-doped sample investigated here is 755.

The second possible interpretation of the data is that $\rho_0 = 1$ for all cases but the size of the trapping regions are

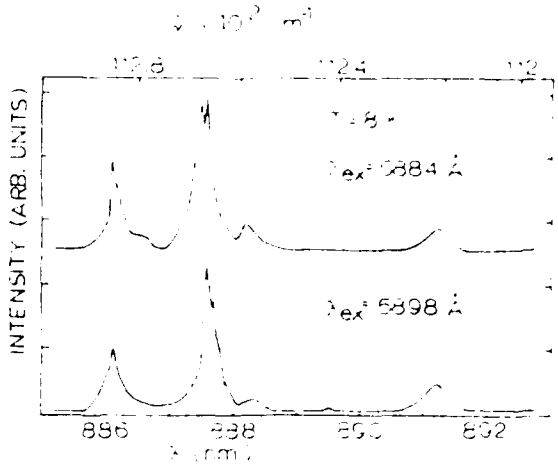

FIG. 7. Spectrum of Nd^{3+} in $YVO_4:Nd^{3+}$ (3%) for two wavelengths of laser excitation.

different for the three activators. However pursuing this line of reasoning leads to the conclusion that the trapping radius for Er^{3+} is of the order of 1830 Å which is unphysically large. It also predicts such a slow hopping time that only one step could take place in a random walk which is not consistent with the observed time-independent energy transfer rate. Thus we conclude that the first approach to interpreting the data is the correct one.

From the analysis of the data described above the diffusion length at room temperature is determined from

$$l = (2D\tau_H)^{1/2} \tag{11}$$

to be 8.8×10^{-5} cm. The diffusion coefficient can be expressed as $D = D_1 \exp(-\Delta E_a/kT)$ where ΔE_a is the activation energy for hopping. The value of D_1 is found to be 5.4×10^{-1} cm^2 sec^{-1}.

III. SITE-SELECTION SPECTROSCOPY

The Nd^{3+} ions can be directly excited with a dye laser using rhodamine 6G dye. When this is done structure can be observed in each of the spectral transitions due to the excitation of ions in different types of crystal field sites. This struc-

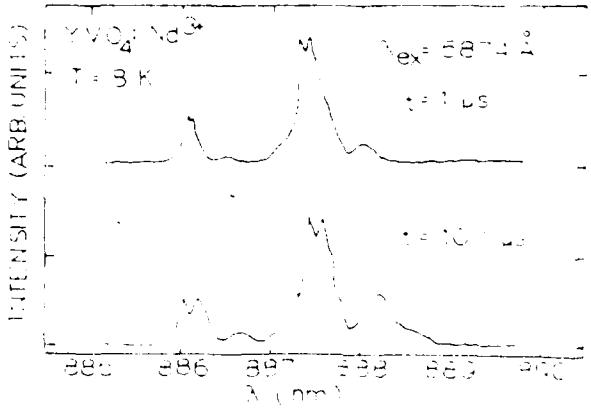

FIG. 8. Spectrum of Nd^{3+} in $YVO_4:Nd^{3+}$ (3%) at two times after the laser excitation pulse.

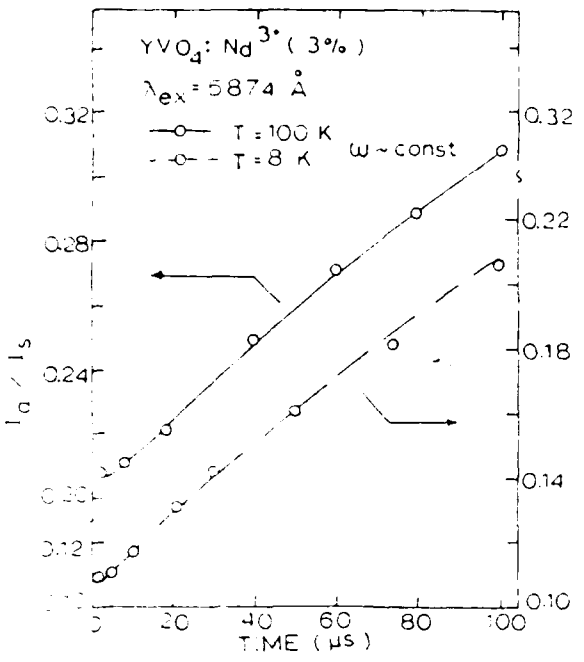

FIG. 9. Ratios of the integrated fluorescence intensities of sensitizer and activator Nd^{3+} ions as a function of time after the laser pulse for YVO_4: Nd^{3+} (3%). (See text for explanation of the theoretical lines.)

ture changes with laser wavelength due to the selective excitation of ions in different sites as shown in Fig. 7. Energy transfer takes place between Nd^{3+} ions and this can again be characterized through time-resolved spectroscopy techniques. Figure 8 shows a typical emission spectrum near 890 nm at two times after the excitation pulse. For both transitions shown, the high energy structure decreases and the low energy structure increases as a function of time after the laser pulse. Designing the high-energy structure as transitions due to ions in selectively excited "sensitizer" sites and the low energy structure as transitions due to ions in "activator" sites, energy transfer from sensitizers to activators can be characterized by plotting the ratio of the integrated fluorescence intensities as a function of time after the laser pulse. The results of doing this at low and high temperatures are shown in Fig. 9.

The solid lines in Fig. 9 represent the best theoretical fits to the data based on the model shown in Fig. 10. This is similar to the model used in Sec. II to analyze the host-sensitized energy transfer results except that direct excitation of the activators is allowed and no significant difference could be detected in the fluorescence lifetimes of the ions in the sensitizer and activator sites. The rate equations for the excited state populations in this model are given by

$$dn_s/dt = W_s - Bn_s - \omega_{sa} n_s, \tag{12}$$

$$dn_a/dt = W_a + \omega_{sa} n_s - Bn_a. \tag{13}$$

These can be solved assuming delta-function excitation and a specific time dependence for the energy transfer rate. It was found that the best fits to the data at all temperatures were obtained with time-independent energy transfer rates. For

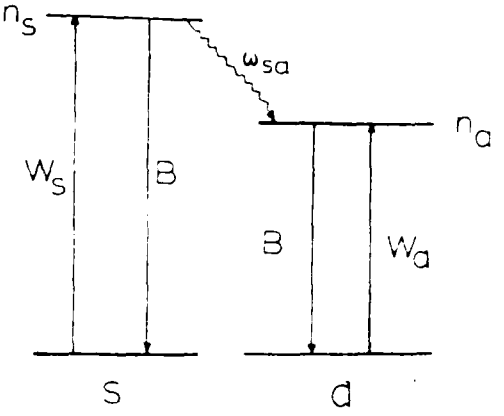

FIG. 10. Rate equation model for explaining energy transfer between Nd^{3+} ions in YVO_4.

this case the solutions to Eqs. (12) and (13) give

$$I_a/I_s = K''\{[n_a(0)/n_s(0) + 1]\exp(\omega_{sa} t) - 1\}, \tag{14}$$

where the radiative decay rates are assumed to be the same for sensitizers and activators. The solid lines in Fig. 9 represent the best fit to the experimental data obtained using Eq. (14) and treating ω_{sa} and K'' as adjustable parameters. The temperature dependence of the energy transfer rate can be obtained using Eq. (14) and measured fluorescence intensity ratios at short and long times after the excitation pulse. The results are shown in Fig. 11. The rate appears to be approximately constant at low temperatures and then increases significantly above about 25 K. The activation energy for this increase is found to be about 15 cm^{-1}. This is essentially the same as the crystal field splitting of the $^4F_{3/2}$ level in this system.

The temperature dependence described above is indicative of a two-phonon-assisted energy transfer process involving a real intermediate level.[11] In this case the energy trans-

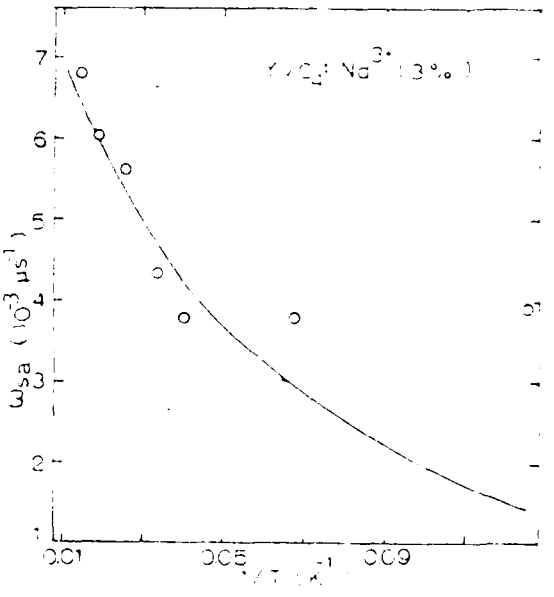

FIG. 11. Temperature dependence of the rate of energy transfer between Nd^{3+} ions in YVO_4: Nd^{3+} (3%). (See text for explanation of the theoretical line.)

TABLE II. Nd^{3+} → Nd^{3+} energy transfer parameters.

Parameters	YVO_4:Nd^{3+} (3.8×10^{20} cm^{-3})
C_1 (cm^{-1})	3.6×10^{-40}
C_2 (cm^{-1})	1.8×10^{-39}
ΔE_{aa} (cm^{-1})	1.6
ΔE_{ab} (cm^{-1})	7.9
δ (cm^{-1})	15
Γ (cm^{-1})	4.9
$J_1^2 R_{aa}^6$ (cm^4)	4.15×10^{-50}
$J_2^2 R_{ab}^6$ (cm^4)	9.41×10^{-50}
R_{ab} (cm)	8.56×10^{-8}
D (cm^{2}sec^{-1})	1.3×10^{-7}
τ_0 (μs)	6.3×10^{3}

[a] $T = 295$ K. [b] $T = 75$ K.

fer rate is given by[13]

$$W_{ab} = 71.6 C_1 C_2 R^{-6} (\Gamma/\hbar)[1 + \exp(\Delta E_{aa}/kT)]^{1/3} \cdot \left(\frac{J_1^2}{\Delta E_{aa}^2} + \frac{J_2^2}{4\Gamma^2}\right)^{1/3} \cdot \left(\frac{J_1^2}{\Delta E_{aa}^2} + \frac{2J_2^2}{\Delta E_{ab}^2 + 8\Gamma^2}\right)^{1/3} \exp(-\delta/kT), \quad (15)$$

where J_1 and J_2 are the ion-ion interaction strengths involving the initial and intermediate states, respectively, Γ is the width of the intermediate state, and δ is the energy of the phonon needed to change the ion from the initial to the intermediate state. In this case the intermediate state is the upper crystal field component of the $^4F_{3/2}$ level, so δ is 15 cm^{-1}. The width of this level is measured from the transition between it and the ground state to be 4.9 cm^{-1}. ΔE_{aa} is measured to be about 7.9 cm^{-1}. ΔE_{ab} is taken to be about one-third of the inhomogeneous linewidth of the sensitizer transition which is measured to be 1.6 cm^{-1}. This is consistent with previous results on garnet samples.[13] The squared matrix elements can be expressed in terms of Judd-Ofelt parameters as[14]

$$J^2 = \frac{(3)(e^2/R^6)^2}{(2J_a + 1)(2J_b + 1)} \left(\sum \Omega_\lambda \langle J_a \| U^{(\lambda)} \| J' \rangle^2\right) \cdot \left(\sum \Omega_\lambda \langle J_b \| U^{(\lambda)} \| J'' \rangle^2\right). \quad (16)$$

The summations over reduced matrix elements have been evaluated for the $^4F_{3/2}$ to $^4I_{9/2}$ transitions of Nd^{3+} in YVO_4 and are given by[5]

$$J_1^2 = 4.15 \times 10^{-50} R^{-6} \text{cm}^4, \qquad J_2^2 = 9.41 \times 10^{-50} R^{-6} \text{cm}^4, \quad (17)$$

where the population differences between the "a" and "b" components of the $^4F_{3/2}$ level have been taken into account. With these considerations, Eq. (15) predicts values for the energy transfer rate at different temperatures shown as a solid line in Fig. 11. This is in good agreement with the values obtained experimentally at high temperatures but predict smaller values for the energy transfer rates than those observed at low temperatures. The theoretical parameters for this model are summarized in Table II.

IV. DISCUSSION AND CONCLUSIONS

The results of the investigation of host-sensitized energy transfer in YVO_4:Nd^{3+} are consistent with the model proposed previously from studies of yttrium vanadate with other types of trivalent rare-earth impurities.[6,7] In this model the host excited state considered to be a charge transfer transition localized on a VO_4^{3-} molecular ion. This can be treated as a Frenkle exciton which is self-trapped at low temperature and undergoes thermally activated hopping among the other vanadate molecular ions at high temperatures. Previous work indicates that the mechanism responsible for the exciton hopping is exchange interaction and the large Stokes shift due to lattice relaxation in the excited state is the cause of the self-trapping at low temperatures. Table I compares some of the relevant model parameters obtained from studies of YVO_4 samples doped with Eu^{3+}, Er^{3+}, and Nd^{3+}. The trapping probability per visit to an activator site and the thermal activation energy for trapping are found to be significantly different for the samples with the three different impurity ions. The reason for the different trapping probabilities is not known but it should be noted that they increase with increasing number of 4f electrons and decreasing ionic radius. Additional activators in this host should be investigated to determine the relevance of this correlation.

At low temperatures where the excitons are self-trapped the results indicate that energy transfer to Nd^{3+} ions takes place by a single-step electric dipole-dipole interaction process. This is consistent with the results found from investigating Eu^{3+} and Er^{3+} doped samples.[6] In the previous cases the values of R_0 which characterize this process were found to be of the order of a few angstroms and in agreement with the predicitons of spectral overlap measurements. For the data described here for Nd-doped samples R was found to be significantly larger than for other activators and even larger than that predicted by spectral overlap considerations. The reason for this is not presently understood.

A previous site-selection spectroscopy investigation has been carried out on Eu^{3+} ions in YVO_4 crystals.[7] In that case it was found that the results were consistent with energy transfer by a single-step resonant electric dipole-dipole interaction process but the data analysis was complicated by having three distinct types of sites. The results obtained here are consistent with a multistep diffusion type of energy transfer with the mechanisms for diffutions and trapping both involving two-phonon-assisted processes. One reason for the significant difference in energy transfer characteristics for different impurity ions may be due to the much higher concentration of Nd^{3+} ions in the YVO_4:Nd^{3+} samples. The model used to explain these results is similar to that used for interpreting the results of similar investigation of Nd-doped garnet crystals.[13,15] The main difference in the models used for these two systems is that in the garnet hosts the intermediate state for the phonon-assisted energy transfer is the first level of the ground state manifold whereas for the yttrium vanadate host it is the upper component of the metastable state. The reason for this may be that the splitting of $^4F_{3/2}$ level is much smaller in YVO_4 crystals than it is in garnets.

It should be emphasized that the agreement between

theory and experiment at high temperatures, shown in Fig. 11, is quite good considering that there are no adjustable parameters in the theory. The poorer agreement at low temperatures indicates that other energy transfer processes are becoming important in this temperature range.

The origin of the different types of crystal field sites for the Nd^{3+} ions is not known but such site multiplicity has been observed in this system by previous investigators.[16] It is well known that a major problem with yttrium orthovanadate crystals is the presence of imperfections introduced during crystal growth. Chemical or structural defects located near to Nd^{3+} ions could result in nonequivalent sites. The sites which are selectively excited by the laser are the dominant types of sites for Nd^{3+} ions in the activator type of sites.

The value of D found here for energy migration among Nd^{3+} ions in YVO_4 is within the range of values between 10^{-9} and 10^{-14} found for other rare-earth ions in solids. The diffusion coefficient for energy migration among the Nd^{3+} ions is given by

$$D = 3.4C_1^{4/3}R_{ss}^6\left(J_1^2 + J_2^2\frac{2(\Delta E_{ss})^2}{(\Delta E_{ss})^2 + 8\Gamma^2}\right) \times [2\Gamma/\hbar(\Delta E_{ss})^2][1 + \exp(\Delta E_{ss}/kt)]\exp(-\delta/kT) \quad (18)$$

and is found to be 1.3×10^{-12} cm^2 sec^{-1} at 295 K. This is somewhat smaller in the vanadate host than in the garnet host due to the increased value inhomogeneous broadening of the transitions.

An attempt was also made to fit the data using a Monte Carlo computer simulation procedure[17] to account for the the fact that the Nd^{3+} "exciton" is hopping on a lattice of randomly distribution sites. A good fit to the data is shown in Fig. 9 for the 100 K data assuming a critical interacation distance of $R_0 = 23$ Å which is similar to the results obtained for Nd^{3+} ions in garnet hosts.

In conclusions, laser time-resolved spectroscopy techniques have been used to determine the characteristics of both host-sensitized energy transfer and energy migration among activator ions in YNO_4:Nd^{3+} crystals. Understanding these processes is of fundamental importance in the use of this material in laser and phosphor applications.

ACKNOWLEDGMENTS

This work was supported by the U.S. Army Research Office. The author are grateful to L.G. DeShazer for supplying us with the samples used in this work.

[1]A.K. Levine and F.C. Palilla, Appl. Phys. Lett. 5, 118 (1964).
[2]J.R. O'Conner, Appl. Phys. Lett. 9, 407 (1966).
[3]J.J. Rubin and L.G. VanUitert, J. Appl. Phys. 37, 2970 (1966).
[4]G. Blasse, Philips Res. Rep. 23, 344 (1968).
[5]P.P. Yaney and L.G. DeShazner, J. Opt. Soc. Am. 66, 1405 (1976).
[6]C. Hsu and R.C. Powell, J. Lumin. 10, 273 (1975); G.E. Venikouas and R.C. Powell, J. Lumin. 16, 29 (1978).
[7]G.E. Venikouas and R.C. Powell, Phys. Rev. B 17, 3456 (1978).
[8]T.S. Lomheim and L.G. DeShazer, J. Appl. Phys. 49, 5517 (1978).
[9]J.G. Sliney, K.M. Leung, M. Birnbaum, and A.W. Tucker, J. Appl. Phys. 50, 3778 (1979).
[10]C. Brecher, H. Samelson, A. Lempicki, R. Riley, and T. Peters, Phys. Rev. 155, 178 (1978).
[11]T. Holstein, S.K. Lyo, and R. Orbach, Phys. Rev. Lett. 36, 891 (1976).
[12]Z.G. Soos and R.C. Powell, Phys. Rev. B 6, 4035 (1972).
[13]L.D. Merkle and R.C. Powell, Phys. Rev. B 20, 75 (1979).
[14]T. Kushida, J. Phys. Soc. Jpn. 34, 1318 (1973); 34, 1327 (1973); 34, 1334 (1973).
[15]M. Zokai, R.C. Powell, G.R. Imbusch, and B. DiBartolo, J. Appl. Phys. 50, 5930 (1979).
[16]Kh. S. Bagdasarov, G.A. Bogomolova, A.A. Kaminskii, and V.I. Popov, Sov. Phys. Dokl. 13, 516 (1968).
[17]H.C. Chow and R.C. Powell, Phys. Rev. (to be published).

Journal of Luminescence 22 (1981) 349 - 358
North-Holland Publishing Company

TIME-RESOLVED SITE-SELECTION SPECTROSCOPY STUDIES OF $NdAl_3(BO_3)_4$ CRYSTALS

Dhiraj K. SARDAR and Richard C. POWELL

Physics Department, Oklahoma State University, Stillwater, Oklahoma 74078, USA

Original manuscript received 30 May 1980
Revised manuscript received 8 December 1980

A pulsed, tunable dye laser was used to selectively excite Nd^{3+} ions in nonequivalent crystal field sites in $NdAl_3(BO_3)_4$ crystals and energy transfer between ions in different types of sites was studied by monitoring the time evolution of the fluorescence spectrum. The results show that the energy transfer rate varies as $t^{-1/2}$ and increases with temperature. The predictions of various models of phonon-assisted energy transfer are compared to the results.

1. Introduction

Neodymium aluminum borate, $NdAl_3(BO_3)_4$, is one of the several "stoichiometric laser materials" which have gained recent interest due to their use in minilaser applications [1,2]. In these materials a high concentration of Nd^{3+} ions can be present (5.43×10^{21} cm^{-3} for $NdAl_3(BO_3)_4$) without strong concentration quenching of the fluorescence emission. Since these materials are relatively new, there are still many aspects of their physical properties that are not well characterized and understood.

$NdAl_3(BO_3)_4$ (NAB) has a complex crystal structure with marked deviation from inversion symmetry and significant isolation of the Nd polyhedra [3,4]. The strong odd-parity crystal field admixture of the f and d configurations results in a short radiative lifetime and the highest cross section of any Nd material. Although laser action has been observed in NAB, the spectroscopic properties of the material have not been well characterized [5,6]. One property of special interest which has not been investigated is the interaction between Nd^{3+} ions which may lead to fluorescence quenching.

We report here the results of a study of energy transfer among Nd^{3+} ions in NAB crystals. Time-resolved site-selection spectroscopy techniques were employed to determine the magnitude, time dependence, and temperature dependence of the rate of energy transfer between Nd^{3+} ions in nonequivalent types of crystal field sites. Several possible interpretations of the results are discussed.

0022-2313/81/0000-0000/$02.50

2. Experimental techniques

The samples consisted of small single crystal pieces of $NdAl_3(BO_3)_4$. These were mounted on the cold finger of a cryogenic refrigerator capable of varying the temperature from about 10 K up to room temperature. A block diagram of the experimental apparatus is shown in fig. 1. A nitrogen laser-pumped tunable dye laser was used to excite the sample. Using rhodamine 6G, a pulse of less than 10 ns in duration and about 0.4 Å halfwidth was obtained. The sample fluorescence was focused onto the entrance slit of a one-meter monchromator and detected by a cooled RCA C31034 photomultiplier tube. The signal was averaged by a boxcar integrator triggered by the laser so that either the lifetimes or the fluorescence spectra at different times after the excitation pulse could be recorded.

The wavelength of the dye laser excitation light was approximately 5920 Å which is absorbed in one of the higher excited states of the Nd^{3+} ions. After relaxation of the $^4F_{3/2}$ metastable state, the emission to the various components of the $^4I_{9/2}$ ground state manifold was monitored. The lifetime of fluorescence was found to be 20 μs and independent of temperature between 10 and 295 K.

The fluorescence spectrum of $NdAl_3(BO_3)_4$ at 11 K in the region from 8780 to 8940 Å is shown in fig. 2 for two different excitation wavelengths. The lines from each transition exhibit a significant amount of structure and the dominant structural components vary significantly with excitation wavelength. The

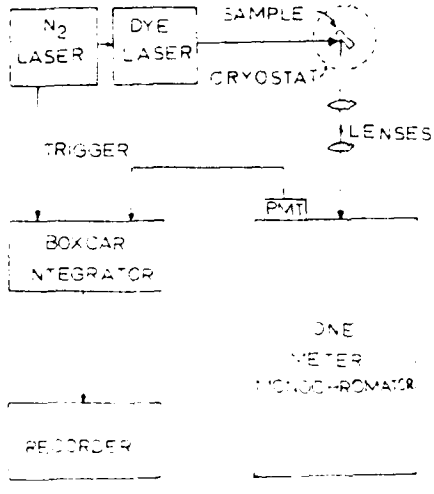

Fig. 1. Block diagram of experimental apparatus

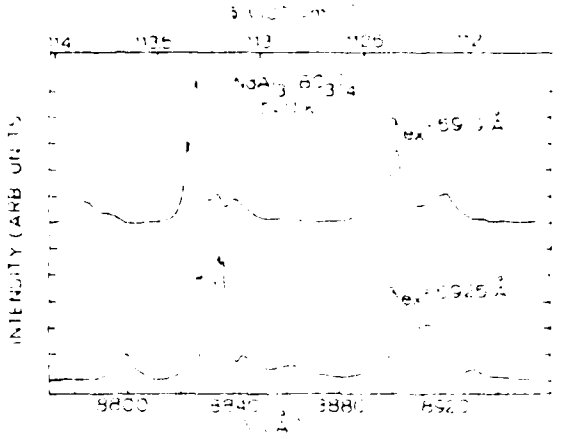

Fig. 2. Fluorescence spectra of $NdAl_3(BO_3)_4$ at 11 K for two different excitation wavelengths

relative intensities of these peaks vary in a uniform, continuous way between the two extremes shown in fig. 2 as the laser wavelength is scanned from 5919 to 5925 Å. This structure can be attributed to the presence of ions in slightly different types of crystal field sites. By tuning the dye laser wavelength, ions in specific types of sites are selectively excited. Energy transfer between ions in spectrally different sites can be studied by monitoring the time evolution of the fluorescence spectra after the laser pulse. Fig. 3 shows the spectrum at two times after the excitation pulse for a specific excitation wavelength at low

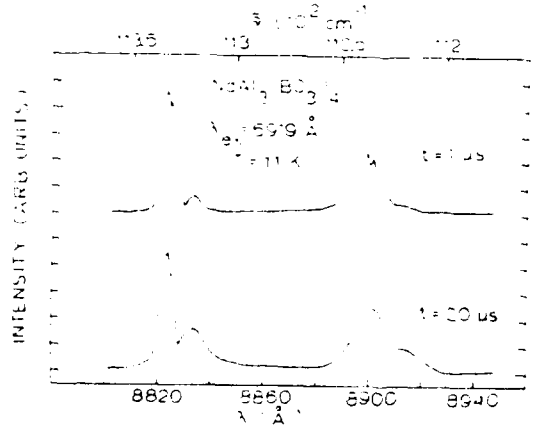

Fig. 3. Fluorescence spectra of $NdAl_3(BO_3)_4$ at 11 K at two times after the excitation pulse.

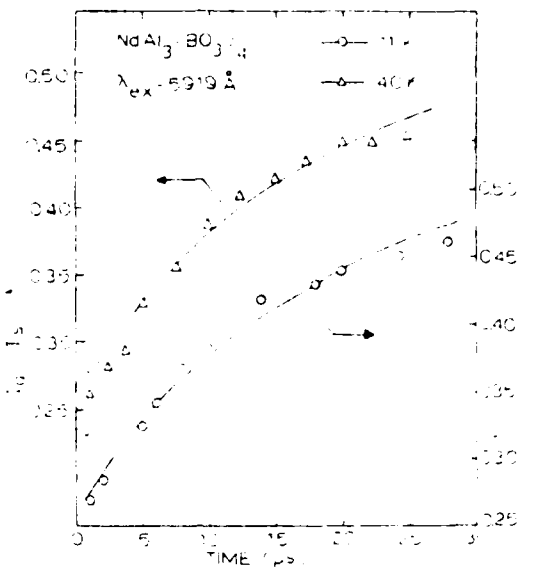

Fig. 4. Ratios of the integrated fluorescence intensities of activator and sensitizer transitions as a function of time after the excitation pulse at 11 K and 40 K. See text for explanation of theoretical lines.

temperature. At short times, the high energy components of the transitions are dominant; as time increases the low energy components grow in intensity with respect to the high energy lines.

The quantitative analysis of energy transfer from Nd^{3+} ions in sites producing the high energy transitions (sensitizers) to ions in sites resulting in the low energy transitions (activators) can be obtained by plotting the time dependence of the ratios of the integrated fluorescence intensities of the activator and sensitizer transitions. The results are shown in fig. 4 for 11 and 40 K. At higher temperatures the lines are broadened to the extent that the transitions from ions in nonequivalent sites cannot be resolved accurately. The solid lines in the figure represent theoretical fits to the data discussed in the following section.

3. Interpretation

The time-resolved spectroscopy results can be interpreted using the phenomenological rate parameter model shown in fig. 5. The "sensitizer" ions are those in the site preferentially excited by the laser at a rate W_s, whereas the

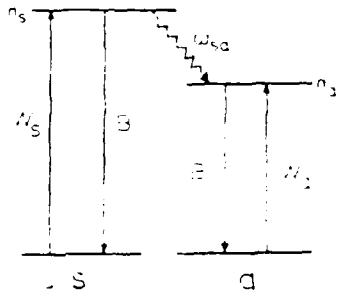

Fig. 5. Model for interpretation of energy transfer data. See text for explanation of symbols.

"activators" are ions in sites which receive the energy through energy transfer as well as being excited by the laser at a rate W_a. n_s and n_a are the concentrations of ions in the excited states, ω_{sa} is the rate of energy transfer, and B is the fluorescence decay rate which was found to be approximately the same for ions in both types of sites.

The rate equations describing the time evolution of the populations of excited states are

$$dn_s/dt = W_s - Bn_s - \omega_{sa} n_s, \tag{1}$$

$$dn_a/dt = W_a - Bn_a + \omega_{sa} n_s. \tag{2}$$

These equations can be solved assuming a delta-function excitation pulse and an explicit time dependence for the energy transfer rate. A variety of different theoretical models were tested, but it was found that the best fits to the data at both low and high temperatures were obtained with an energy transfer rate which varied as $t^{-1/2}$. The solutions of eqs. (1) and (2) are

$$n_s(t) = n_s(0)\, e^{-Bt - 2\omega t^{1/2}}, \tag{3}$$

$$n_a(t) = n_s(0)\left[e^{-Bt} - e^{-Bt - 2\omega t^{1/2}}\right] + n_a(0)\, e^{-Bt}, \tag{4}$$

where the time dependence of the energy and transfer rate is written explicitly as $\omega_{sa} = \omega t^{-1/2}$. The ratio of integrated fluorescence intensities is then given by

$$\frac{I_a}{I_s} = K\left\{\left(\frac{n_a(0)}{n_s(0)} + 1\right) e^{2\omega t^{1/2}} - 1\right\}, \tag{5}$$

where K is a constant containing factors including the radiative emission rates. The solid lines in fig. 4 represent the predictions of this expression treating K, ω and $n_a(0)/n_s(0)$ as adjustable parameters.

The temperature dependence of the energy transfer rate was determined by measuring the fluorescence intensities at different times after the excitation

pulse as a function of temperature and fitting the data using eq. (5). The results are shown in fig. 5. The transfer rate was found to be approximately constant below 25 K and to increase at higher temperatures.

4. Discussion and conclusions

The time dependence of the energy transfer rate is a sensitive indicator of the mechanism of energy transfer. The $t^{-1/2}$ variation observed here can be due to several types of processes: single-step electric dipole–dipole interaction between randomly distributed sensitizers and activators; multistep energy migration on a one-dimensional lattice; and trap-modulated energy migration in three dimensions. The first of these possibilities is generally the most common and can be verified through theoretical predictions of the magnitude of the energy transfer rate. At 11 K the measured value of ω_{da} is 0.20 μs^{-1}. The theoretical expression for the rate of single-step electric dipole–dipole energy transfer among randomly distributed ions is [7]

$$\omega_{da} = (\pi^{3/2}/2)C_a R_0^3 (\tau_s)^{-1/2}, \tag{6}$$

where C_a is the concentration of activators, τ_s is the intrinsic fluorescence decay time of the sensitizers and the critical interaction distance is given by [5]

$$R_0 = \left[\frac{3}{4}\frac{e^2}{mc^2}\frac{\eta_s f_a \Omega}{(2\pi n \bar{\nu}_a)^4}\right]^{1/6}, \tag{7}$$

where η_s is the quantum efficiency of the sensitizer, f_a is the oscillator strength of the activator, $\bar{\nu}_a$ is the average wave number in the region of spectral overlap, and Ω is the spectral overlap integral. Using the measured value of the energy transfer rate in eq. (6) along with the values of $C_a = 1.4 \times 10^{20}$ cm^{-3} determined by comparing relative spectral intensities at different excitation wavelengths and $\tau_s = 50$ μs which is the value measured in lightly doped borate samples [9] gives a measured value of $R_0 = 3.0$ Å. This can be compared to the theoretical value predicted by eq. (7), where f_a is calculated from spectral measurements to be 2.3×10^{-6} and the overlap integral is approximated by the overlap of two Lorentzian lines

$$\Omega \approx \frac{1}{\pi}\frac{\Delta\bar{\nu}_a + \Delta\bar{\nu}_s}{(\Delta\bar{\nu}_a + \Delta\bar{\nu}_s)^2 + (\bar{\nu}_a'' - \bar{\nu}_s'')^2}. \tag{8}$$

At 11 K the predicted value is $R_0 = 7.6$ Å. The difference in the predicted and measured values of R_0 is significant. Although some of the values of the parameters used in obtaining these results are rough estimates, such as η_s and Ω, any reasonable choice of values given at least a factor of 2 difference between the two determinations of R_0.

The inconsistency described above indicates that the single-step mechanism is not responsible for the observed energy transfer in this system. The second type of possible energy transfer process having the observed time dependence is a random walk in one dimension. In this case the Nd^{3+} ion in the excited metastable state is treated as a Frenkel exciton which can migrate to other sensitizer ions before becoming trapped at an activator site. The energy transfer rate for a random walk process can be expressed as the rate at which the exciton sample new sites multiplied by the fraction of total sites occupied by activators [10]. Using the expression for the sampling function for a one-dimensional lattice gives [11]

$$\omega_{sa} = (2\pi^{1/2}/3)N_a[\Gamma(R_{ss}/R_0)^6]^{1/2}t^{-1/2}, \qquad (6)$$

where it has been assumed that each step in the random walk takes place by an electric dipole–dipole interaction mechanism between ions separated by a distance R. The closest Nd ion separation in $NdAl_3(BO_3)_4$ crystals is 5.91 Å. Using this and the measured value of the energy transfer rate in eq. (6) gives a value of $R_0 = 7.2$ Å which is consistent with the theoretical predictions of eq. (5).

The third possibility that the observed energy transfer characteristics are due to trap-modulated energy migration in three dimensions can not be easily proven or disproven since any type of trap distribution necessary to fit the data can be postulated [12]. An important question is whether or not exciton motion restricted to one dimension is feasible in this type of crystal. The published crystal structure of $NdAl_3(BO_3)_4$ indicates that a Nd ion site has 6 nearest neighbor Nd ions in various crystallographic directions [3]. However, more recent structural measurements describe this crystal as having a two-dimensional layered structure [13]. The feasibility of a preferred migration direction must await publication of the details of this structure. It should be emphasized that theoretical models for fitting the TRS data are very sensitive to the time dependence of the proposed energy transfer mechanism and attempts to fit the data with two-dimensional or three-dimensional random walk models or with single-step higher order multipole processes were all unsuccessful.

The observed temperature dependence of the energy transfer rate can provide further information about the nature of the energy transfer mechanism and the role played by phonons at high temperatures. Several different processes can contribute to the increase in the transfer rate with increasing temperature. These include the increase in the spectral overlap integral, the increase in the number of phonons available to make up the mismatch between sensitizer and activator transitions ($\Delta E_{sa} \approx 12$ cm^{-1}), and the increase in population of higher energy sensitizer and activator levels which can take part in the transfer process [14]. For this case the first two types of processes were

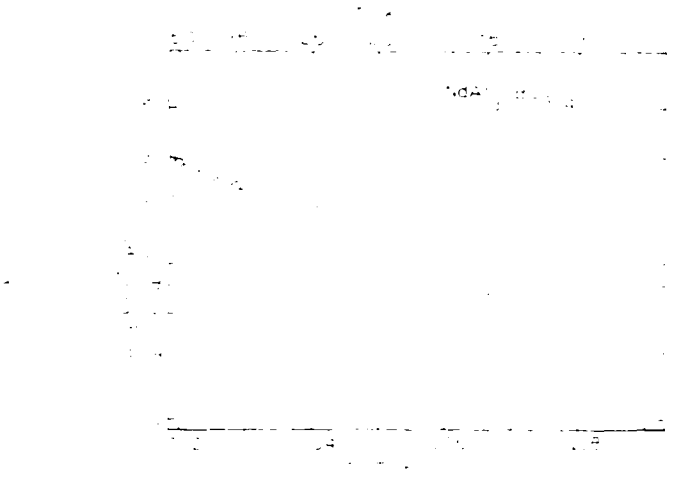

Fig. 6. Temperature dependence of the energy transfer rate. See text for explanation of the theoretical line.

found to be inconsistent with the data shown in fig. 6. The third mechanism can be applied to either single-step or multistep transfer. For a single-step process the expression for the energy transfer rate in eq. (6) would be written as the sum of transfer rates for each set of transitions weighted by the populations of the initial states of the transitions. The observed temperature dependence is not consistent with populating the first excited level of the ground state manifold of the activator, $E_{a2} \approx 60$ cm^{-1}. A qualitative fit to the data shown in fig. 6 can be obtained assuming the important activation energy is $\Delta E_{ab} \approx 25$ cm^{-1} which is needed to populate the higher crystal field component of the metastable state of the sensitizer. However, the room temperature spectrum shows that the b–1 transition is less intense than the a–1 transition and thus, energy transfer should not increase as the b level becomes populated from the a level [9].

The most consistent fit to the data is found from the one-dimensional random walk theory described by expressing eq. (9) as a sum over the thermally activated transitions involved in the migration. If the sum is simplified to include only the terms for the ground state and the first excited component the energy transfer rate is

$$\omega_{sa} = (2\pi)^{1/2} N_a \left\{ t_{HH}^{-1} \frac{1}{1 + e^{-\Delta E_{ab}/2kT}} \right\}^{1/2}$$

$$+\left[t_{H2}^{-1}\frac{e^{-\Delta E_{12}/kT}}{1-e^{-\Delta E_{12}/kT}}\right]^{1/2}t^{-1/2}, \quad (10)$$

where t_{H1} and t_{H2} are the hopping times involving the two types of transitions. The good fit to the data shown by the solid line in fig. 6 was found with $\Delta E_{12} \approx 60$ cm^{-1}, $t_{H1}^{-1} \approx 0.075$ ns^{-1} and $t_{H2}^{-1} \approx 6.75$ μs^{-1}. Both the value of the activation energy and the fact that $t_{H2}^{-1} \gg t_{H1}^{-1}$ are consistent with spectral observations. The magnitude of t_{H1}^{-1} is consistent with the theoretical prediction $t_{H1}^{-1} = \tau_0^{-1}(R_0/R)^6$.

In summary, the energy transfer characteristics of NAB crystals are consistent with a one-dimensional random walk in which the hopping rate increases as the first excited component of the ground state multiplet becomes thermally activated. The diffusion coefficient at low temperatures is $D = \frac{1}{2}R^2 t_{H1} = 1.3 \times 10^{-13}$ cm^2 sec^{-1}. These characteristics are quite different from those found in other Nd^{3+}-doped crystals [15]. The differences may be associated with the different crystal structure of NAB which still must be clarified. It should be pointed out that the conventional approach to the study of energy transfer has been used in this investigation in that a phenomenological rate parameter model was utilized to obtain the primary characteristics of the transfer rate from the experimental data and secondary information was obtained from comparison with the predictions of standard theories. More sophisticated theories are now being developed which raise questions about some aspects of this conventional approach [16] but they are not yet established to the point where they can be used to analyze new data such as that obtained in this study.

Acknowledgements

This research was supported by the U.S. Army Research Office. The authors are grateful to Professor G. Blasse for supplying the samples, and appreciate the helpful discussions with Dr. W. Zwicker concerning the crystal structure of NAB.

References

[1] S.R. Chinn, H.Y-P. Hong and J.A. Pierce, Laser Focus 12 (1976) 64.
[2] H.G. Danielmeyer, Festkorperprobleme (Advances in Solid State Physics, ed. H.J. Queisser (Pergamon/Vieweg, Braunschweig, 1975) p. 253.
[3] H.Y-P. Hong and K. Dwight, Mat. Res. Bull. 9 (1974) 1661.
[4] O. Jarchow, F. Lutz and K.H. Klaska, Diskussionstagung der Arbeitsgemeinschaft Kristallographie 29 (1972) 162.

[5] V.I. Bilak, I.I. Kuratev, N.I. Leonyuk, V.A. Pashkov, A.V. Pashkova, I.I. Timchenko and A.V. Shestakov, Sov. Phys. Dokl. 23 (1978) 299.
[6] H.D. Hattendorff, G. Huber and H.G. Danielmeyer, J. Phys. C11 (1978) 2599.
[7] M. Inokuti and F. Hirayama, J. Chem. Phys. 15 (1965) 1978.
[8] D.L. Dexter, J. Chem. Phys. 21 (1953) 836.
[9] S.R. Chinn and H.Y.-P. Hong, Optics Comm. 15 (1975) 345.
[10] Z.G. Soos and R.C. Powell, Phys. Rev. B6 (1972) 4035.
[11] E.W. Montroll, Proc. Symp. Appl. Math. Am. Math. Soc. 16 (1963) 193.
[12] R.C. Powell and Z.G. Soos, Phys. Rev. B5 (1972) 1547.
[13] H.G. Danielmeyer, presented at the International Laser Symposium, 1979.
[14] M.J. Weber, Phys. Rev. B4 (1971) 2932.
[15] J.M. Flaherty and R.C. Powell, Phys. Rev. B19 (1979) 32.
L.D. Merkle and R.C. Powell, Phys. Rev. B20 (1979) 75.
M. Zokai, R.C. Powell, G.F. Imbusch and B. DiBartolo, J. Appl. Phys. 51 (1980) 5950.
D.K. Sardar and R.C. Powell, J. Appl. Phys. 51 (1980) 2829.
[16] D.L. Huber, Phys. Rev. B20 (1979) 2307, 5363.
K.K. Ghosh and D.L. Huber, J. Lumin. 21 (1980) 225.
K.K. Ghosh, J. Hazarty and D.L. Huber, Phys. Rev. B22 (1980) 2537.

ENERGY TRANSFER AMONG NEODYMIUM IONS IN GLASS HOSTS

Larry D. Merkle, Richard C. Powell and Edwin E. Freed
Physics Department, Oklahoma State Univ.*, Stillwater, OK 74078, USA

and
Marvin J. Weber
Lawrence Livermore National Laboratories, **Livermore, CA 90017, USA

Energy transfer between Nd^{3+} ions in silicate, germanate, phosphate, and pentaphosphate glasses has been studied between 12 and 300 K. The results at 12 K agree with relative values predicted for electric dipole-dipole energy transfer. Very different temperature dependences are observed for the energy transfer in these samples.

Tunable dye lasers have proven to be an important tool in probing the optical properties of ions in disordered host materials such as glasses. We report here the results of using laser excited time-resolved site-selection spectroscopy techniques to study the energy transfer between Nd^{3+} ions in spectrally different sites in four different glass hosts.

The compositions of the glasses investigated are listed in Table 1. The experimental apparatus used in this work has been described previously [1]. Rhodamine 6G was used in the dye laser to obtain an excitation pulse with a 0.4 bandwidth. This excited the $^4I_{9/2} \rightarrow {}^2G_{7/2}$ $^4G_{5/2}$ transition and the fluorescence emission from the $^4F_{3/2} \rightarrow {}^4I_{9/2}$ transition was observed.

Table 1: Summary of Results

PARAMETER	LD2	LG	LP	NP
C(10^{20}Nd/cm^3)	1.33	3.02	4.85	35.8
τ_{fl}(μs)	290	215	175	30.5
τ(μs)	260	122	45	4
λ_{eff}(nm)	34.4	39.5	20.5	12.5
τ^{-1} (s^{-1})	633	1000	2410	2

COMPOSITIONS (mol.%): LD2-50SiO_2, 27.5 Li_2O, 5.0 , 17.5 Al_2O_3; LG-47.5GeO_2, 12.5 Li_2O; LP-52 P_2O_5, 28 Li_2O, 5 , Al_2O_3; NP-93.5 P_2O_5, 1.5 Na_2O.

*Sponsored by the National Science Foundation under Grant No. DMR-7910153 and the U.S. Army Research Office.
**Work performed under the auspices of the U.S. Department of Energy by the Basic Energy Sciences and Laser Programs at Lawrence Livermore National Laboratory.

AD-A110 886 OKLAHOMA STATE UNIV STILLWATER DEPT OF PHYSICS F/G 7/4
CHARACTERIZATION OF THE OPTICAL PROPERTIES OF LASER AND PHOSPHO--ETC(U)
JAN 82 R C POWELL DAAG29-80-C-0052

UNCLASSIFIED ARO-16182.11-P NL

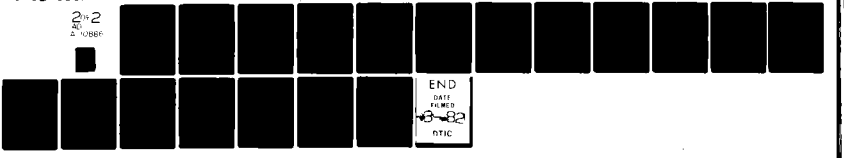

END
DATE FILMED
3-82
DTIC

Figure 1 shows examples of the fluorescence. For all of the samples the selectively excited spectra evolves with time toward the broadband excited spectra. The fluorescence decay times vary across the emission band and the amount of variation is different for each sample and becomes less at high temperatures. The lifetimes measured at the peaks of the emission bands at 12 K are listed in Table 1.

The results described above show that laser excitation selectivity excites Nd^{3+} ions in different types of local site environments and that energy transfer takes place between ions in these different types of local sites. The function describing the energy transfer can be written as [2].

$$a(t)=\int_{\omega_1}^{\omega_2} [I(\omega,t)-I(\omega,\infty)]d\omega \Big/ \int_{\omega_1}^{\omega_2} [I(\omega,o)-I(\omega,\infty)]d\omega.$$

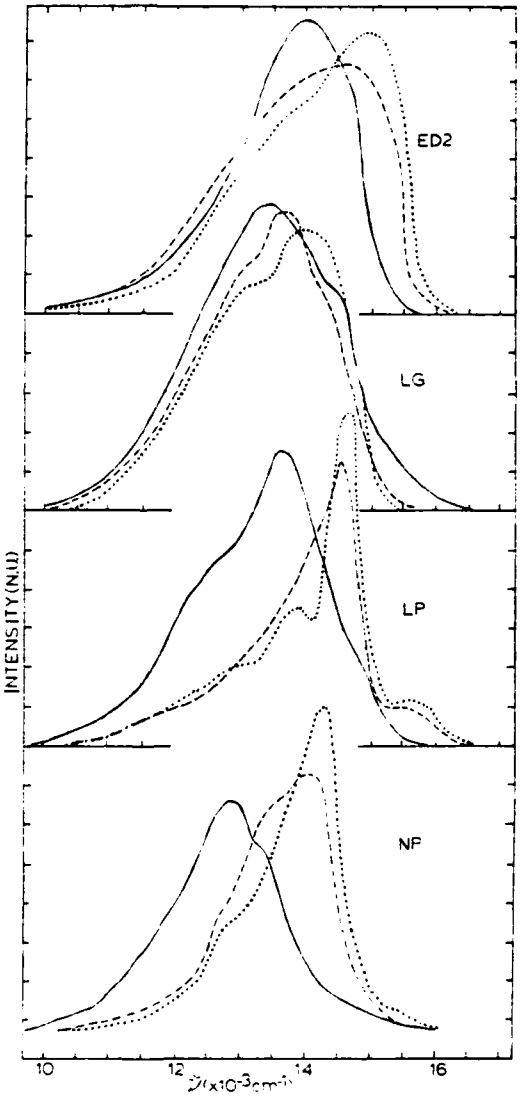

Figure 1
Normalized emission spectra at 12 K —— broad band excitation; .... laser excitation at short times (10 μs for ED2, LG, and LP and 1 μs for NP); ---- laser excitation at long times (400 μs for ED2, 600 μs for LG, 300 μs for LP and 50 μs for NP).

a(t) can be approximated by an exponential curve with the e^{-1} time given by the values of α listed in Table 1.

The rate of energy transfer between two Nd^{3+} ions separated by a distance R can theoretically be estimated by:

$$P = \frac{1}{(2J_A+1)(2J_B+1)}(2/3)(2\pi/\hbar)\cdot e^4/R^6 \quad L \sum_{t=2,4,6} \Omega^A_t \, |\langle J_A| \, |U^{(t)}| \, |J_A'\rangle|^2$$

$$\times \sum_{t=2,4,6} \Omega^B_t \, |\langle J_B| \, |U^{(t)}| \, |J_B'\rangle|^2.$$

This assumes a resonant electric dipole-dipole interaction. L is the integrated spectral overlap and the line strengths are expressed in terms of the Judd-Ofelt parameters Ω^I_t and the reduced matrix elements of the unit tensor operator. The matrix elements and Judd-Ofelt parameters were calculated from spectral data and the results were used in Eq. (2) along with estimates of average values of R obtained from the known concentrations assuming uniform distributions of Nd ions. The spectral overlap integral in this case involves all of the transitions between the various Stark levels of the excited state and ground state manifolds. This is proportional to the extent of splitting of the J-manifolds which can be approximated by the effective linewidth $\delta\lambda_{eff}$ 3 and these are listed in Table 1. Note that $\delta\lambda_{eff}$ is actually measured for the $^4F_{3/2} \rightarrow {}^4I_{11/2}$ transition but this is proportional to the effective width of the $^4F_{3/2} \rightarrow {}^4I_{4/2}$ transition 3.

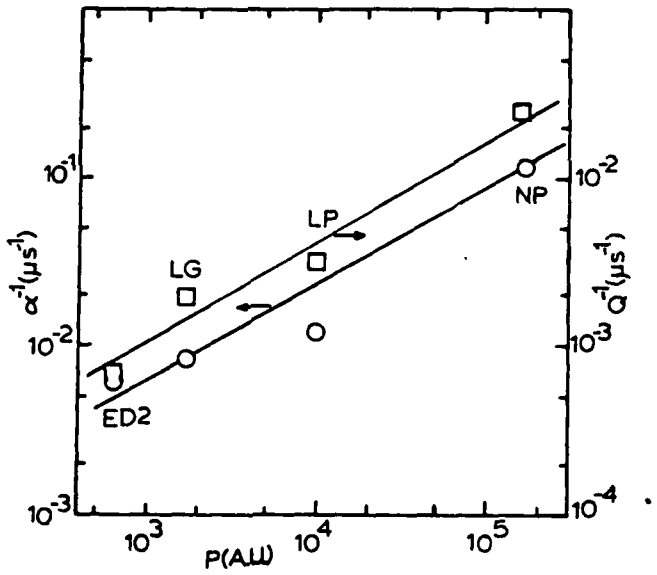

Figure 2

Measured energy transfer and quenching rates at 12 K plotted versus theoretically predicted electric dipole-dipole energy transfer rates.

As a rough approximation we assume the variation in $\delta\tilde{\nu}$ from sample to sample is proportional to the effective line widths (3). In Fig. 2 the measured values of α^{-1} at 12 K are plotted versus the predictions for P expressed in arbitrary units. α^{-1} varies uniformly with P from sample to sample which shows that the glass composition effects the strength of the energy transfer through L and Ω.

Another parameter of interest is the radiationless quenching rate $Q^{-1} = \tau_{fl}^{-1} - \tau_{rad}^{-1}$ where τ_{fl} is the fluorescence decay time and τ_{rad} is the radiative decay time. The values of Q^{-1} at 12 K are plotted versus P in Fig. 2. The variation of Q^{-1} with P is the same as that of α^{-1} which indicates that the physical

processes causing the differences in α^{-1} from sample to sample have similar effects on Q^{-1}.

The temperature dependences of α are quite different as shown in Fig. 3. Since there are several different physical processes which can contribute to the temperature dependence of the energy transfer rate it is difficult to give a definitive interpretation to the observed results. One possible interpretation which is also consistent with the different spectral characteristics seen in Fig. 1 is the following. Energy transfer in the NP and LP glasses may be associated with single-phonon assisted process involving stimulated phonon emission whereas the transfer mechanism in the LG glass may be a single-phonon assisted process involving spontaneous phonon emission. The behavior of the ED2 glass can be explained either by two-phonon assisted processes or enhanced absorption transition strengths due to thermally populating higher Stark components of the ground state manifold. Further studies are currently underway to correlate energy transfer properties with properties of the glass hosts with different compositions.

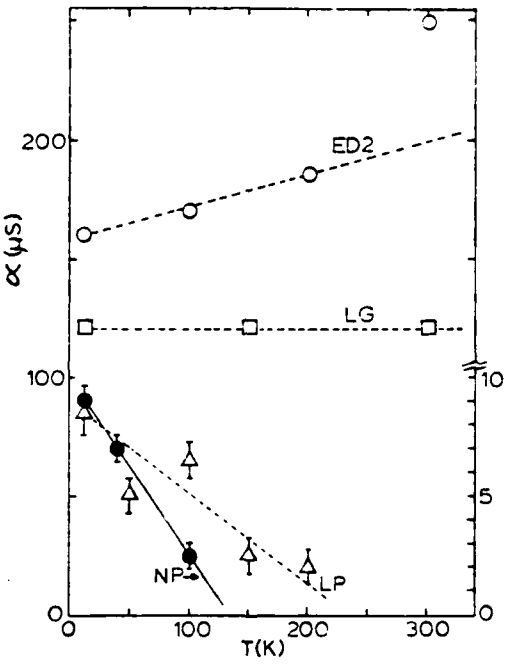

Figure 3
Temperature dependences of average ion-ion energy transfer times.

REFERENCES

(1) Merkle, L.D. and Powell, R.C., Energy transfer among Nd^{3+} ions in garnet crystals, Phys. Rev B 20 (1979) 75-84.

(2) Brawer, S.A. and Weber, M.J., Observation of fluorescence line narrowing, hole burning, and ion-ion energy transfer in neodymium laser glass, Appl. Phys. Lett. 35 (1979) 31-33.

(3) Pellegrino, J.M., Yen, W.M. and Weber, M.J., Composition dependence of Nd^{3+} homogeneous linewidths in glasses, J. Appl. Phys. 51 (1980) 6332-6336.

V. MISCELLANEOUS STUDIES

The manuscript in Section V.1 describes the results obtained using photoacoustic spectroscopy techniques to determine the quantum efficiencies of several different Nd^{3+} doped samples. In Section V.2 results are presented on the spectroscopic property of ruby crystals under hydrostatic pressure.

V.1

Radiationless decay processes of Nd^{3+} ions in solids

Richard C. Powell, Dean P. Neikirk, and Dhiraj Sardar

Department of Physics, Oklahoma State University, Stillwater, Oklahoma 74074

(Received 8 August 1979; revised 31 December 1979)

Laser photoacoustic spectroscopy measurements were made on Nd^{3+} ions in garnet, vanadate, and pentaphosphate host crystals. The variations of signal intensities with chopping frequency of the incident light are not in agreement with the predictions of standard photoacoustic signal generation theory. The results are distinctly different for concentrated and dilute Nd-doped crystals, indicating that the mechanisms for generating heat have different characteristics in these two types of samples. The determination of radiative quantum efficiencies of these materials by photoacoustic spectroscopy techniques is also described. These results are compared with those obtained by other methods.

INTRODUCTION

Photoacoustic spectroscopy (PAS) techniques have recently received a great deal of interest as a method for characterizing radiationless relaxation processes of ions in solids.[1-5] We describe here the results of PAS investigations of Nd^{3+} ions in several different types of host crystals. The data is interpreted in terms of radiationless decay, concentration quenching, and energy migration processes and a method for determining the quantum efficiencies of the samples is described. Problems with understanding the signal generation process with laser excitation, and problems with the accuracy of quantitative measurements are discussed.

Our experimental setup for PAS measurements has been described previously.[3,4] The only difference for the work described here is that the individual lines of an argon ion laser were used as the excitation source. The laser power was continuously monitored and stabilized at a level of 0.15 W. The exciting light was chopped at frequencies varying from 110 to 2700 Hz and focused onto the samples which were placed on the quartz exit window of the PA cell. The microphone was mounted at 90° to the exciting light and behind a baffle to prevent scattered laser light from reaching it. The signal was sent through a preamplifier to a lock-in amplifier and read out on a digital voltmeter after adjusting the lock-in phase for signal maximum. The signal to noise ratio was better than 100 to 1 in all cases and the measured background cell signal was at least 200 times smaller than the sample PA signal.

The samples investigated were all single crystals between 1 and 2 mm thick and between 5 and 10 mm on a side with polished faces. Three types of samples were studied: the garnets $Y_3Al_5O_{12}$ (0.85% Nd), $Y_3Ga_5O_{12}$ (0.25% Nd), $Y_3(Al_{0.5}Ga_{0.5})_5O_{12}$ (0.85% Nd), and $Nd_3Ga_5O_{12}$; the vanadate YVO_4 (2.0% and 3.0% Nd); and the pentaphosphates $Nd_xY_{1-x}P_5O_{14}$ with x ranging from 0.1 to 1.0.

Two types of experiments were performed: the measurement of PA signal intensity versus chopping frequency and the determination of quantum efficiencies.

I. PA SIGNAL VERSUS CHOPPING FREQUENCY

The PA signals at maximum phase were recorded at 12 or more chopping frequencies ν_c after excitation with the 5145-Å line of the argon laser. Examples of the results are shown in Figs. 1–3. For both samples of YVO_4:Nd^{3+}, the PA signal varies as ν_c^{-1} throughout the entire range of frequencies. For all three of the lightly doped garnet samples, a ν_c^{-1} dependence was also observed as shown for $Y_3Al_5O_{12}$:Nd^{3+} in Fig. 2. However, for the concentrated neodymium gallium garnet sample the PA signal was observed to vary as $\nu_c^{-3/2}$ throughout the entire frequency range. For the pentaphosphate crystals the 10% Nd sample exhibits a PA signal intensity which varies as ν_c^{-1} over the entire frequency range while the PA signal for the 100% Nd sample varies as ν_c^{-1} up to about 450 Hz and then varies as $\nu_c^{-3/2}$ at higher frequencies. Samples with intermediate Nd concentrations have PA signals which vary as ν_c^{-n} where n is intermediate between 1.0 and 1.5.

Understanding the results described above poses a difficult problem in the light of current theories for photoacoustic signal generation. Three parameters are necessary for theoretical analysis of PA measurements: the sample thickness l, the optical penetration depth l_{op}, and the thermal diffusion length l_{th}. For the samples investigated l is between 1 and 2 mm. The optical penetration depth is characterized as $1/\alpha$ where α is the absorption coefficient at the wavelength of the exciting light. For the laser line used for excitation, l_{op} is of the order of 80 mm for the lightly doped samples and approximately 0.7 mm for the concentrated Nd samples. The former ($l_{op} > l$) is the "optically thin" case while the latter ($l_{op} < l$) is the "optically thick" case.

The thermal diffusion length is given by $l_{th} = \sqrt{\beta/\pi\nu_c}$, where β is the thermal diffusivity. For garnet crystals[6] β is about $5.0 \times 10^{-2}\ cm^2 s^{-1}$, whereas in NdP_5O_{14}, β is anisotropic with the largest value being about[7] $1.0 \times 10^{-2}\ cm^2 s^{-1}$. The thermal diffusivity of YVO_4 should be of the same magnitude as that for the garnets and pentaphosphates. Thus for the range of chopping frequencies investigated, l_{th} varies from about 55 down to 10 μm. For all samples $l_{th} \ll l$, which is the "thermally thick" case. Also, $l_{th} < l_{op}$ for all samples investigated.

For a thermally thick case with $l_{th} < l_{op}$ as investigated here the Rosencwaig-Gersho (RG)[8] theory predicts that the PA signal intensity will vary as $\nu_c^{-3/2}$. Only if $l_{th} > l_{op}$ should a ν_c^{-1} dependence be observed. Obviously there is a striking difference between these theoretical predictions and the data shown in Figs. 1–3 for the lightly doped samples. A possible explanation for this discrepancy is the difference in dimensionality between theory and experiment. The RG theory is based on a one-dimensional model where the thermal gradient at the boundary between the excited surface and the gas causes uniform heat flow back into the cell. In the experiments described here only a small area of the total sample

 0030-3941/80/050486-05$00.50

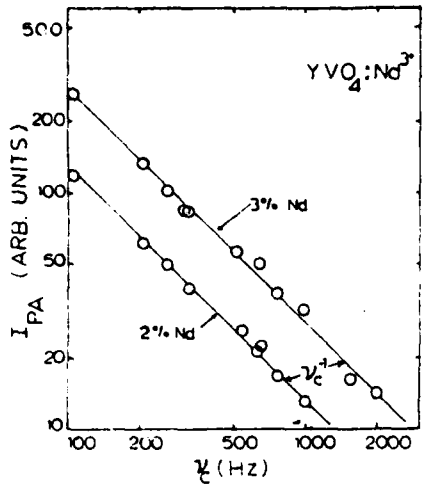

FIG. 1. Photoacoustic signal intensity as a function of chopping frequency for Nd-doped YVO_4 crystals.

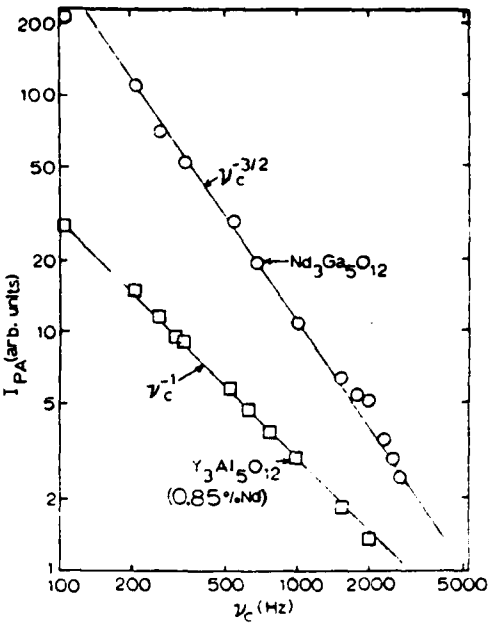

FIG. 2. Photoacoustic signal intensity as a function of chopping frequency for Nd^{3+} ions in garnet crystals.

surface is excited by the laser and the heat is generated in a cylindrical volume within the crystal. Near the front surface the dominant temperature gradient is still that between the sample and the gas, and the heat generated in this region diffuses to the surface and contributes to the PA signal as predicted in the one-dimensional model. However, in the interior region of the sample the dominant temperature gradient is radially outward from the heated cylinder. A three-dimensional photoacoustic theory which accurately models the details of our experiment has recently been developed.[9] The predictions of this theory have been shown to be in excellent agreement with our data with no adjustable parameters.

II. DETERMINATION OF QUANTUM EFFICIENCY

The accurate determination of absolute quantum efficiencies of ions in solids has been an experimental problem of interest for many years. It has been hoped that PAS techniques will provide a method for doing this and we describe there the results of measuring the quantum efficiencies of the neodymium-doped crystals. The maximum PA signal intensity and the phase at signal maximum were recorded for excitation wavelengths of 4765 Å and 5145 Å at chopping frequencies of 312 and 1000 Hz.

The PA signal at phase angle θ can be described by

$$I_a(\theta) = C(P_a/E_a) \sum_{i,j} \phi_{ij}^{nr} E_{ij} \cos[\psi + \tan^{-1}(2\pi\nu_c\tau_i) - \theta], \quad (1)$$

where P_a and E_a are the power absorbed and the energy of the level where absorption occurs, C is a factor accounting for the properties of the cell and detection system, and ϕ_{ij}^{nr} is the probability for a nonradiative transition between levels i and j separated by energy E_{ij} where the initial state has a lifetime τ_i. The summation is over all relaxation processes that occur after absorption. ψ is the phase shift due to the detection process.

The summation in Eq. (1) can be evaluated by considering the energy-level scheme and transitions for Nd^{3+} ions shown in Fig. 4. For the lines of the argon laser used for excitation, absorption occurs in either the $^4G_{11/2}$ or $^2G_{9/2}$ levels at energies E_7 and E_6. This is followed by a cascade of nonradiative decay processes to the $^4F_{3/2}$ metastable state. From this level radiative decay can occur with a rate W_R to the various ^4I_J multiplets with branching ratios b_{5i}. Nonradiative decay processes within the ^4I term return the ion to the ground state. The metastable state can also relax through direct nonradiative processes with a rate W_{NR} or through cross relaxation transitions with neighboring Nd^{3+} ions. This process is generally referred to as concentration quenching and occurs at a rate W_X. The quantum efficiency, probability of non-

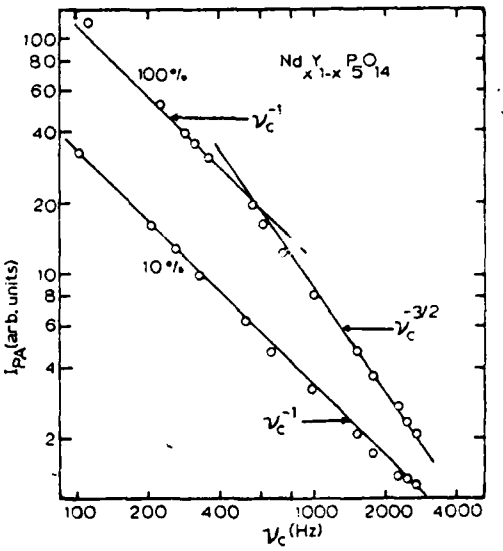

FIG. 3. Photoacoustic signal intensity as a function of chopping frequency for $Nd_xY_{1-x}P_5O_{14}$ crystals.

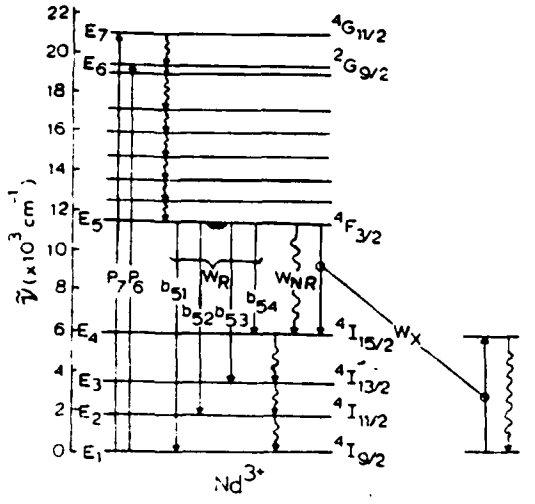

FIG. 4. Energy levels and transitions for Nd^{3+} ions.

radiative decay, and probability of concentration quenching of the metastable state are given by

$$QE = W_R/(W_R + W_{NR} + W_X), \tag{2}$$

$$P_{NR} = W_{NR}/(W_R + W_{NR} + W_X), \tag{3}$$

$$P_X = W_X/(W_R + W_{NR} + W_X), \tag{4}$$

where

$$QE + P_{NR} + P_X = 1. \tag{5}$$

All of the sample properties needed for Eqs. (1)–(5), such as energy levels, branching ratios,[10] and lifetimes are known for Nd^{3+} ions in $Y_3Al_5O_{12}$, YVO_4, and $Nd_xY_{1-x}P_5O_{14}$ crystals. Since only the $^4F_{3/2}$ level has a long enough lifetime to cause a phase shift in the PA signal, the evaluation of Eq. (1) with the model of Fig. 4 gives

$$I_a(\theta) = C(P_a/E_{a1})|E_{a5}\cos(\psi - \theta) + (E_{51} - kQE)\cos[\psi + \tan^{-1}(2\pi\nu_c\tau_5) - \theta]|, \tag{6}$$

where

$$k = E_{51} - b_{54}E_{41} - b_{53}E_{31} - b_{52}E_{21}, \tag{7}$$

and τ_5 is the lifetime of the $^4F_{3/2}$ level.

One of the problems in making absolute photoacoustic intensity measurements is the determination of the factor C representing cell and system response characteristics. To eliminate this factor we took the ratio of PA signals at two different excitation wavelengths. If we assume that the response characteristics of the system are approximately constant at least over a limited spectral region, the unknown factor cancels out and upon solving for the quantum efficiency gives

$$QE = \frac{AE_{75}\cos(\psi - \theta_7) + AE_{51}\cos[\psi + \tan^{-1}(2\pi\nu_c\tau_5) - \theta_7] - E_{65}\cos(\psi - \theta_6) - E_{51}\cos[\psi + \tan^{-1}(2\pi\nu_c\tau_5) - \theta_6]}{k\{A\cos[\psi + \tan^{-1}(2\pi\nu_c\tau_5) - \theta_7] - \cos[\psi + \tan^{-1}(2\pi\nu_c\tau_5) - \theta_6]\}}, \tag{8}$$

where

$$A = (I_{a6}/I_{a7})(E_{61}/E_{71})(P_7/P_6). \tag{9}$$

The phase shift due to equipment response ψ poses another problem. This was handled by deriving a second equation found from maximizing Eq. (6) with respect to θ and again solving for quantum efficiency:

$$QE = \frac{1}{k}\left\{\frac{E_{a5}\sin(\psi - \theta_a)}{\sin[\psi + \tan^{-1}(2\pi\nu_c\tau_5) - \theta_a]} + E_{51}\right\}. \tag{10}$$

Similar equations exist for the two different excitation wavelengths. These two equations along with Eq. (8) can be solved simultaneously in an iterative way to obtain a unique value for QE. To check the uniqueness of the result, the procedure was repeated for data obtained at both chopping frequencies.

The quantum efficiencies obtained by the above procedure are listed in Table I. $Y_3Al_5O_{12}$:Nd was the only one of the garnet samples analyzed because some of the important parameters, such as branching ratios, are not yet established for the gallium garnet and mixed garnet host crystals. A value of 0.60 was found for the quantum efficiency of Nd^{3+} in this host. This is much smaller than the value of 0.91 that is predicted by Judd-Ofelt theoretical calculations.[11] However, it is quite close to the value of 0.56 obtained by Singh *et al.*[12] by direct measurement techniques and the values of 0.48 and 0.63 obtained by using indirect laser-pumping techniques.[13,14] The variations in measured values may be due to samples having different Nd^{3+} concentrations and thus different levels of concentration quenching. Polycrystalline powders of $Y_3Al_5O_{12}$:Nd have been found to have a quantum efficiency close to 1.0 but this is greatly reduced when single crystals are formed.[15] This has been attributed to crystal defects acting as quenching centers[15] and thus explains the apparent discrepancy between measured values and theoretical predictions.

The results obtained for the 2.0% and 3.0% Nd-doped YVO_4 crystals give quantum efficiencies of 9.59 and 0.54, respectively. Calculations by Judd-Ofelt theory[16] predict a QE

TABLE I. Quantum efficiencies.

Sample	QE PAS method	QE Other methods	Reference
$Y_3Al_5O_{12}$		0.91	(10)
		0.56	(11)
(0.85% Nd)	0.60	0.48	(12)
		0.63	(13)
YVO_4		0.72	(15)
(2.0% Nd)	0.59	0.53	(a)
(3.0% Nd)	0.54	0.51	(a)
$Nd_xY_{1-x}P_5O_{14}$		0.40	(16)
(100% Nd)	0.45	0.50	(b)
(50% Nd)	0.60	0.66	(b)
(10% Nd)	0.90	1.00	(b)

(a) From lifetime measurements and the radiative lifetime of (15).
(b) From lifetime quenching measurements of (4).

value of 0.72. For the relatively high concentrations of Nd in our samples, concentration quenching will lower the measured QE from this theoretical value. Use of the calculated radiative lifetime and our measured fluorescence lifetimes predicts values of QE of 0.53 and 0.51 for our samples. No direct measurements of QE for Nd in YVO_4 are available for comparison.

For NdP_5O_{14} crystals a value of QE of 0.45 was obtained, which is close to the value obtained by Auzel *et al.*[17] through relative PAS measurements on powdered samples. The combination of this result with the measured concentration quenching of the fluorescence lifetime[4] predicts a QE for the $^4F_{3/2}$ level in the absence of concentration quenching in this system of 0.90. This is consistent with the values of QE found for lightly doped $Nd_xY_{1-x}P_5O_{14}$ as listed in Table I. No direct measurements of quantum efficiency in this system is available for comparison.

III. DISCUSSION AND CONCLUSIONS

The results presented here on the frequency dependence of the PA signal intensity on a variety of lightly doped and heavily doped samples show that there is still much work to be done in developing an accurate theoretical description of PA signal generation under typical experimental conditions. An attempt was made to better simulate the one-dimensional model upon which theoretical calculations have been based by using a lens to disperse the incident laser beam over most of the sample surface. However, when this was done a very different frequency dependence of the signal was obtained which was less than linear over most of frequency range, reached a maximum at about 400 Hz, and decreased at lower frequencies. This erratic dependence appears to be due to scattered-light and cell-surface effects. The experiments were again repeated with no lens used, resulting in an excited area of about 1 mm in radius. The results obtained under these conditions are the same as those shown in Figs. 1–3. Finally, to ensure that scattered light was not affecting the results obtained with small-area excitation, the laser was tuned to 4880 Å. This wavelength of light is not absorbed efficiently by Nd^{3+} ions and, therefore, the sample PAS signal should be essentially zero while the scattered light signal should be approximately the same as for the 5145-Å excitation. It was found that the scattered light signal was approximately one-and-one-half order of magnitude smaller than the smallest sample PAS signals. It should be emphasized that the specular reflection from the polished sample surface came back out through the front window of the cell and was measured to be approximately the same for both excitation wavelengths. These experiments indicate that experimental artifacts such as scattered light are not affecting the data. Also for samples of the type investigated here the small-diameter laser beam appears to be favorable to the dispersed excitation source and it is important to further develop theoretical models to account for these types of experimental conditions.

Recent work has been presented which accounts for some of the three-dimensional aspects of the heat flow problem.[18,19] The results of Quimby and Yen[18] indicate that no matter where the heat enters the cell from the sample, the one- and three-dimensional models are equivalent as long as cell-wall effects are not important. However, for the experiments described in this paper the important point is that in true three-dimensional heat flow inside the sample, some of the heat that is predicted to reach the surface in a one-dimensional flow model will actually never reach the surface within a duty cycle of the experiment. McDonald[19] has recently developed a three-dimensional photoacoustic theory based on a point source lying on the axis of a cylindrical sample. The new theory developed by Chow[9] gives a rigorous result for arbitrary beam profile. This theory is the most appropriate one for comparing with data obtained from our experimental geometry and the good fit that is obtained indicates that these data are affected by the three-dimensional aspects of the experiment. The data of Quimby and Yen[18] can also be fit well by this theory.

Another possibility for interpreting the results could be the dominance of the thermal expansion contribution to the PA signal.[20] This term will dominate only if $\beta_T \gg \mu_g/(l_s T_0)$, where β_T is the thermal expansion coefficient, μ_g is the thermal diffusion length in the gas, l_s is the sample thickness, and T_0 is the ambient temperature. For an air-filled cell at a frequency of 100 Hz, $\mu_g \simeq 2.5 \times 10^{-2}$ cm. For $T_0 = 300$ K and a typical sample thickness of 0.15 cm, the right-hand side of the inequality was found to be about 5×10^{-4} K^{-1}. Since the thermal expansion coefficients of the type of materials investigated here[21] are of the order of 7×10^{-6} K^{-1}, the inequality does not hold and thus thermal expansion makes a negligible contribution to the PA signal.

The method of measuring quantum efficiencies by photoacoustic techniques appears to give results generally consistent with other predictions and measurements. The procedure of eliminating unknown system-response properties by obtaining the ratio of PA signals at two different excitation wavelengths was first suggested by Rockley and Waugh[22] for determining the QE of organic dye molecules. Two other attempts have been made to obtain the QE of Nd^{3+} ions in solids. Auzel *et al.*[17] studied powdered samples of concentrated stoichiometric neodymium materials and eliminated equipment response factors by forming a calibration curve from samples of known quantum efficiencies. Quimby and Yen[5] investigated Nd^{3+} in a glass host and eliminated the problem of equipment response factors by measuring lifetime and PA signal changes on a series of samples with different concentrations. Their results extrapolated to very low concentrations imply that the QE for this system is between 0.65 and 0.75 depending on the Nd sites selectively excited by the laser. These values are less than the value of 0.9 measured by other techniques and theoretically predicted.[23,24] The chopping frequency used in this previous work was only 22 Hz and this eliminated the necessity for treating the phase-shift differences of the PA signal generated by phonons given off in different relaxation processes. For our experimental setup we found that the signal to noise ratio decreased below about 100 Hz and thus in our case more accurate data could be obtained at the higher chopping frequencies. Experimentally this problem of phase-shift differences could be eliminated by pumping directly into the $^4F_{3/2}$ level.

The most significant problem in the method of obtaining QE's described here is the accurate determination of the parameter A given in Eq. (9). A change in this parameter by an amount of only 0.01 can change the value of QE by about 0.10. For the type of samples studied the ratio of PA signal inten-

sities can be measured accurately and the ratio of the energies of the excitation lines is known exactly. The problem is in accurately determining the ratio of the power absorbed at the two excitation wavelengths. The major difficulties arise in measuring the amount of light scattered at the cell window and sample surface and in determining the exact absorption coefficients for sharp absorption lines at the positions of very narrow band laser lines. Thus the values of QE quoted in Table I should be considered to have an error range of as much as ±0.10.

In conclusion, PAS techniques can be used to obtain information on radiationless relaxation processes of ions in solids. However, it is important to develop better theoretical descriptions of the signal generation process when narrow-beam-diameter laser excitation sources are used. Quantum efficiencies can be determined even in complicated cases involving numerous radiationless processes if enough information is known concerning energy levels and branching ratios. However, absolute measurements are difficult and it is important to develop methods of eliminating cell- and system-response properties.

ACKNOWLEDGMENT

This work was supported by the U.S. Army Research Office.

[1]For a comprehensive review, see A. Rosencwaig, "Photoacoustic Spectroscopy," in *Advances in Electronics and Electron Physics* (Academic, New York, 1978), Vol. 46, pp. 207–311 and references therein.

[2]J. C. Murphy and L. C. Aamodt, "Photoacoustic spectroscopy of luminescent solids: Ruby," J. Appl. Phys. 48, 3502–3509 (1977); C. Aamodt, J. C. Murphy, and J. G. Parker, "Size considerations in the design of cells for photoacoustic spectroscopy," J. Appl. Phys. 48, 927–933 (1977).

[3]L. D. Merkle and R. C. Powell, "Photoacoustic spectroscopy investigation of radiationless transitions in Eu^{3+} ions in KCl crystals," Chem. Phys. Lett. 46, 303–306 (1977); R. G. Peterson and R. C. Powell, "Photoacoustic spectroscopy investigation of radiationless relaxation processes of Cr^{3+} in crystals," Chem. Phys. Lett. 53, 366–368 (1978).

[4]J. M. Flaherty and R. C. Powell, "Concentration quenching in $Nd_xY_{1-x}P_5O_{14}$ crystals," Phys. Rev. B 19, 32–42 (1979).

[5]R. S. Quimby and W. M. Yen, "Photoacoustic measurement of absolute quantum efficiencies in solids," Opt. Lett. 3, 181–183 (1978).

[6]P. H. Klein and W. J. Croft, "Thermal conductivity, diffusivity, and expansion of Y_2O_3, $Y_3Al_5O_{12}$, and LaF_3 in the range 77°–300°K," J. Appl. Phys. 38, 1603–1607 (1967).

[7]S. R. Chinn and W. K. Zwicker, "Thermal conductivity and specific heat of NdP_5O_{14}," J. Appl. Phys. 49, 5892–5895 (1978).

[8]A. Rosencwaig and A. Gersho, "Theory of the photoacoustic effect with solids," J. Appl. Phys. 47, 64–69 (1976).

[9]H. C. Chow (unpublished).

[10]T. S. Lomheim and L. G. DeShazer, "New Procedure of Determining Neodymium Fluorescence Branching Ratios as Applied to 25 Crystal and Glass Hosts," Opt. Commun. 24, 89–94 (1978).

[11]W. F. Krupke, "Radiative Transition Probabilities Within the $4f^3$ Ground Configuration of Nd:YAG," IEEE J. Quantum Electron. 7, 153–159 (1971).

[12]S. Singh, R. G. Smith, and L. G. Van Uitert, "Stimulated-emission cross section and fluorescent quantum efficiency of Nd^{3+} in yttrium aluminum garnet at room temperature," Phys. Rev. B 10, 2566–2572 (1974).

[13]T. S. Lomheim and L. G. DeShazer, "Determination of optical cross sections by the measurement of saturation flux using laser-pumped laser oscillators," J. Opt. Soc. Am. 68, 1575–1779 (1978).

[14]C. J. Kennedy and J. D. Barry, "New evidence on the quantum efficiency of Nd:YAG," Appl. Phys. Lett. 31, 91–92 (1977).

[15]S. Singh, W. A. Bonner, W. H. Grodkiewicz, M. Grasso, and L. G. Van Uitert, "Nd-doped yttrium aluminum garnet with improved fluorescent lifetime of the $^4F_{3/2}$ state," Appl. Phys. Lett. 29, 343–345 (1976).

[16]T. S. Lomheim and L. G. DeShazer, "Optical-absorption intensities of trivalent neodymium in the uniaxial crystal yttrium orthovanadate," J. Appl. Phys. 49, 5517–5522 (1978).

[17]F. Auzel, E. Meichenin, and J. C. Michel, "Determination of Quantum Yield of Self-Activated Mini-Laser Materials by Photoacoustic Spectroscopy," J. Luminescence 18/19, 97–100 (1979).

[18]R. S. Quimby and W. M. Yen, "Three-dimensional heat-flow effects in photoacoustic spectroscopy of solids," presented at the Photoacoustic Spectroscopy Meeting, Ames, Iowa, August 1979; Appl. Phys. Lett. 35, 43–45 (1979); J. Appl. Phys. (to be published).

[19]F. A. McDonald, "Three-dimensional theory of the photoacoustic effect," Appl. Phys. Lett. (to be published).

[20]F. A. McDonald and G. C. Wetsel, Jr., "Generalized theory of the photoacoustic effect," J. Appl. Phys. 49, 2313–2322 (1978).

[21]M. Birnbaum and L. G. DeShazer, "Low Threshold cw Nd Laser Oscillator at 1060 nm Study," final report for NASA by The Aerospace Corporation (unpublished).

[22]M. G. Rockley and K. M. Waugh, "The photoacoustic determination of fluorescence yields of dye solutions," Chem. Phy. Lett. 54, 597–599 (1978).

[23]E. M. Dianov, A. Ya. Karasik, A. A. Kut'enkov, V. B. Neustruev, and I. A. Shcherbakov, "Einstein coefficients, stimulated emission cross sections, and absolute quantum efficiencies of luminescence from the metastable state $^4F_{3/2}$ of Nd^{3+} in laser glasses and garnet crystals," Sov. J. Quantum Electron. 6, 90–94 (1976).

[24]C. B. Layne, W. H. Lowdermilk, and M. J. Weber, "Nonradiative Relaxation of Rare-Earth Ions in Silicate Laser Glass," J. Quantum Electron. 11, 798–799 (1975).

EFFECTS OF PRESSURE ON THE SPECTRA AND LIFETIMES OF RUBY

$Al_2O_3:Cr^{3+}$ results and interpretation

The change in the fluorescence lifetime of the R lines of the ruby sample with pressure is shown in figure 5. Despite the relatively large scatter in the data inherent in making

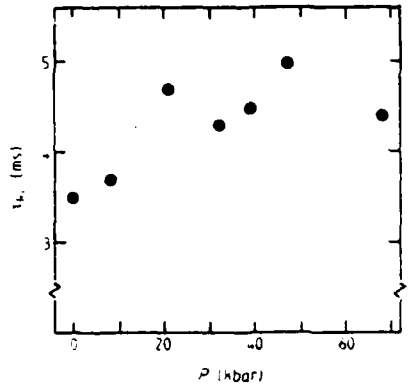

Figure 5. Pressure dependence of the lifetime of the R_1 fluorescence in ruby.

measurements on such a small sample, it is clear that the lifetime increases with increasing pressure. All decay curves were observed to be single exponentials. It is not clear at this time whether these results are due to a decrease in the radiative or non-radiative decay rate of the ^2E levels of Cr^{3+} with increasing pressure.

The detailed fluorescence spectrum of ruby observed at one atmosphere has been reported previously (Powell and Di Bartolo 1972). The peaks at 7017 Å and 7049 Å are the N_2 and N_1 lines, respectively, arising from exchange coupled pairs of Cr^{3+} ions. The peaks at 6977 Å, 6985 Å, and 6996 Å also arise from pairs, whereas the longer-wavelength peaks correspond to vibronic sidebands of the R_1 transition (Kushida and Kikuchi 1967). The pressure dependence of the peak positions is plotted in figure 6 with approximate rates of change of the line positions with pressure listed in table 3. It can be seen that N_1 is more sensitive to hydrostatic pressure than N_2, which is consistent with the uniaxial stress data of Mollenauer and Schawlow (1968). This difference has been attributed to the details of the interaction between third-nearest-neighbour pairs giving rise to N_1 and fourth-nearest-neighbour pairs giving rise to N_2.

For vibronic lines, table 3 also gives the pressure-induced energy shifts relative to the R_1 line shift. These shifts in phonon energies can be used to estimate mode Grüneisen

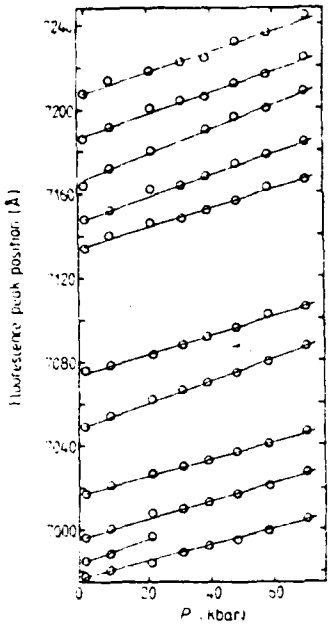

Figure 6. Pressure dependence of the long-wavelength side peaks of the R fluorescence of ruby.

Table 3. Pressure shifts and Grüneisen parameters from the long-wavelength side peaks of the ruby R fluorescence.

	Positions at 1 bar					
	λ (Å)	$\bar{\nu}$ (cm^{-1})	$\bar{\nu}_{R_1} - \bar{\nu}$ (cm^{-1})	$\frac{d\bar{\nu}}{dP}$ (cm^{-1} $kbar^{-1}$)	$\frac{d\bar{\nu}_{R_1}}{dP} - \frac{d\bar{\nu}}{dP}$ (cm^{-1} $kbar^{-1}$)	γ
	6977	14333	72	-0.82 ± 0.03		
	6985	14316	89	—		
	6996	14294	111	-0.88 ± 0.03		
(N_2)	7017	14251	154	-0.87 ± 0.03		
(N_1)	7049	14186	219	-1.08 ± 0.03		
	7076	14132	273	-0.86 ± 0.04	0.11 ± 0.04	1.0 ± 0.4
	7134	14017	388	-0.86 ± 0.03	0.11 ± 0.03	0.7 ± 0.2
	7148	13990	415	-0.99 ± 0.03	0.24 ± 0.03	1.5 ± 0.2
	7164	13959	446	-1.14 ± 0.04	0.39 ± 0.04	2.2 ± 0.2
	7186	13916	489	-0.98 ± 0.06	0.23 ± 0.06	1.2 ± 0.3
	7208	13873	532	-0.96 ± 0.08	0.21 ± 0.08	1.0 ± 0.4

parameters from the equation

$$\gamma_i = \frac{\partial \ln \omega_i}{\partial \ln V} = \frac{B_T}{\bar{\nu}_i} \frac{\partial \bar{\nu}}{\partial P} \tag{7}$$

where B_T is the isothermal bulk modulus which is about 2.57 Mbar for ruby (Finger and Hazen 1978). The mode γ's obtained from equation (7) and the observed data are listed

in table 3. These are difficult to compare directly with other types of data due to the uncertainty in identifying the vibronic peaks with particular points in the Brillouin zone. However, the values obtained here fall in the same range as the Al_2O_3 mode γ's determined from the pressure derivatives of elastic moduli (Gerlich 1970).

The pressure variations of the lifetime of the ruby R lines and the positions of the N lines and vibronic peaks demonstrate the variety of effects that can be studied with pressure techniques. The lifetime change most probably reflects changes in the nature of the crystal field. The different variations in the positions of the N_1 and N_2 lines reflect changes in the exchange interactions between the pairs of Cr^{3+} ions. The change in vibronic peaks can be attributed to changes in the lattice phonons with increased pressure. All of these areas warrant further study, but it is obvious that the application of hydrostatic pressure can provide a great deal of useful information on the spectral dynamics of impurity ions in solids.

REFERENCES

Finger L W and Hazen R M 1978 *J. Appl. Phys.* **49** 5823

Gerlich D 1970 *J. Phys. Chem. Solids* **31** 1188

Kushida T and Kikuchi M 1967 *J. Phys. Soc. Japan* **23** 1333

Mollenauer L F and Shawlow A L 1968 *Phys. Rev.* **168** 309

Powell R C and DiBartolo B 1972 *Phys. Stat. Solidi* (a) **10** 315

APPENDIX

DERIVATION OF SUSCEPTIBILITY χ FOR A TWO LEVEL MEDIA*

Consider an absorbing media which will be modeled as an array of two level atoms that can be characterized by dipole moment μ and longitudinal and transverse relaxation times t_1 and t_2, respectively. One can then derive the susceptibility χ, where $\underset{\sim}{P} = \varepsilon_o \chi(\Xi)\underset{\sim}{E}$.

Suppose that a quantum mechanical system is in state $\psi(\underset{\sim}{r},t)$. One can expand $\psi(\underset{\sim}{r},t)$ as $\psi(\underset{\sim}{r},t) = \sum_n C_n(t)U_n(\underset{\sim}{r})$ where $U_n(\underset{\sim}{r})$ are a complete orthonormal set of functions and $C_n(t)$ is the n^{th} time dependent expansion coefficient. An operator A has expectation value

$$\langle A \rangle = \sum_{nm} C_m^* A_{mn} C_n$$

where $A_{mn} = (U_m, AU_n)$.

The ensemble average $\overline{\langle A \rangle}$ is given by $\overline{\langle A \rangle} = \sum_{mn} \rho_{mn} A_{mn}$ where $\rho_{mn} = \overline{C_m^* C_n}$ or

$$\overline{\langle A \rangle} = \sum_n (\rho A)_{nn} = \mathrm{Tr}(\rho A) . \qquad (A-1)$$

Now consider an ensemble of two-level atoms interacting with a time-harmonic electromagnetic field. The density matrix is a 2x2 matrix

---

*See A. Yariv, Quantum Electronics (Wiley, New York, 1975).

with elements ρ_{11}, ρ_{22}, ρ_{12}, $\rho_{21} = \rho_{12}^*$. The interaction hamiltonian $H'(t)$ is of the dipole type, and can be written as $H'(t) = -\mu E(t)$. Since the dipole transitions are between states of definite parity, $\mu_{11} = \mu_{22} = 0$; and the phases of $U_1(\underline{r})$ and $U_2(\underline{r})$ can be chosen such that $\mu_{22} = \mu_{21} = \mu$. One can then write the interaction hamiltonian as

$$H'(t) = \begin{pmatrix} 0 & -\mu E(t) \\ -\mu E(t) & 0 \end{pmatrix} .$$

The unperturbed hamiltonian H_o is given by

$$H_o = \begin{pmatrix} \varepsilon_1 & 0 \\ 0 & \varepsilon_2 \end{pmatrix}$$

where ε_2 is the energy of the excited state and ε_1 is the energy of the ground state.

Thus the hamiltonian H is given by

$$H = \begin{pmatrix} \varepsilon_1 & -\mu E(t) \\ -\mu E(t) & \varepsilon_2 \end{pmatrix} . \qquad \text{(A-2)}$$

The ensemble average $\overline{\langle \mu \rangle}$ of the dipole moment induced by $E(t)$ is given by

$$\overline{\langle \mu \rangle} = \mathrm{Tr}(\rho\mu) = \mu(\rho_{12}+\rho_{21}) = \mu(\rho_{21}+\rho_{21}^*) . \qquad \text{(A-3)}$$

The density matrix satisfies

$$\frac{d\rho}{dt} = \frac{-i}{\hbar} [H,\rho] . \qquad \text{(A-4)}$$

which becomes

$$\frac{d\rho}{dt} = \frac{-i}{\hbar}\begin{pmatrix} \mu E(t)(\rho_{21}-\rho_{21}^*) & -\mu E(t)(\rho_{22}-\rho_{11})-(\epsilon_2-\epsilon_1)\rho_{21}^* \\ \mu E(t)(\rho_{22}-\rho_{11})+(\epsilon_2-\epsilon_1)\rho_{21} & \mu E(t)(\rho_{21}-\rho_{21}^*) \end{pmatrix} . \quad (A-5)$$

Defining the resonant frequency $\omega_o = \frac{\epsilon_2-\epsilon_1}{\hbar}$, it follows from (A-5) that

$$\frac{d\rho_{21}}{dt} = -i\omega_o\rho_{21} + \frac{i\mu}{\hbar} E(t)(\rho_{11}-\rho_{22}) \quad (A-6)$$

$$\frac{d\rho_{22}}{dt} = \frac{i\mu E(t)}{\hbar} (\rho_{21}-\rho_{21}^*) \quad (A-7)$$

and using the normalization condition,

$$\frac{d}{dt} (\rho_{11}-\rho_{22}) = \frac{2i\mu}{\hbar} E(t)(\rho_{21}-\rho_{21}^*) . \quad (A-8)$$

The above equations of motion for the density matrix do not include collisional effects. When the perturbing field E(t) is turned off, one expects the off diagonal terms in the density matrix to vanish as the relative phase coherence among the eigenfunctions of the ensemble is lost via collisions. These collisions will conserve the average energy of each level, but cause a loss of information about the phases of the wavefunctions. The jth diagonal element of the density matrix represents the fraction of the systems in the ensemble that will give the answer E_j when the energy is measured. If one takes into account only collisions, these will be given by the Boltzmann factors, and the equilibrium density matrix ρ^{ℓ} is

$$\rho^{\ell} = \frac{1}{Q}\begin{bmatrix} \ell^{-\varepsilon_1/k_bT} & 0 \\ 0 & \ell^{-\varepsilon_2/k_bT} \end{bmatrix}$$

where Q = partition function = $\ell^{-\varepsilon_1/k_bT} + \ell^{-\varepsilon_2/k_bT}$.

If the perturbing field is turned off, the density matrices will decay back to equilibrium with decay constant t^{-1} as

$$\frac{d\rho_{jk}}{dt} = -\frac{(\rho_{jk} - \rho_{jk}^{\ell})}{t_{jk}},$$

Because of the normalization condition, for a two-level system the relaxation times of the diagonal elements must be equal and is called the longitudinal relaxation time t_1. Since $\rho_{12} = \rho_{21}^*$, the off diagonal relaxation times are also equal and is called the transverse relaxation time t_2. The transverse relaxation time can be thought of as a phase coherence relaxation time.

After including collisional effects, (A-6) and (A-8) become

$$\frac{d\rho_{21}}{dt} = -i\omega_o\rho_{21} + \frac{i\mu}{\hbar}(\rho_{11}-\rho_{22})E(t - \frac{\rho_{21}}{t_2} \qquad \text{(A-9)}$$

$$\frac{d}{dt}(\rho_{11}-\rho_{22}) = \frac{2i\mu E(t)}{\hbar}(\rho_{21}-\rho_{21}^*) - \frac{(\rho_{11}-\rho_{22}) - (\rho_{11}^{\ell}-\rho_{22}^{\ell})}{t_1}. \qquad \text{(A-10)}$$

If one assumes that the local perturbing field E(t) is harmonic, $E(t) = E_o\cos\omega t$; then if $\omega \approx \omega_o$ the slowly varying variable $\sigma_{21}(t)$ may be defined as

$$\rho_{21}(t) = \sigma_{21}(t)\ell^{-i\omega t}. \qquad \text{(A-11)}$$

Substituting into (A-9), and throwing out the nonsynchronous term $\ell^{i\omega t}$ which averages to zero, Equation (A-9) becomes

$$\frac{d\sigma_{21}}{dt} = i(\omega-\omega_o)\sigma_{21} + \frac{i\mu E_o}{2\hbar}(\rho_{11}-\rho_{22}) - \frac{\sigma_{21}}{t_2} . \qquad (A-12)$$

Substituting (A-11) into (A-10) and throwing out the nonsynchronous terms $\ell^{2i\omega t}$ and $\ell^{-2i\omega t}$ which average to zero, one obtains

$$\frac{d}{dt}(\rho_{11}-\rho_{22}) = \frac{i\mu E_o}{\hbar}(\sigma_{21}-\sigma_{21}^*) - \frac{(\rho_{11}-\rho_{22}) - (\rho_{11}-\rho_{22})^{\ell}}{t_1} . \qquad (A-13)$$

To obtain the steady state solutions to the density matrix, the left hand side of (A-12) and (A-13) is set equal to zero. The precession frequency Ω is defined as

$$\Omega = \frac{\mu E_o}{2\hbar}$$

and the steady-state solutions to (A-12) and (A-13) are

$$Re(\sigma_{21}) = \frac{-\Omega t_2^2(\rho_{11}-\rho_{22})^{\ell}(\omega-\omega_o)}{1 + 4\Omega^2 t_1 t_2 + t_2^2(\omega-\omega_o)^2} \qquad (A-14)$$

$$Im(\sigma_{21}) = \frac{\Omega t_2(\rho_{11}-\rho_{22})^{\ell}}{1 + 4\Omega^2 t_1 t_2 + t_2^2(\omega-\omega_o)^2} \qquad (A-15)$$

$$\rho_{11}-\rho_{22} = (\rho_{11}-\rho_{22})^{\ell}\left\{\frac{1 + (\omega-\omega_o)^2 t_2^2}{1 + (\omega-\omega_o)^2 t_2^2 + 4\Omega^2 t_2 t_1}\right\} . \qquad (A-16)$$

If N is the density of active atoms or ions, then $\Delta N = N(\rho_{11}-\rho_{22})$ is the average density of the population difference between the two levels,

and $\Delta N^{\ell} = N(\sigma_{11}-\sigma_{22})^{\ell}$ is the population difference between the two levels at zero field. From (A-16),

$$\Delta N = \Delta N^{\ell} \{\frac{1 + (\omega-\omega_o)^2 t_2^2}{1 + (\omega-\omega_o)^2 t_2^2 + 4\Omega^2 t_2 t_1}\} .$$

The macroscopic polarization P is given by

$$P = N\overline{<\mu>} \text{ or, using (A-3),}$$

$P = N\mu(\sigma_{21} + \sigma_{21}^*)$ which can be expressed in terms of σ_{21} as

$$P = 2N\mu(\mathrm{Re}(\sigma_{21})\cos\omega t + \mathrm{Im}(\sigma_{21})\sin\omega t) .$$

Substituting in for $\mathrm{Re}(\sigma_{21})$ and $\mathrm{Im}(\sigma_{21})$, one may write the polarization as

$$P = \frac{\mu^2 \Delta N^{\ell} t_2}{\hbar} E_o \{\frac{\sin\omega t + (\omega_o-\omega) t_2 \cos\omega t}{1 + (\omega-\omega_o)^2 t_2^2 + 4\Omega^2 t_2 t_1}\} . \qquad \text{(A-17)}$$

One may now express the polarization in terms of the susceptibility χ as

$$P(t) = \varepsilon_o(\mathrm{Re}(\chi))E_o\cos\omega t - \varepsilon_o(\mathrm{Im}(\chi))E_o \sin\omega t ;$$

comparing with (A-17), it can be seen from observation that

$$\mathrm{Re}(\chi) = \frac{\mu^2 t_2 \Delta N^{\ell}}{\varepsilon_o \hbar} \{\frac{(\omega_o-\omega) t_2}{1 + (\omega-\omega_o)^2 t_2^2 + 4\Omega^2 t_1 t_2}\} \qquad \text{(A-18)}$$

and

$$\mathrm{Im}(\chi) = -\frac{\mu^2 t_2 \Delta N}{\varepsilon_o \hbar} \left\{ \frac{1}{1 + (\omega-\omega_o)^2 + 4\Omega^2 t_1 t_2} \right\} . \qquad \text{(A-19)}$$

Now let k be the magnitude of the wavevector at frequency ω. One can identify $\delta = (\omega-\omega_o)t_2$ as the normalized detuning from line center; $E_s^2 = \frac{\hbar^2}{t_1 t_2 \mu^2}$ as the line center saturation "intensity"; and $\alpha_o = \frac{\mu^2 \Delta N t_2 k}{2\varepsilon_o \hbar}$ as the line center small-signal field attenuation coefficient.

Using (A-18) and (A-19), one may write the two-level atom susceptibility as

$$\chi(E) = -\frac{2\alpha_o}{k} \frac{(i+\delta)}{(1 + \delta^2 + \frac{|E|^2}{|E_s|^2})} . \qquad \text{(A-20)}$$

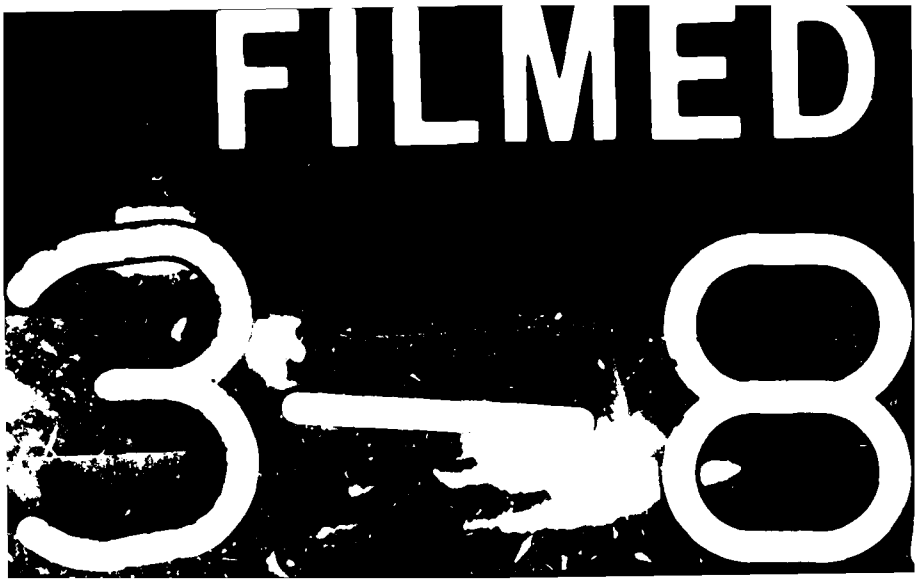
FILMED